NASA TECHNICAL MEMORANDUM

NASA TM X- 74027

NASA TM X-74027

(NASA-TM-X-74027) CALIBRATION AND TEST CAPABILITIES OF THE LANGLEY 7- BY 10- FOOT HIGH SPEED TUNNEL (NASA) 75 p HC A04/MF A01
CSCL 14B
N78-11121
Unclas
G3/09 52811

CALIBRATION AND TEST CAPABILITIES OF THE LANGLEY 7- BY 10-FOOT HIGH SPEED TUNNEL

by

Charles H. Fox, Jr.

and

Jarrett K. Huffman

NASA Langley Research Center

May 1977

This informal documentation medium is used to provide accelerated or special release of technical information to selected users. The contents may not meet NASA formal editing and publication standards, may be revised, or may be incorporated in another publication.

NASA
National Aeronautics and Space Administration

Langley Research Center
Hampton, Virginia 23665

1. Report No.	2. Government Accession No.	3. Recipient's Catalog No.
NASA TM X-74027		

4. Title and Subtitle	5. Report Date
CALIBRATION AND TEST CAPABILITIES OF THE LANGLEY 7- BY 10-FOOT HIGH SPEED TUNNEL	May 1977
	6. Performing Organization Code
7. Author(s)	8. Performing Organization Report No.
Charles H. Fox, Jr. and Jarrett K. Huffman	
	10. Work Unit No.
9. Performing Organization Name and Address	11. Contract or Grant No.
Langley Research Center Hampton, VA 23665	
	13. Type of Report and Period Covered
12. Sponsoring Agency Name and Address	Technical Memorandum
National Aeronautics & Space Administration Washington, DC 20546	14. Sponsoring Agency Code

15. Supplementary Notes

16. Abstract

The results of a new subsonic calibration of the Langley 7- by 10-foot high speed tunnel with the test section in a solid wall configuration are presented. A description of the test capabilities of the 7- by 10-foot high speed tunnel is also given.

17. Key Words (Suggested by Author(s))	18. Distribution Statement
Tunnel Calibration Tunnel Test Capabilities	Unlimited-Star Category-09 Unclassified

19. Security Classif. (of this report)	20. Security Classif. (of this page)	21. No. of Pages	22. Price*
Unclassified	Unclassified	73	$4.50

* For sale by the National Technical Information Service, Springfield, Virginia 22161

INTRODUCTION

The test section of the Langley 7- by 10-foot high speed tunnel is surrounded by a plenum attached to a boundary layer removal compressor. The test section may be configured with longitudinal slots in the floor and ceiling to permit operation at transonic speeds. The test section may also be configured with a solid floor and ceiling for purely subsonic testing. Since plenum suction is not currently available and since the current research program for the facility does not require transonic testing, the test section has been modified to return it to the solid wall configuration. For subsonic testing, the solid wall configuration has the advantages of well defined wall boundary conditions for the calculation of wall interference effects and significantly lower drive energy consumption with respect to the slotted wall configuration.

A test program was initiated to recalibrate the test section in the solid wall configuration. This calibration program consisted of measuring the test section centerline static pressure distribution over the full operating range of the tunnel. The results of this calibration are presented in this report.

Complementing the calibration information is a description of the test capabilities of the 7- by 10-foot high speed tunnel. Particular emphasis has been placed upon providing illustrative examples of the wide variety of test setups which are possible in this facility.

SYMBOLS

ΔA	change in area, m^2 (ft^2)
A_{REF}	reference area, 5.8065 m^2 (62.5006 ft^2)
H_I	total pressure indicated by sonar manometer, Pa(psf)
M	free stream Mach number
P	local static pressure
P_I	static pressure indicated by sonar manometer, Pa(psf)
P_1	static pressure from the calibration probe averaged over the usable test section, Pa (psf)
P_{T_1}	total pressure from the calibration probe, Pa(psf)
q	free stream dynamic pressure, Pa(psf)
R	Reynolds number per unit length
T	free stream stagnation temperature, °C (°F)
α	angle of attack, deg.
β	angle of sideslip, deg.

PART I - TUNNEL CALIBRATION

APPARATUS

The Langley 7- by 10-foot high speed tunnel test section is shown in figure 1. The tunnel is a continuous flow, closed circuit, atmospheric wind tunnel which operates at ambient atmospheric conditions. A more complete description is given in the second part of this report.

Figure 1 shows the calibration probe installed in the test section. The probe geometry is shown in figure 2. The calibration probe is 7.620 cm (3.000 in.) in diameter. The probe contained a total pressure orifice at tunnel station 367.99 and measured the static pressure distribution from tunnel station 317.74 to tunnel station 17.74. The rear of the probe was rigidly attached to the vertical strut of the tunnel sting support system. The front of the probe was held centered in the test section through the use of four cables. These cables also applied a tensile load to the entire probe.

The probe orifices were referenced to a single static orifice in the ceiling at tunnel station 200.29. This orifice was connected to a precision digital U-tube sonar mercury manometer. During normal testing, this ceiling orifice provides the indicated static pressure, as measured by this manometer, for setting the test conditions. A second ceiling orifice located at the same tunnel station but displaced laterally 20.32 cm (8. in.) was cross calibrated against the centerline ceiling orifice. During normal testing, this second orifice provides the reference static pressure for differential pressure transducers.

The probe was equipped with a total pressure orifice which was referenced to a total pressure probe mounted on the right side wall upstream in the entrance cone. This side wall probe was connected to a precision digital U-tube sonar mercury manometer. During normal testing, this sidewall total probe provides the indicated total pressure, as measured by this manometer, for setting the test conditions. A second total probe located on the left side wall was cross calibrated against the right side wall total probe. During normal testing, the left sidewall total probe provides the reference total pressure for differential pressure transducers.

The digital sonar manometers could be read to 3.386 Pa (0.001 inches of mercury). When exposed to the same pressure, the manometers are considered to be in agreement if their readings differ by not more than 10.158 Pa (0.003 inches of mercury). All other pressures were measured by 6894 Pa (1 psi) differential pressure transducers which are quoted as accurate to 0.25 percent of full scale.

RESULTS AND DISCUSSION

In the present closed test section, the basic area distribution through the test section is constant. This distribution is compatible with the slotted test section but results in undesireable longitudinal velocity gradients for the closed test section. While the test section has a moveable floor and ceiling to permit changing the area distribution , these changes in the test section geometry are extremely difficult to accomplish and were not considered feasible for the iterative changes required during the calibration. Therefore, wood fairings were added to the sidewalls of the test section in order to obtain the desired area distribution. Calibration runs were then made and the fairings were modified until an acceptable static pressure distribution was obtained throughout the operating range. The final area distribution of the fairings is presented in figure 3.

The resultant calibration static pressure distribution is shown in figure 4. The associated Mach number distribution is shown in figure 5. An additional iteration on the area distribution could have smoothed out the distribution for the top Mach number run. However, since experience has shown that the maximum Mach number with a normal size model is in the range 0.90 to 0.94, this final iteration was not made. The top Mach number run of figure 5 was omitted in arriving at the tunnel calibration curve. It should be noted that each calibration run presented in figures 4 and 5 represents a unique combination of operating conditions and that the runs at duplicate operating conditions were omitted for clarity. Based on the distributions of figures 4 and 5, the usable test section was judged to lie between stations 185 and 55. The static pressure was averaged over this region and this average was used in obtaining the tunnel calibration curve of figure 6.

The calibration equation which was obtained from a least square fit to the calibration data is:

a) For $\left(\frac{P_I}{H_I}\right) \geq .62474$;

$$\frac{P_1}{P_{T_1}} = .995885\left(\frac{P_I}{H_I}\right) + .004020$$

b) For $\left(\frac{P_I}{H_I}\right) < .62474$;

$$\frac{P_1}{P_{T_1}} = 1.051280\left(\frac{P_I}{H_I}\right) - .030756$$

The nominal power consumption of the tunnel main drive system is shown in figure 7. It should be noted that a Mach number of 0.8 requires approximately 8.1 megawatts for the closed test section. This represents a significant saving in comparison to the approximately 11.5 megawatts required to obtain a Mach number of 0.8 for the slotted test section without boundary layer removal.

The dynamic pressure variation is shown in figure 8 and the Reynolds number variation is presented in figure 9.

The longitudinal gradient in the static pressure distribution of Figure 4 can be interpreted in terms of a buoyancy effect which leads to a buoyancy drag correction. A detailed analysis was performed which separated out the time gradient of the multiplexor from the longitudinal gradient of the pressures. This analysis showed that: (a) in terms of drag coefficient, the buoyancy drag correction is essentially zero in the low Mach number range and in the higher range is less than 0.0001 for models with volume to reference area ratios less than 0.35, and (b) if the buoyancy drag correction became important, for large models at the higher Mach numbers, for example, it would be necessary to survey in the region to be occupied by the model using individual transducers in order to determine the buoyancy correction more accurately. It should be noted that almost all tests conducted in the 7- by 10-foot high speed tunnel involve models with volume to reference area ratios less than 0.35.

PART II - TEST CAPABILITIES

FACILITY DESCRIPTION

The 7- by 10-foot high speed tunnel is a continuous flow subsonic-transonic atmospheric wind tunnel. In the closed test section configuration, the speed range is from very low speed to a speed of approximately M = 0.94 depending on model size.

The test section is 2.007 m (6.584 ft) high and 2.918 m (9.574 ft) wide. The present calibration shows that the usable length is from station 185 to station 55 for a length of 3.302 m (10.833 ft). The mean cross-sectional area of the test section for use in blockage calculations is 5.7717 m^2 (62.1256 ft^2).

The tunnel operates at ambient temperature and pressure and continuously exchanges air with the surrounding atmosphere.

The drive system consists of a motor generator system which powers a 10.5 megawatt (14000 hp) fan motor. The fan motor drives an eighteen blade ducted fan with a diameter of approximately 9.1 m (30 ft). The fan blades are laminated spruce. The fan has a maximum speed of 485 rpm.

FACILITY DIGITAL DATA ACQUISITION, DISPLAY, AND CONTROL SYSTEM

The 7- by 10-foot high speed tunnel is equipped with a digital data acquisition, display, and control system controlled by a dedicated on-site computer. See figure 10. An on-line link to the Langley central computer complex is presently being implemented.

The on-site system presently consists of a Xerox Sigma 3 computer with 49152 words of memory in the central processing unit, an external input/output processor, 4.5 megabytes of rapid access disk, two 9-track tape drives, a card reader, a line printer, a Tektronix 4014 graphics terminal, and a data acquisition unit. The present input capacity of the data acquisition unit is 50 analog channels, 20 digital channels, and 8 tachometer channels. The data acquisition unit also has an output capability sufficient to perform control functions.

Facility Test Capabilities

The 7- by 10-foot high speed tunnel is currently used primarily for fundamental aerodynamic research related to the exploration of new aerodynamic concepts, studies designed to provide improved understanding of flow phenomena required for the development of improved theoretical methods and special experiments to evaluate the range of applicability of advanced theories. However, because of the development over the years of unique test capabilities and equipment for a wide range of static and dynamic testing, the facility is also used periodically for highly specialized tests which would be difficult to perform in other facilities. This wide range of testing capability is illustrated in figures 11 to 40.

A test section schematic is shown in figure 11. The primary model support system is used for the majority of the tests and is referred to as the standard angle of attack sting. This system consists of a vertical strut with a variable pitch angle sting support system which covers an angle range of 24° in the tunnel vertical plane. The model sting is attached to the tunnel sting pod through a variety of knuckles and couplings. The fixed knuckles permit the 24° range to be placed anywhere between a pitch angle of -30° and a pitch angle of 30°. The couplings provide a yaw capability of -15° to 15° and roll capability in 90° increments. The primary model support system actually has two mutually exclusive modes of operation, the pitch mode just described and a translation mode. In the latter mode, the model may be translated vertically from floor to ceiling. The standard angle of attack system is shown in figures 12 to 18 and 32 to 36.

For special tests, models may be mounted on a high angle static stability sting. (See figure 11.) This sting has a computerized controller and provides a pitch capability of -10° to 60° and a roll capability of -180° to 180°. The high angle sting is mounted on the front of the standard sting which is placed in the translation mode. For a selected angle of attack and angle of sideslip, the controller drives the high angle sting to the appropriate pitch and roll angles and translates the standard sting to maintain the model in the center of the test section. The high angle stability sting is shown in figures 19 to 21.

The test section includes a side wall turntable with a pitch rotation capability of 0° to 360° which is available for special tests. (See figure 11.) This system is shown in figures 22 to 24.

It is also possible to mount models on fixed struts as shown in figures 25, 26, and 38.

The facility possesses a complete set of highly specialized dynamic stability test rigs which consist of both special stings and balances. The dynamic stability system also includes its own self-contained computerized data acquisition, display, and control system. For roll stability tests, both a steady state roll rig (see figures 27 and 28) and an oscillatory roll rig (see figures 29 and 30) are available. There is also an oscillatory rig which may be installed for either pitch stability or yaw stability tests (see figure 31).

In addition to these specialized model mounting systems, the facility is also able to perform specialized types of tests. The facility is supplied with high pressure air for use in jet simulation. Powered model testing is made possible by a number of specialized sting-balance arrangements developed for the facility. Powered model installations are illustrated in figures 26, 32 to 35, and 39.

To accomplish specific test objectives, highly specialized model installations may also be made. See figures 37 and 38.

The facility has developed a laser velocimeter system for flow field velocity measurements. This system utilizes a 10 watt Argon ion laser. The flow is seeded with kerosene smoke composed of nominal 1 micron particles. See figures 13, 37(b), and 41.

A variety of flow visualization methods are available for use either alone or in conjunction with other test methods. Classical methods such as tufts and fluorescent oil are used to visualize surface flows. The laser from the laser velocimeter has also been used with different optics to throw a light sheet across the test section. Heavy seeding with kerosene smoke then permits the visualization of complex three dimensional flow fields. See figure 42.

It should be emphasized that, since this facility is used primarily for static stability and control studies and for basic research to support analytical development, the simple model installations of figures 12, 15, and 17 are typical of the majority of tests. The other model installations shown, which represent only a small percentage of the tests, serve to illustrate the flexibility inherent in the facility. The more complicated installations involve considerable setup time, may require extensive calibrations after installation, and consume large blocks of tunnel occupancy time.

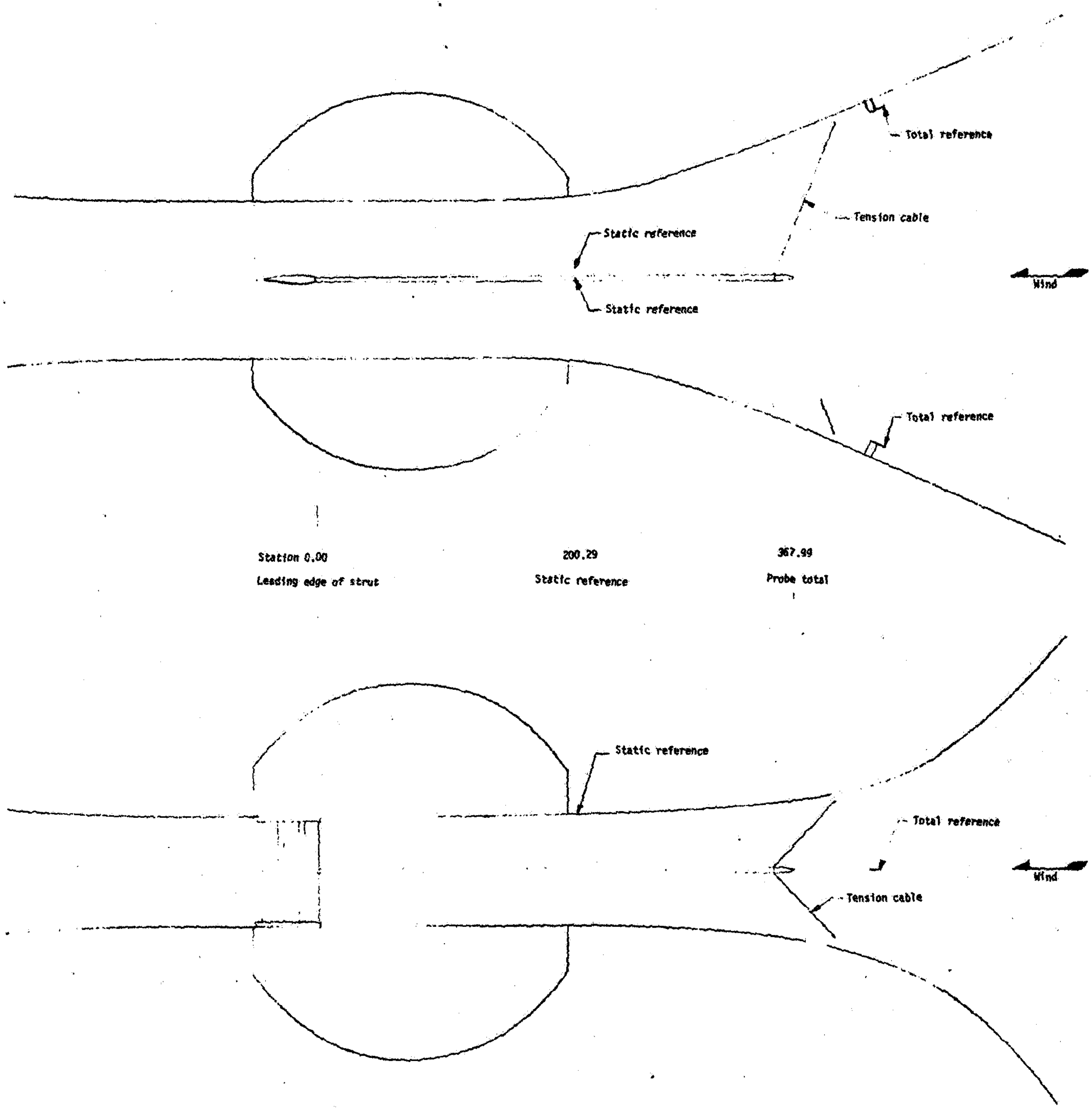

Figure 1. Drawing of the test section of the 7- by 10-foot high speed tunnel showing the calibration probe installation.

ORIGINAL PAGE IS
OF POOR QUALITY

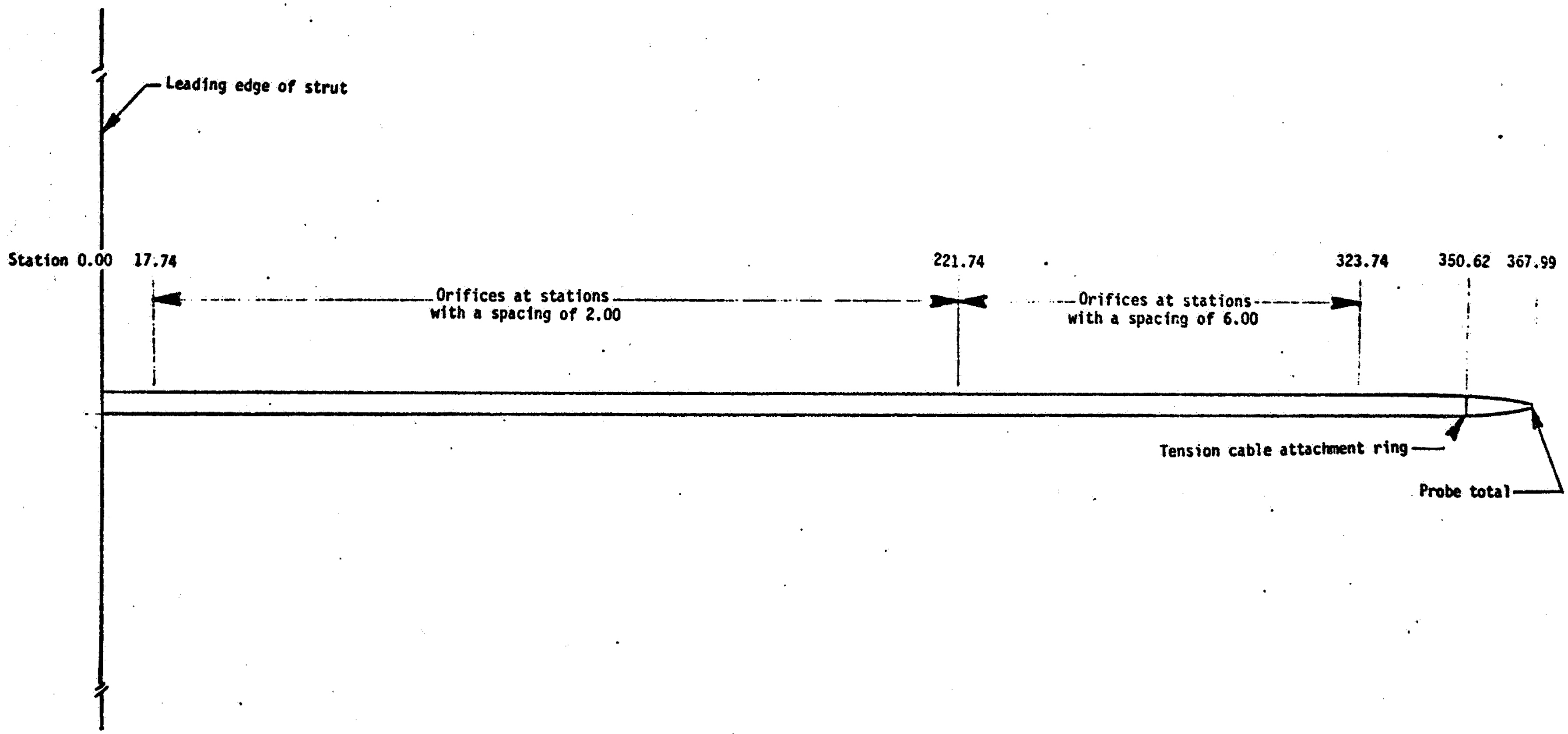

Figure 2. Details of the calibration probe. The constant section has a diameter of 7.62 cm. (3.00 in.)

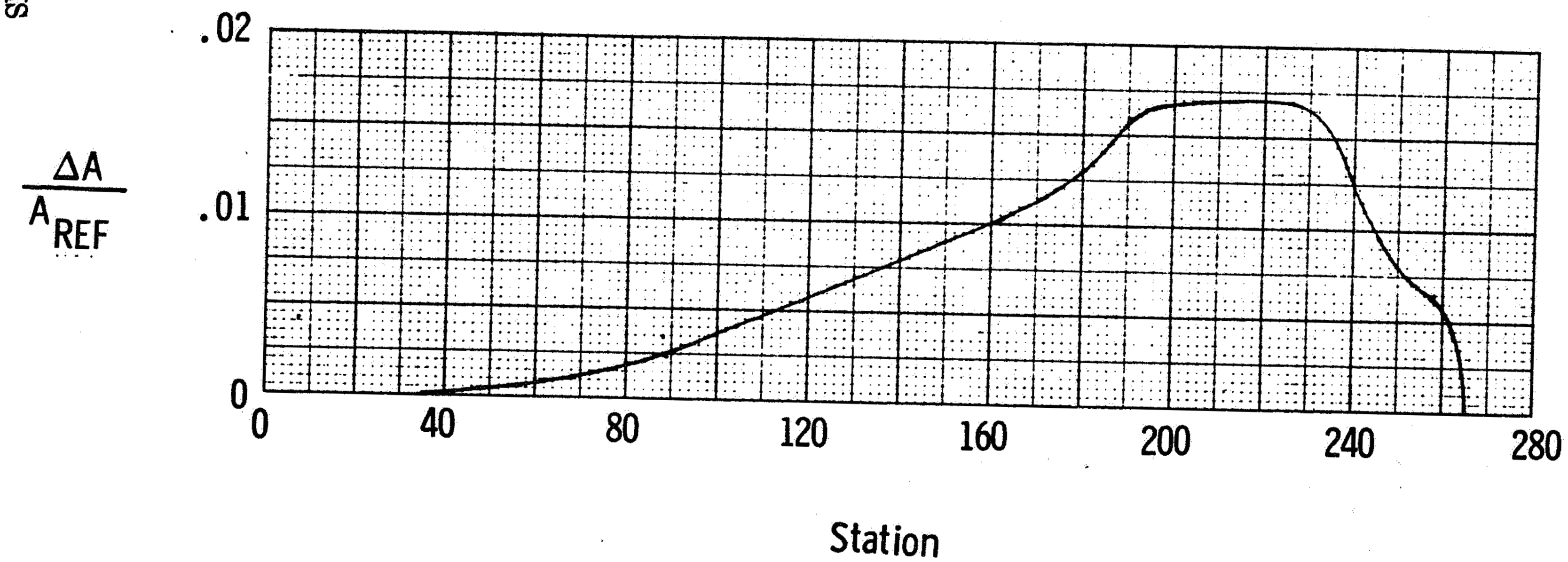

Figure 3. The area distribution of the fairings added to the tunnel walls. The basic test section starts at Station 200 and has a constant cross sectional area, A_{REF}, of 5.8065 m^2 (62.5006 ft^2).

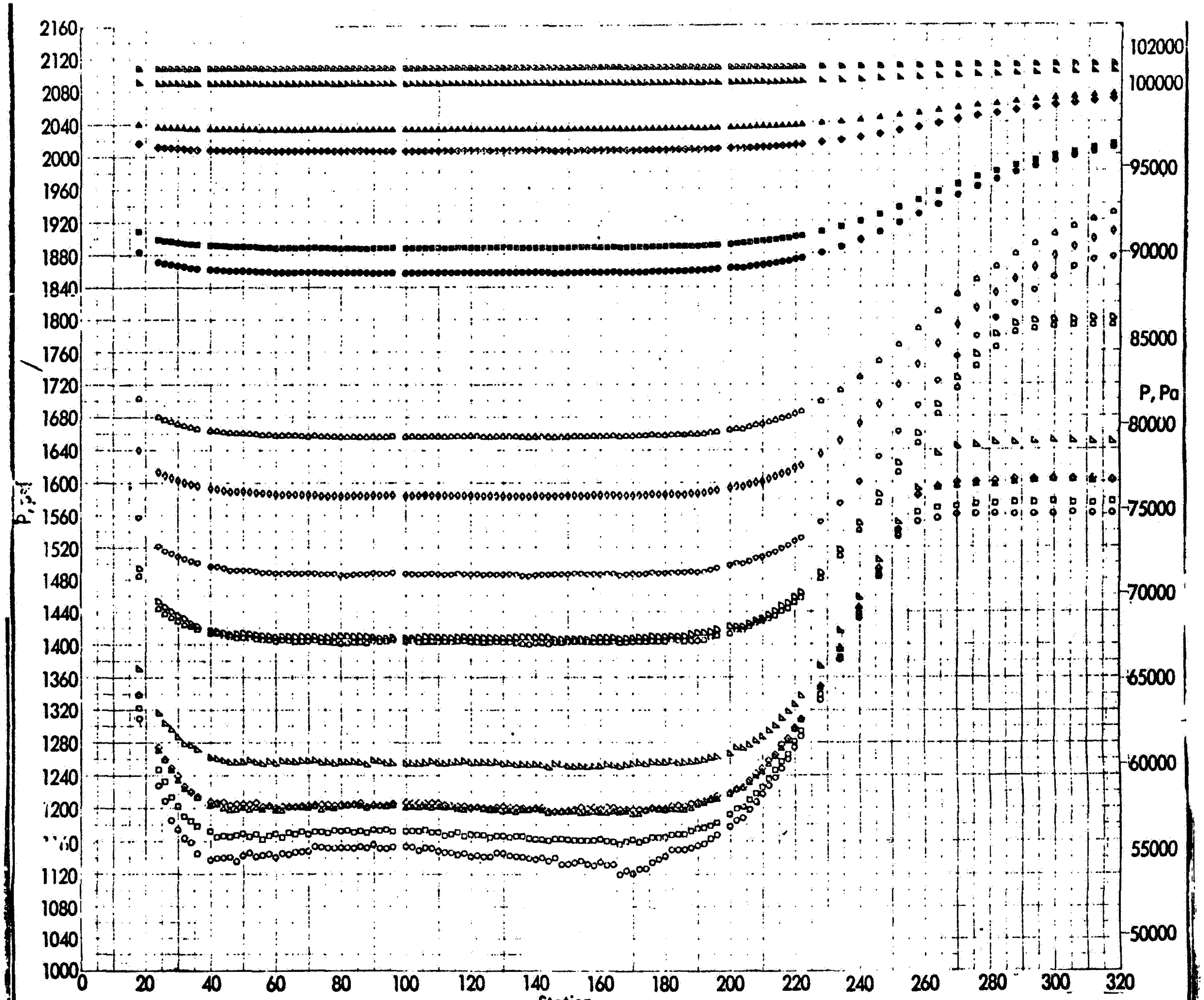

Figure 4. - Static pressure distribution. The usable test section is from station 185 to station 55.

16

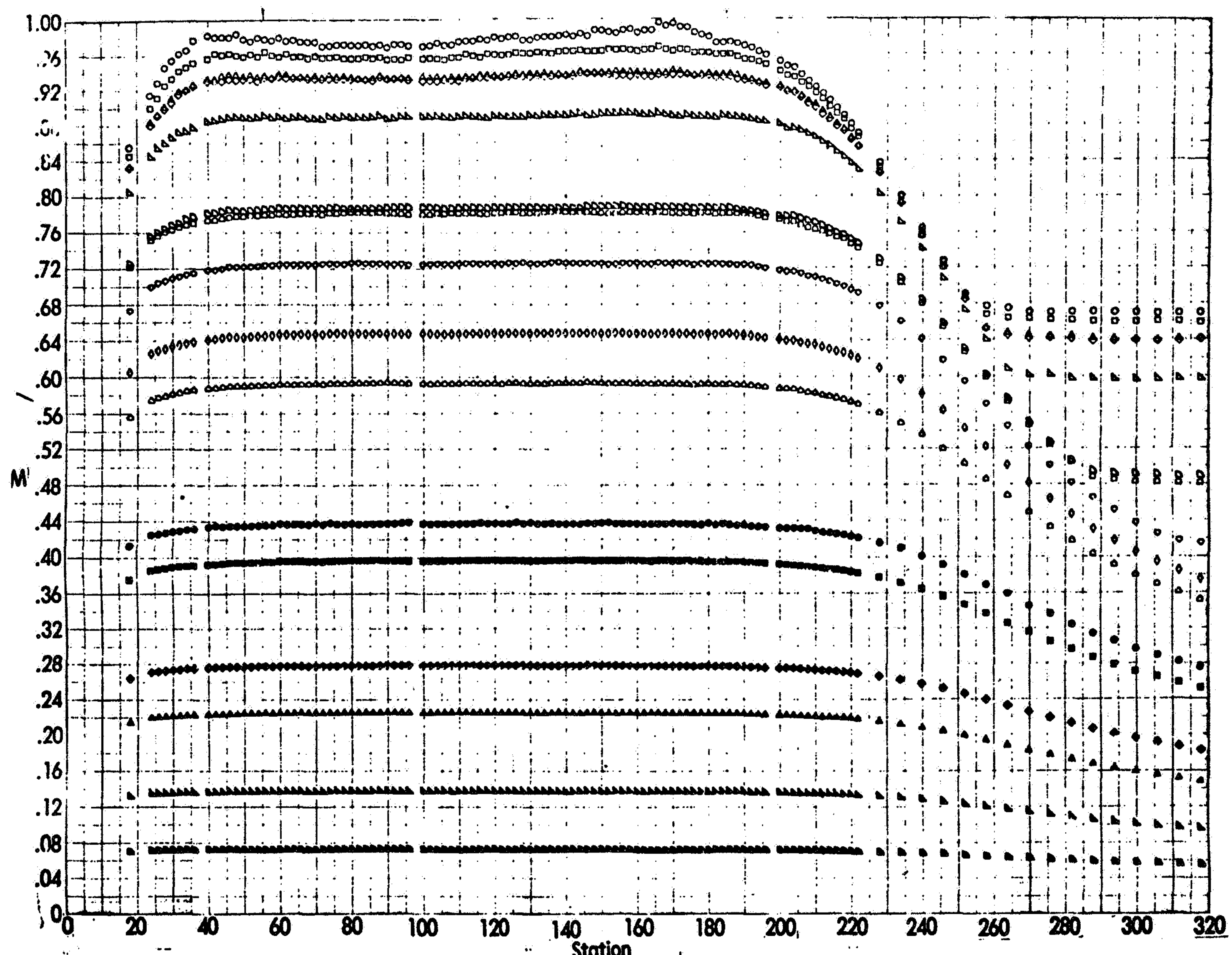

Figure 5.- Mach number distributions. The usable test section is from station 185 to station 55.

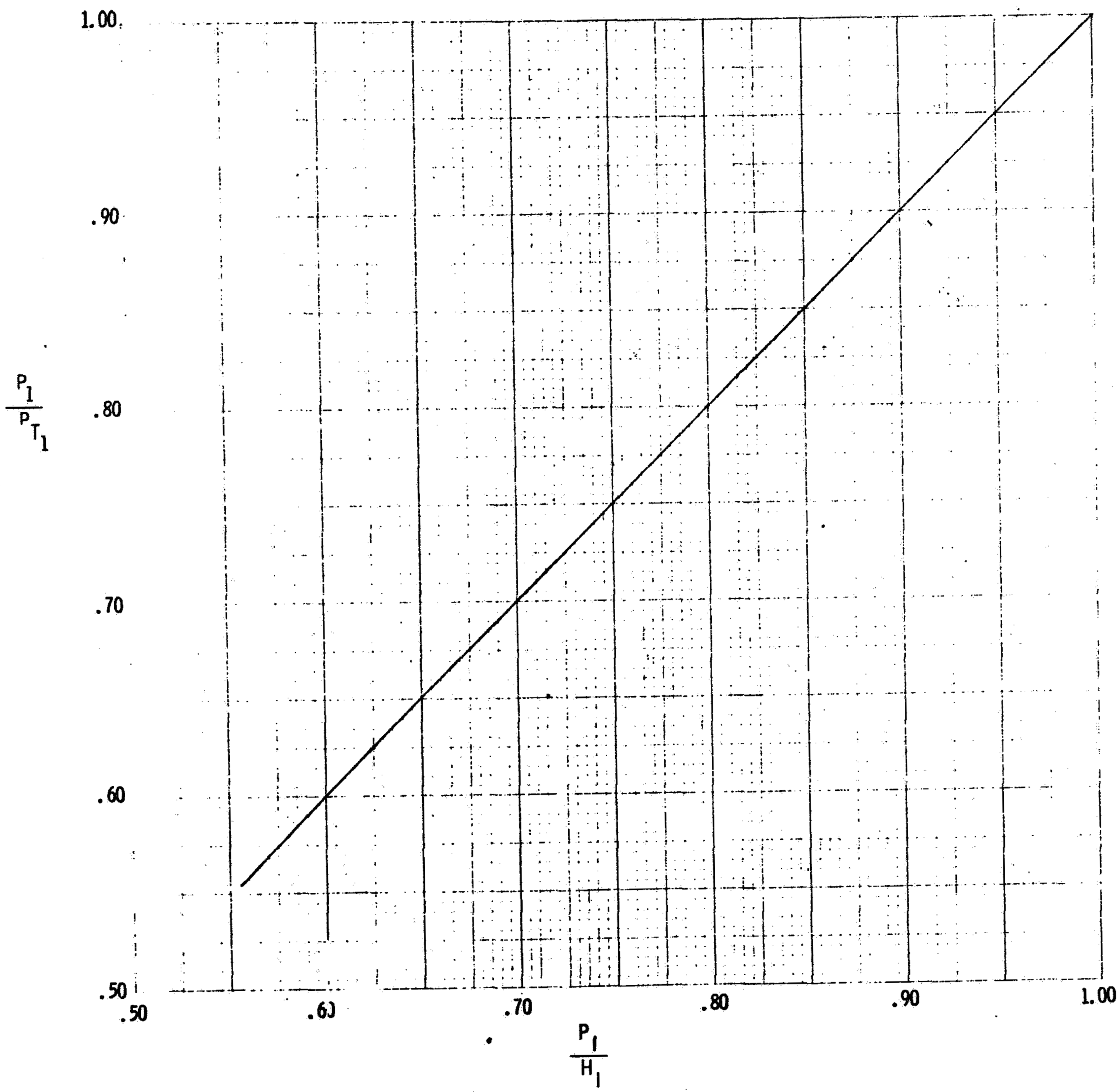

Figure 6. Tunnel calibration curve.

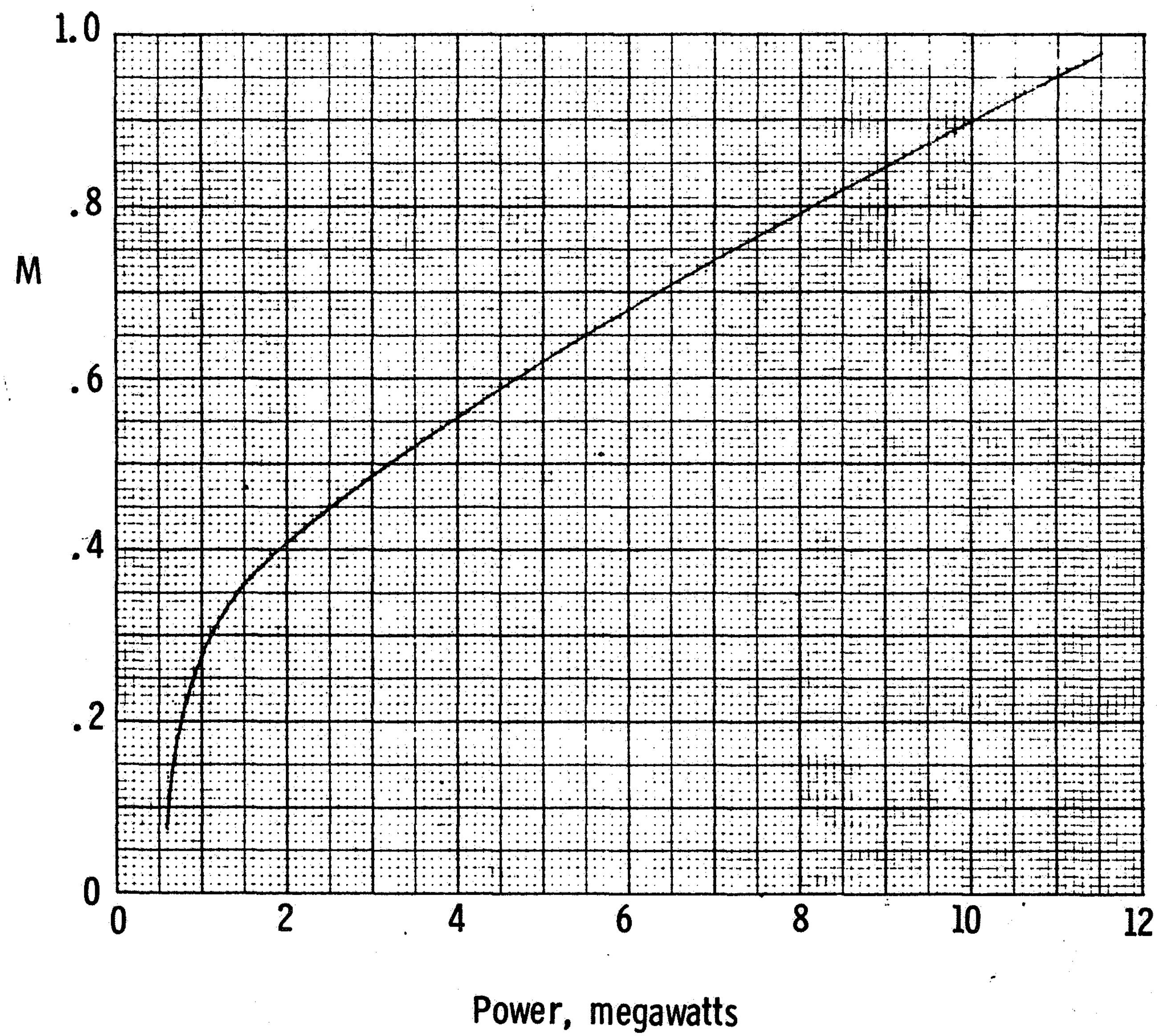

Figure 7. Nominal power consumption of the tunnel main drive system.

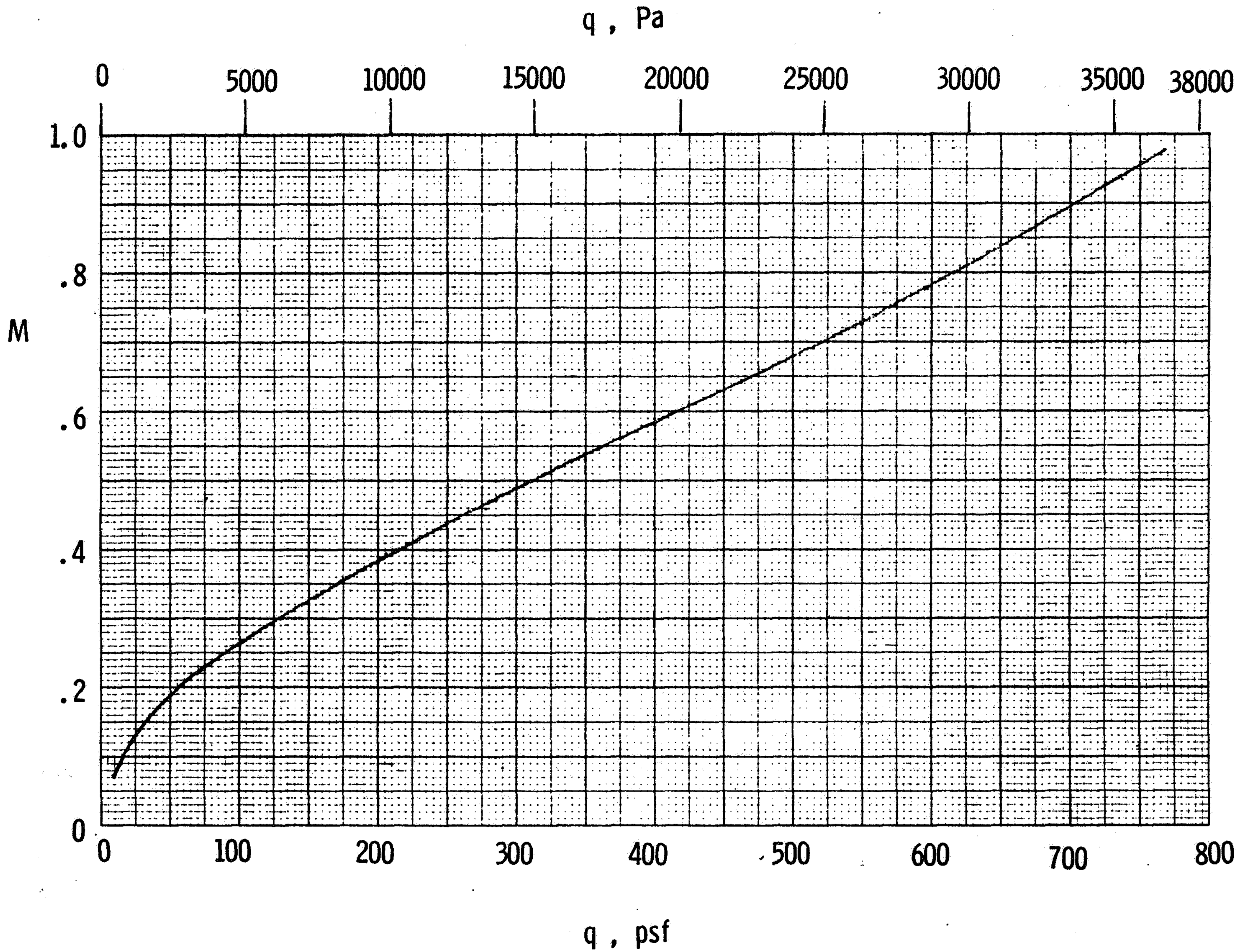

Figure 8. Nominal dynamic pressure variation.

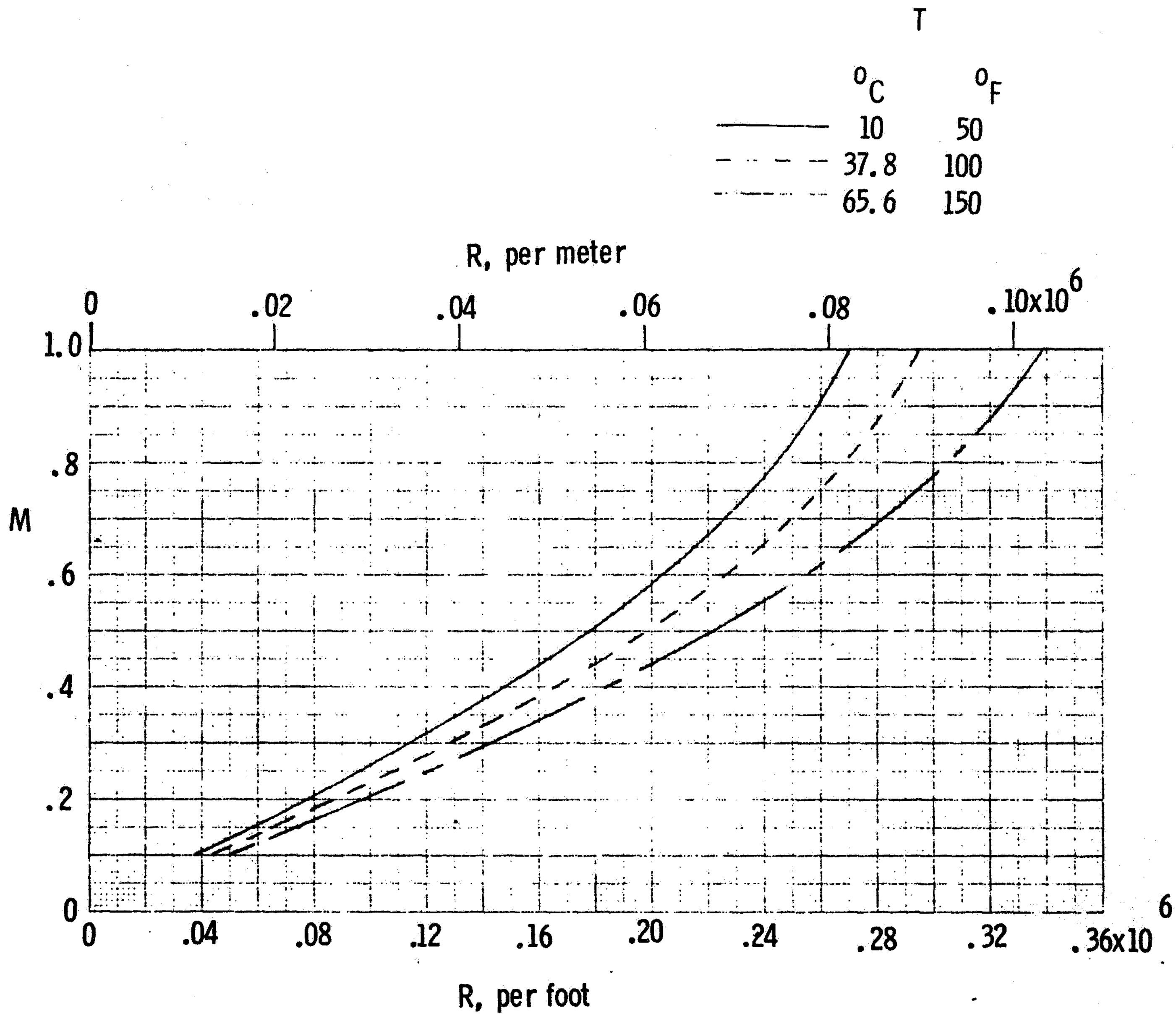

Figure 9. Nominal Reynolds number variation.

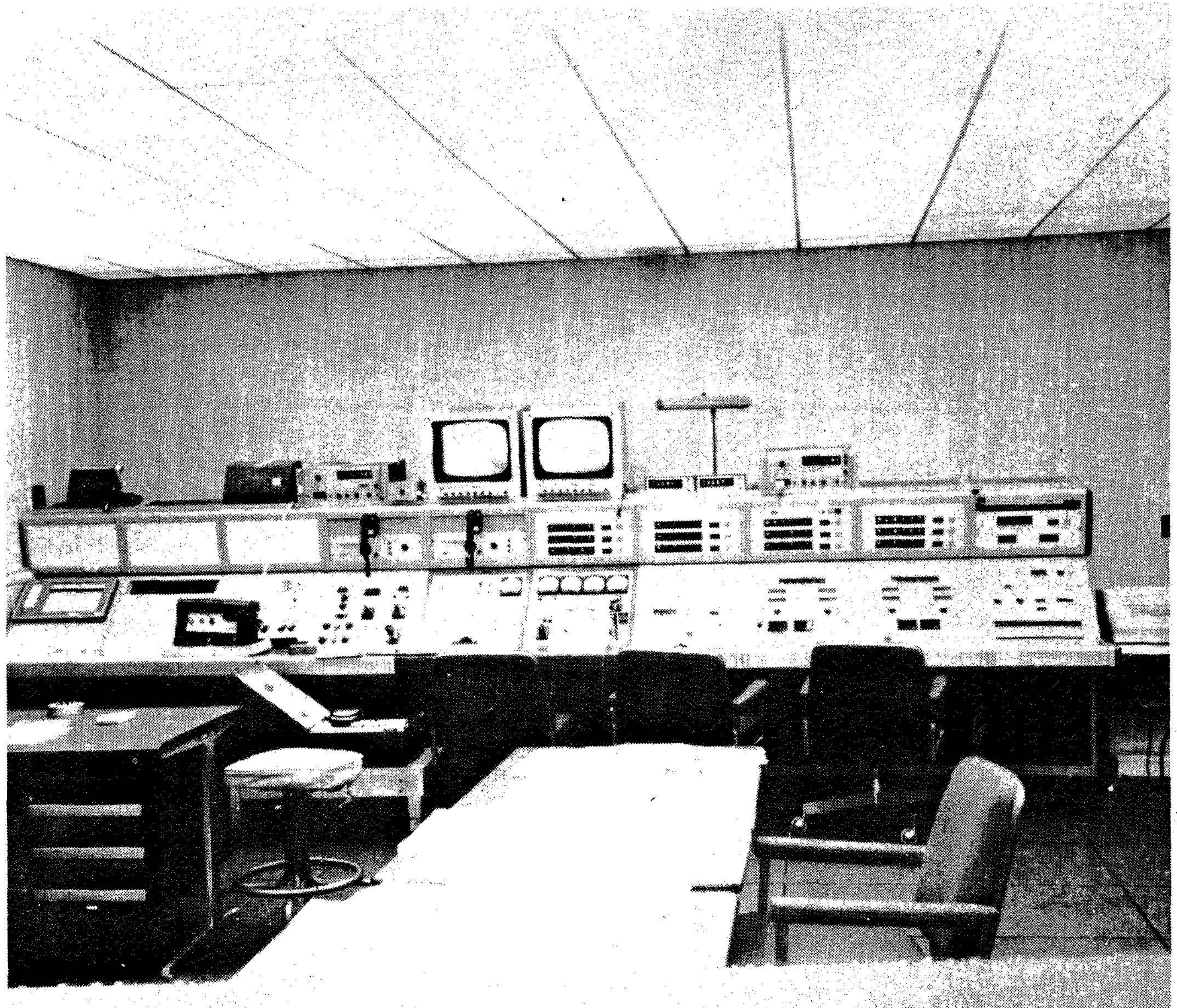

Figure 10. The data acquisition, display, and control system.

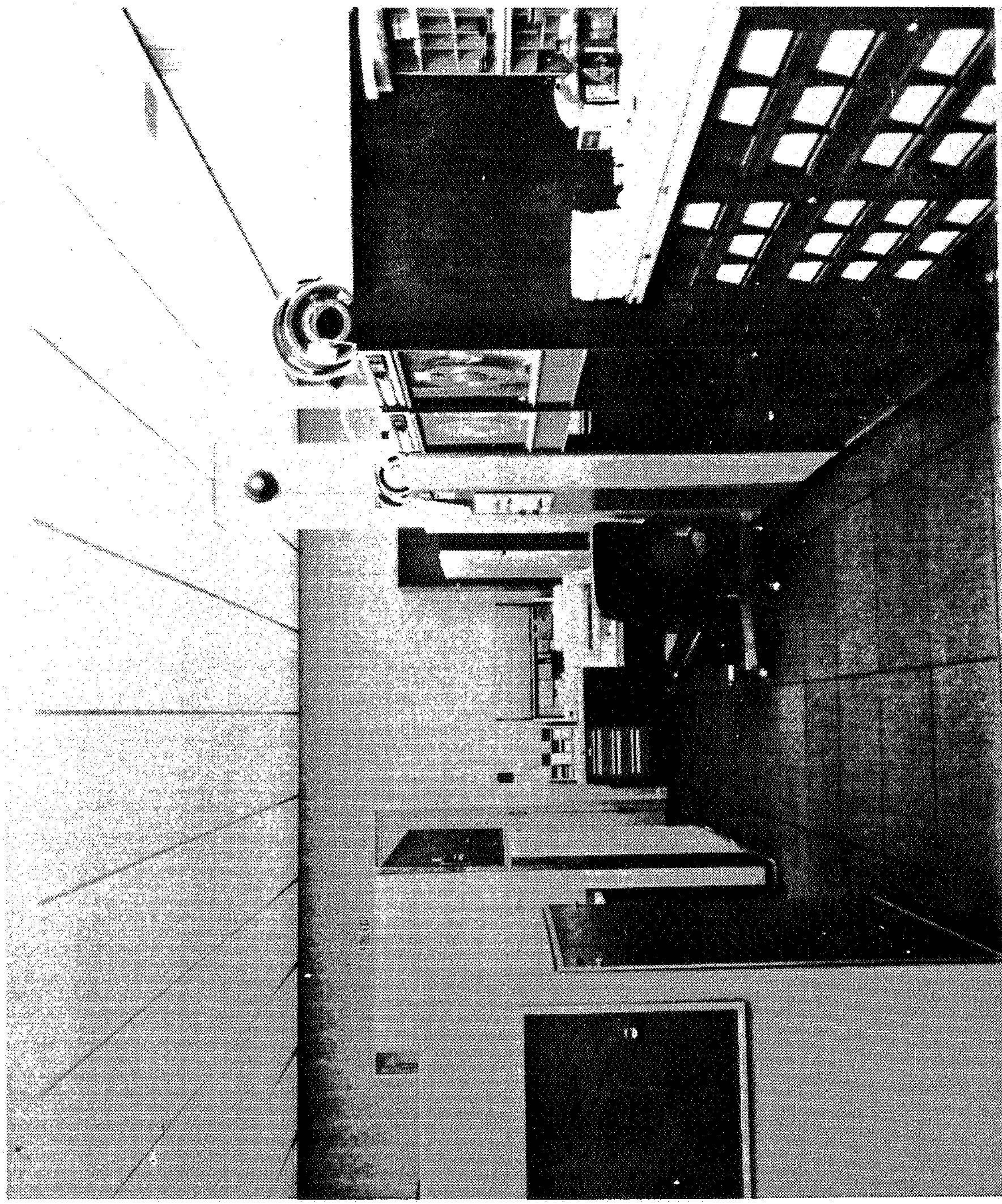

Figure 10. Continued.

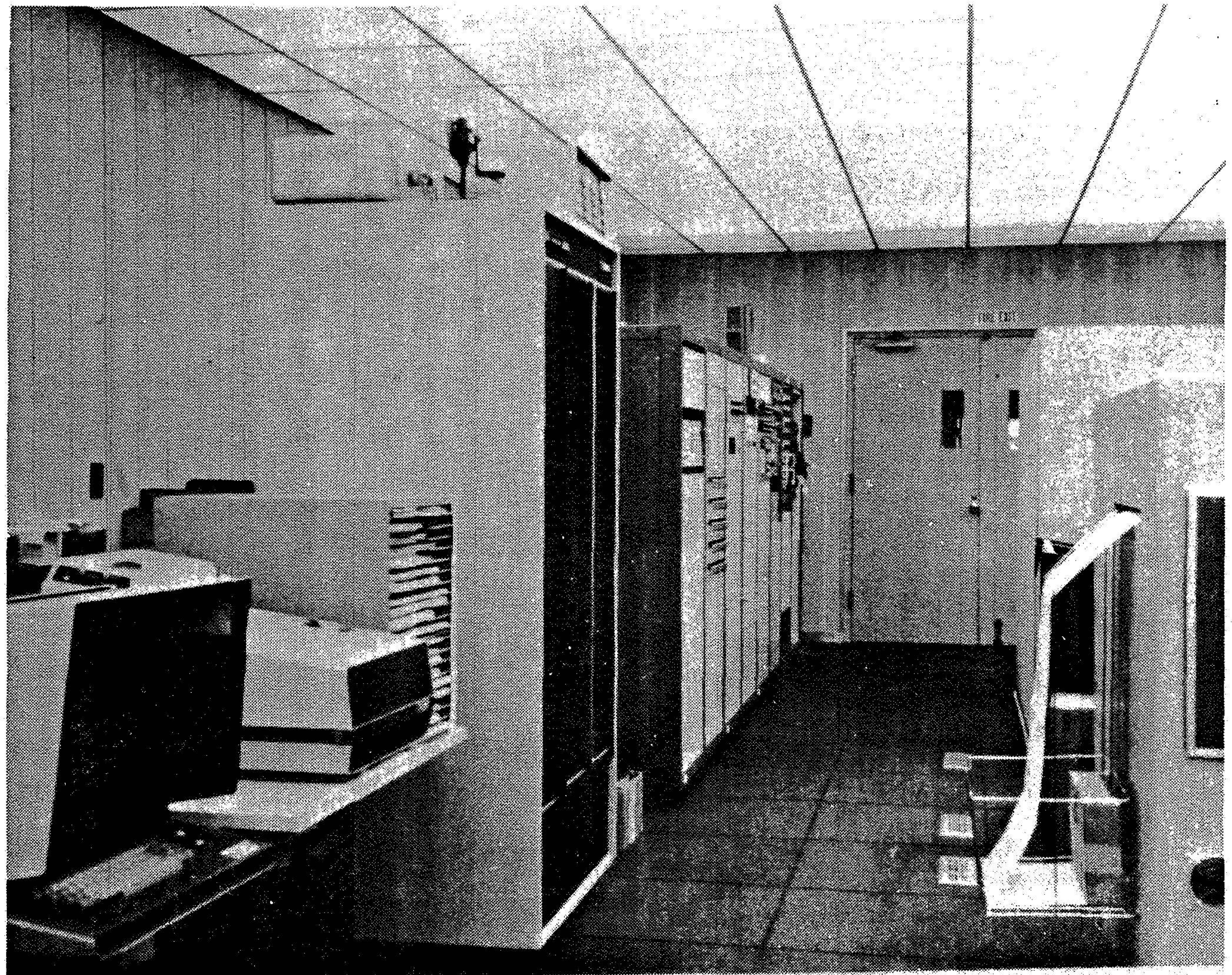

Figure 10. Concluded.

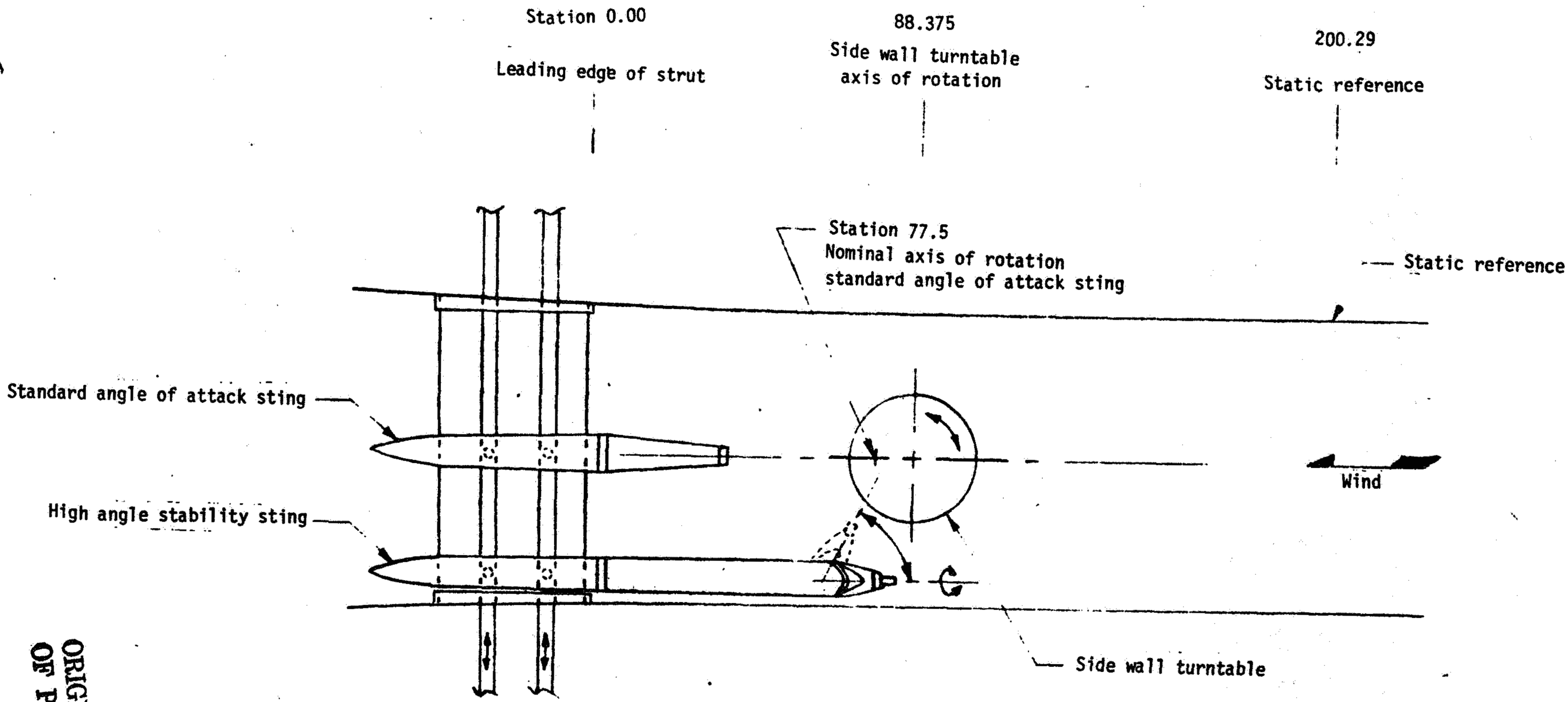

Figure 11. Details of static test setups. Vertical sliders can drive main sting pod in either translation or rotation mode.

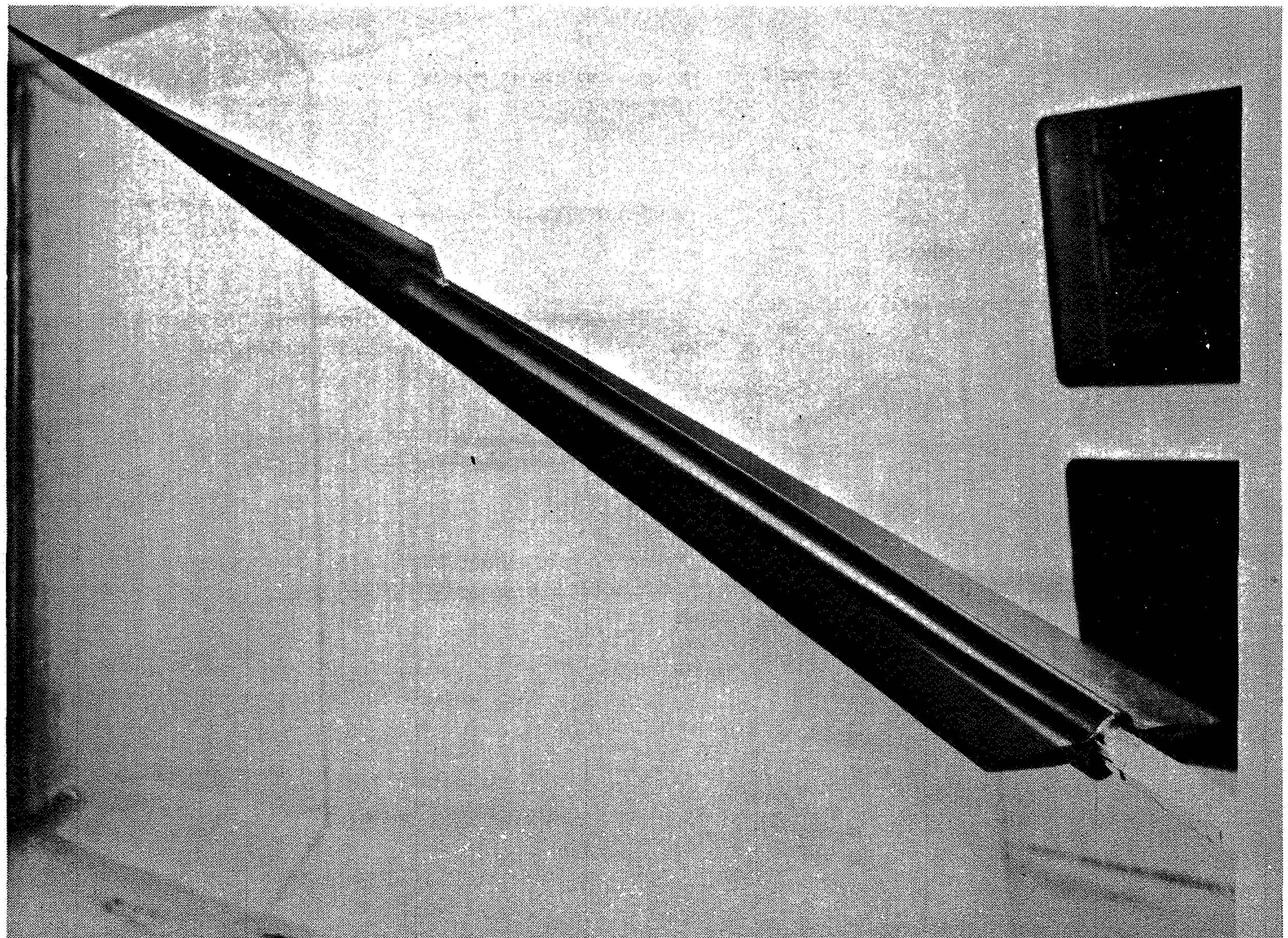

Figure 12. Force models used for theory verification mounted on the standard angle of attack sting.

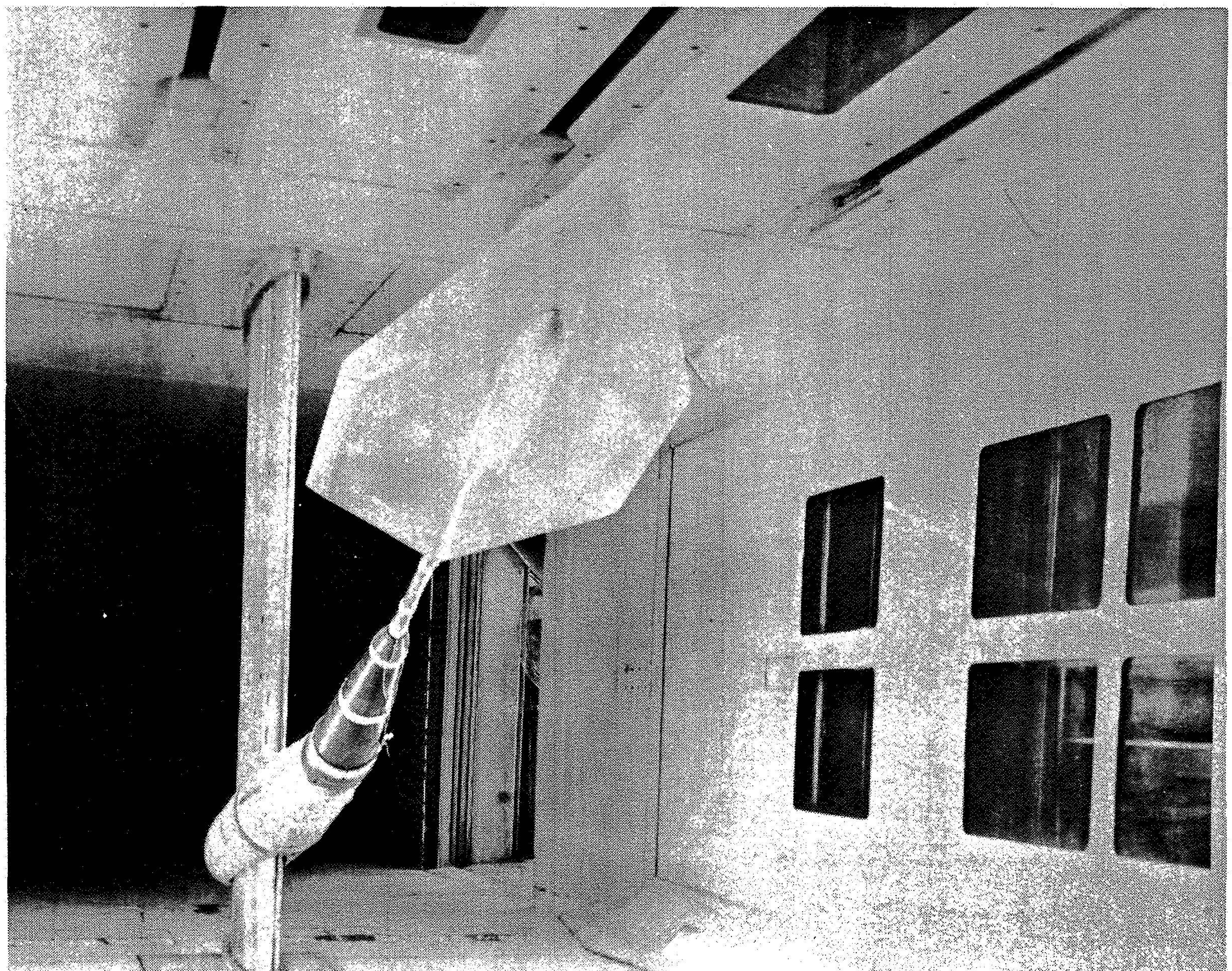

Figure 12. Continued.

ORIGINAL PAGE IS
OF POOR QUALITY

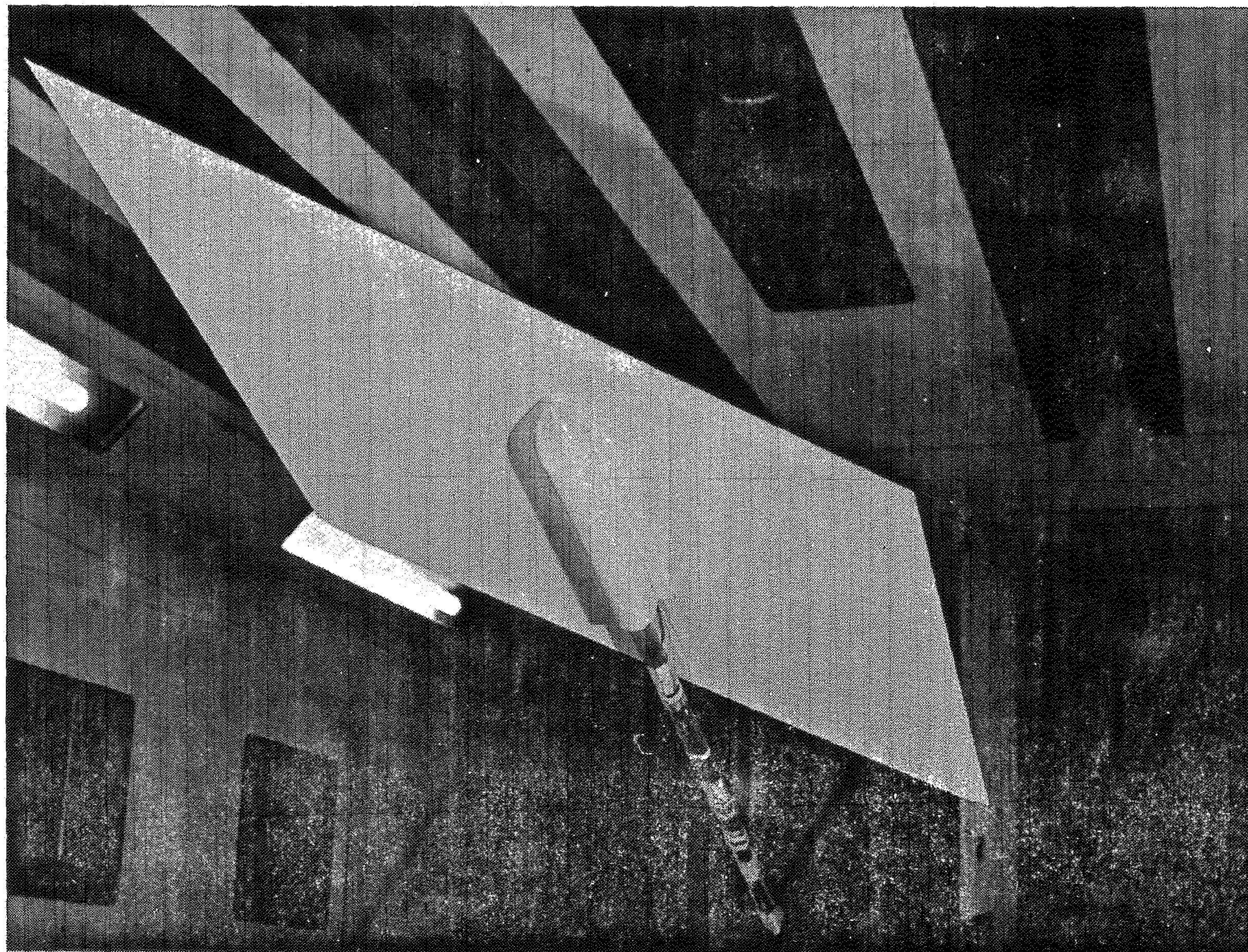

Figure 12. Continued.

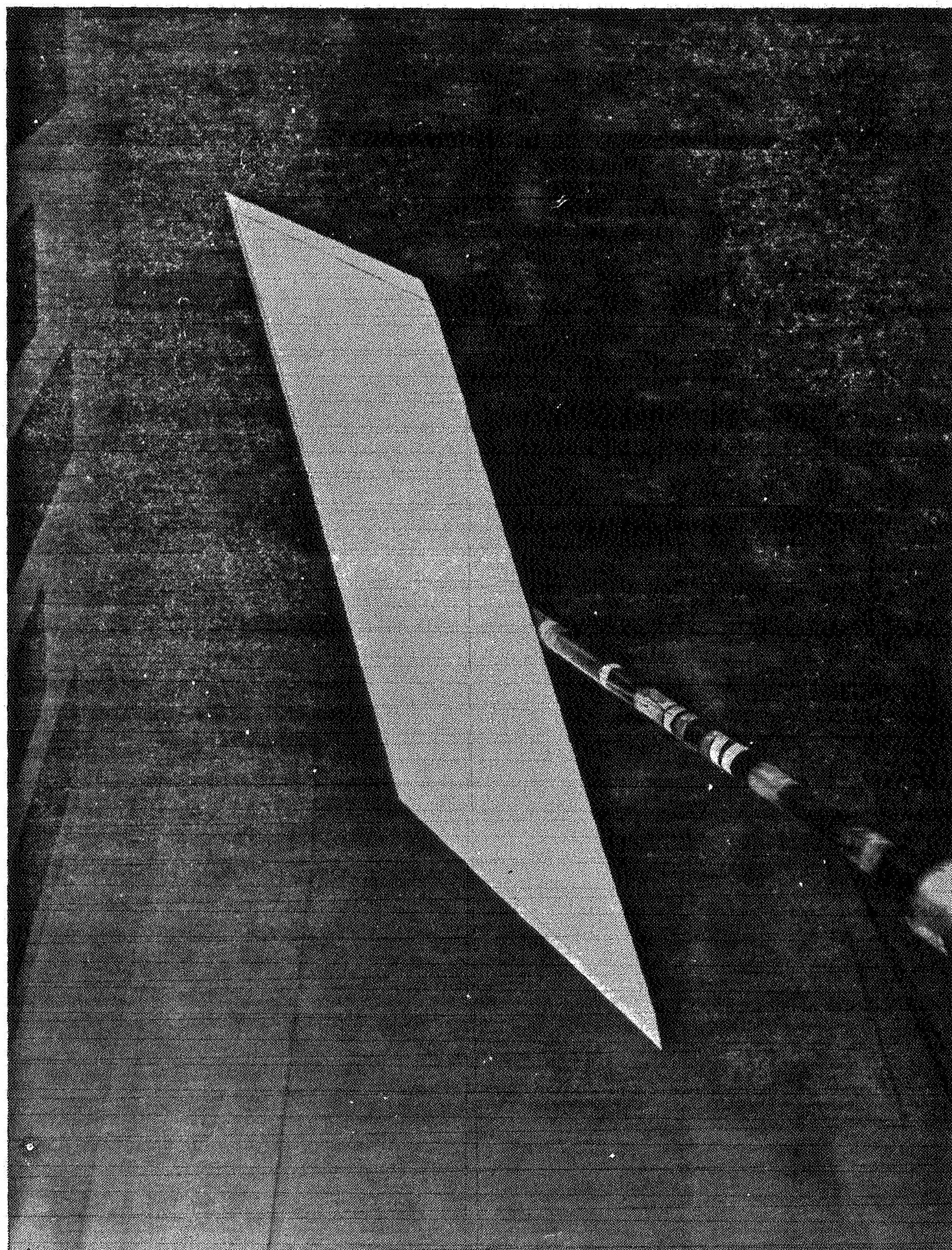

Figure 12. Continued.

ORIGINAL PAGE IS
OF POOR QUALITY

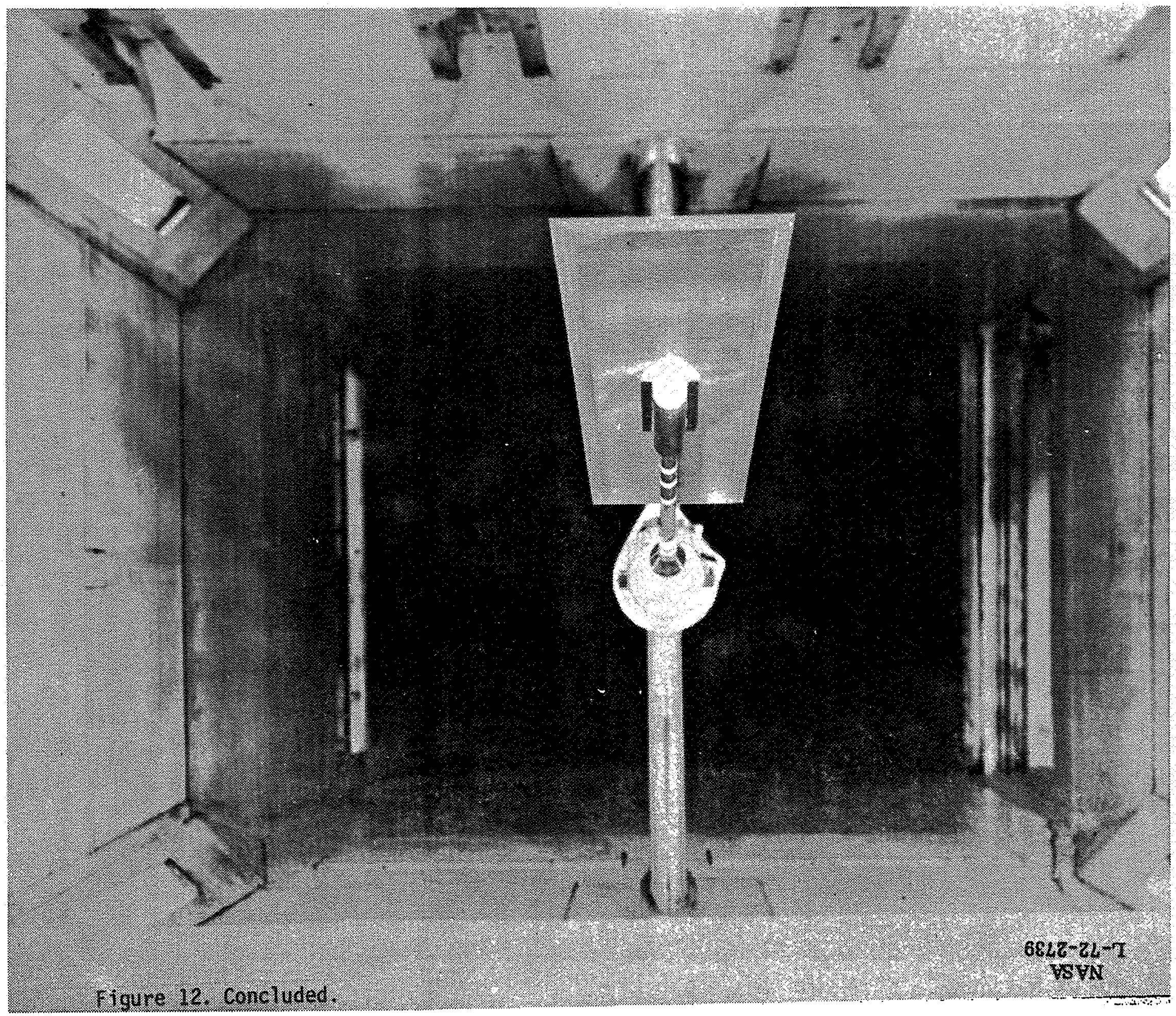

Figure 12. Concluded.

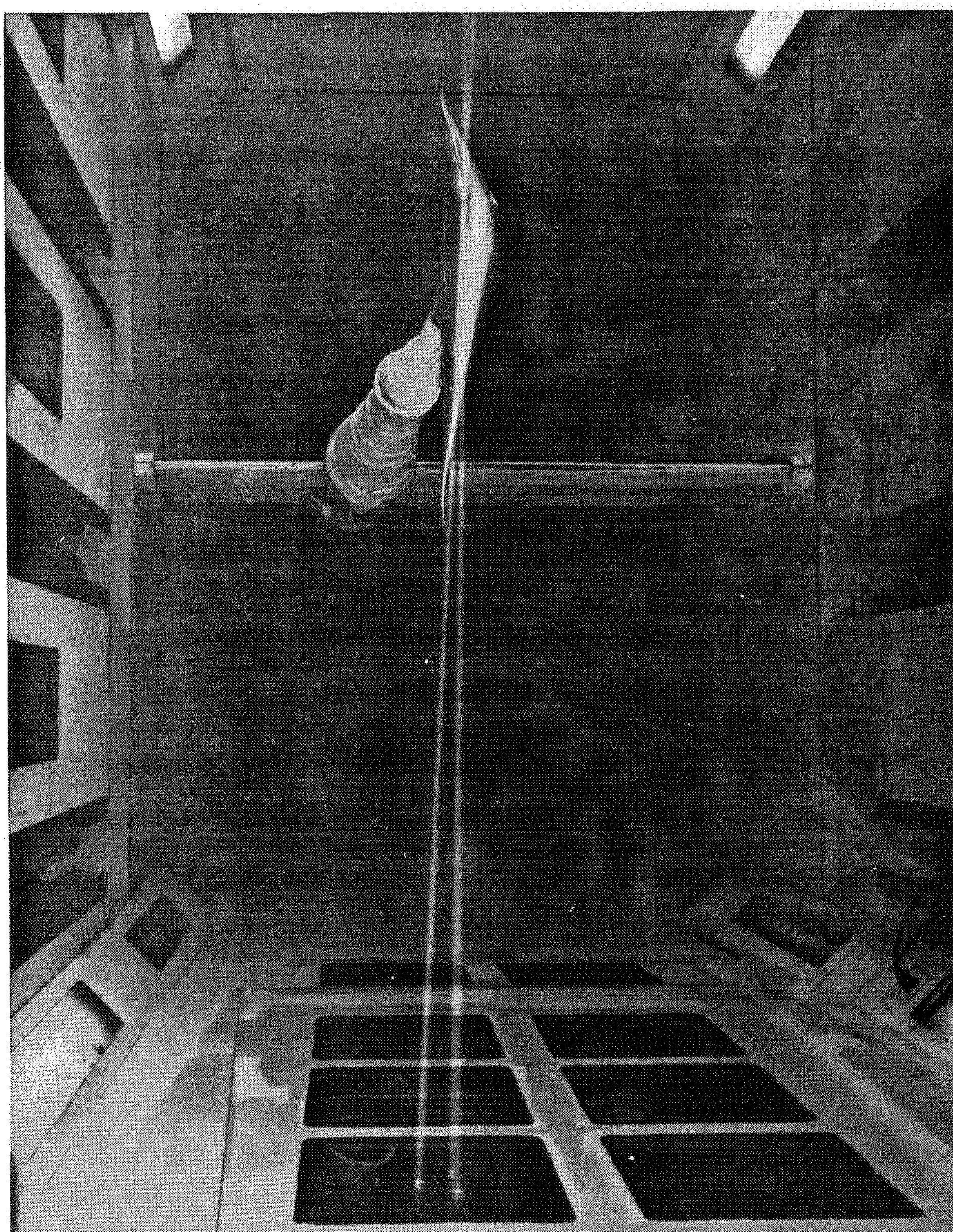

Figure 13. A force and pressure model mounted on the standard angle of attack sting. The light beams of the laser velocimeter are shown.

L-76-4552

ORIGINAL PAGE IS
OF POOR QUALITY

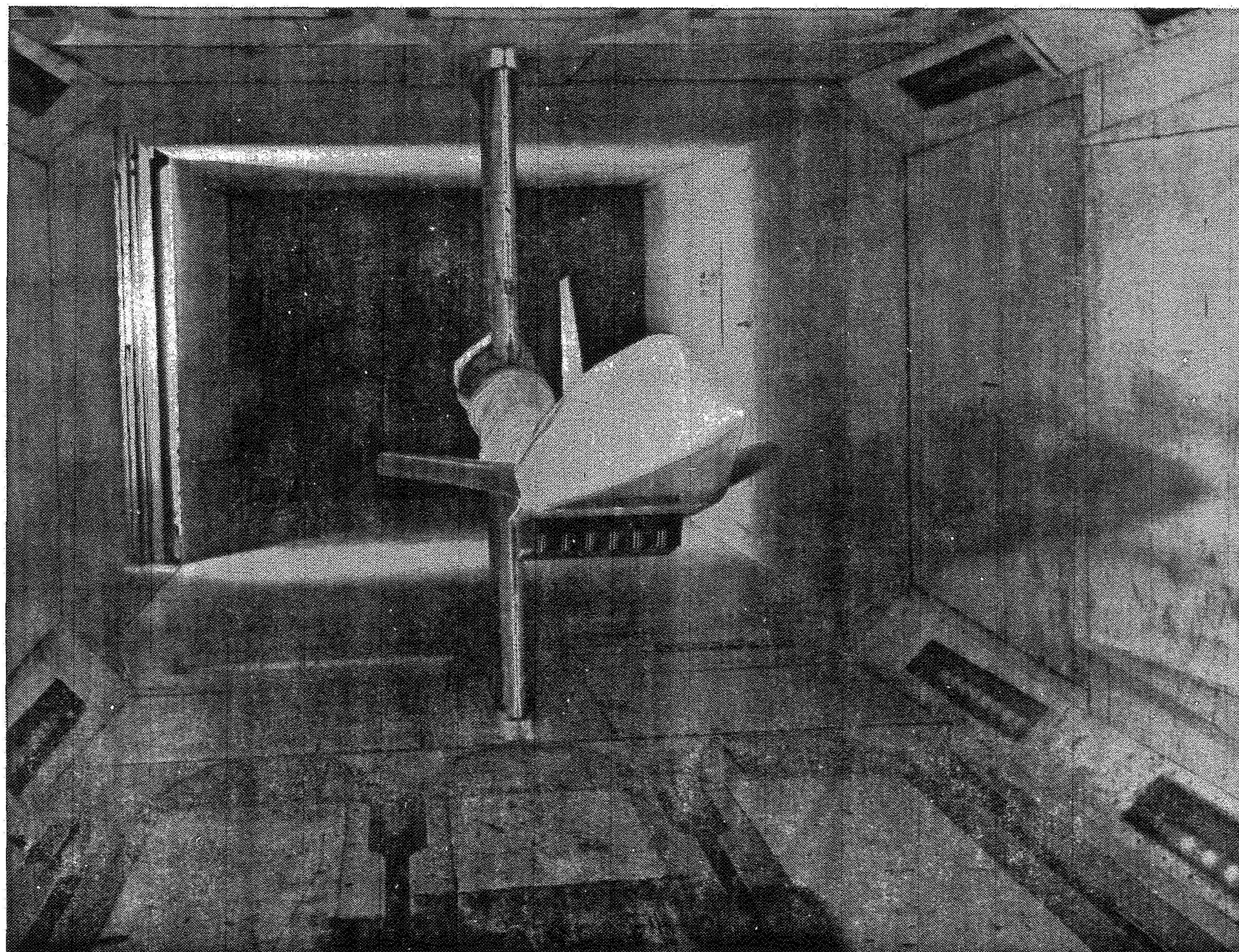

Figure 14. A force and pressure model with an unpowered flow through engine pack mounted on the standard angle of attack sting.

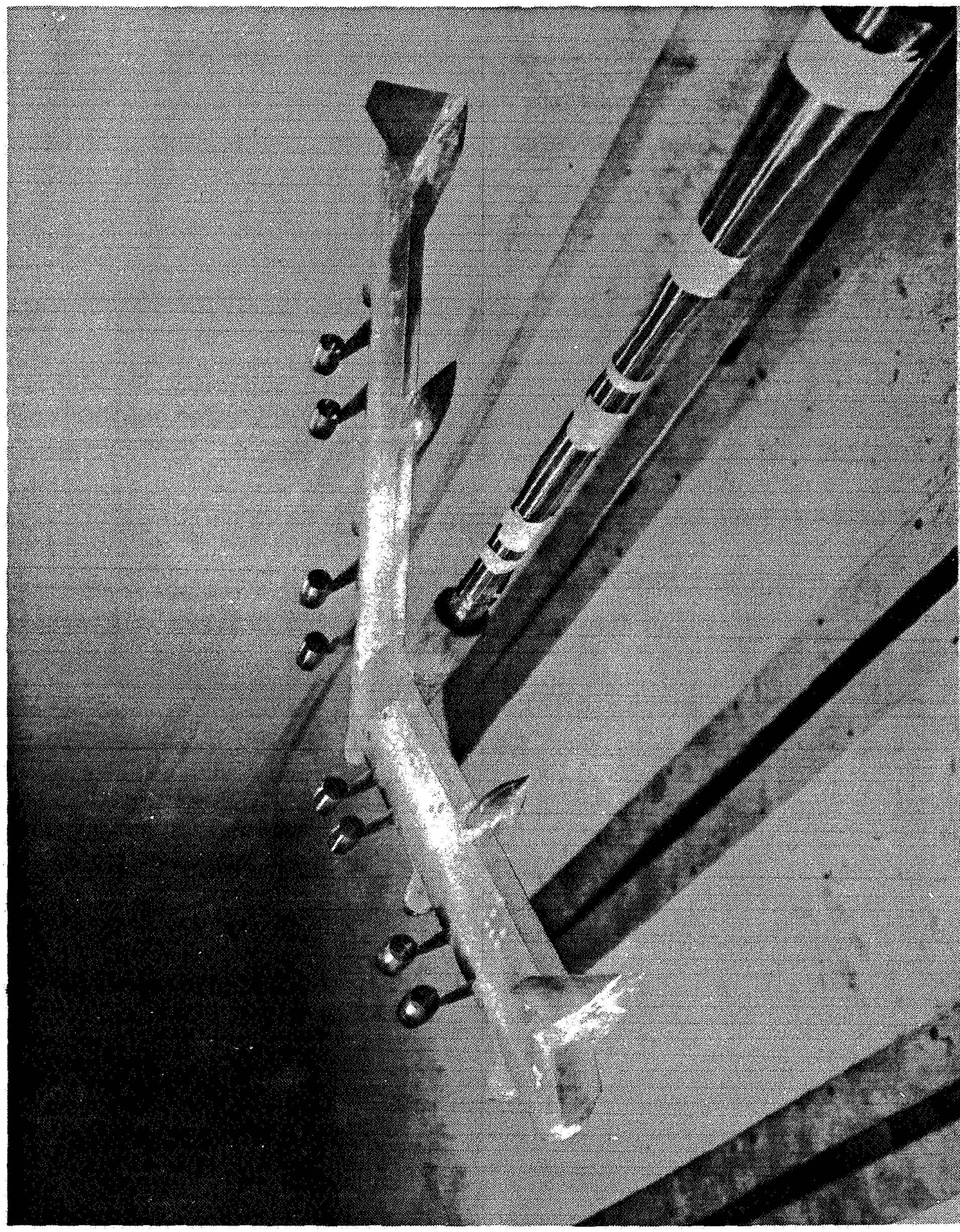

Figure 15. A force model mounted on the standard angle of attack sting.

ORIGINAL PAGE IS
OF POOR QUALITY

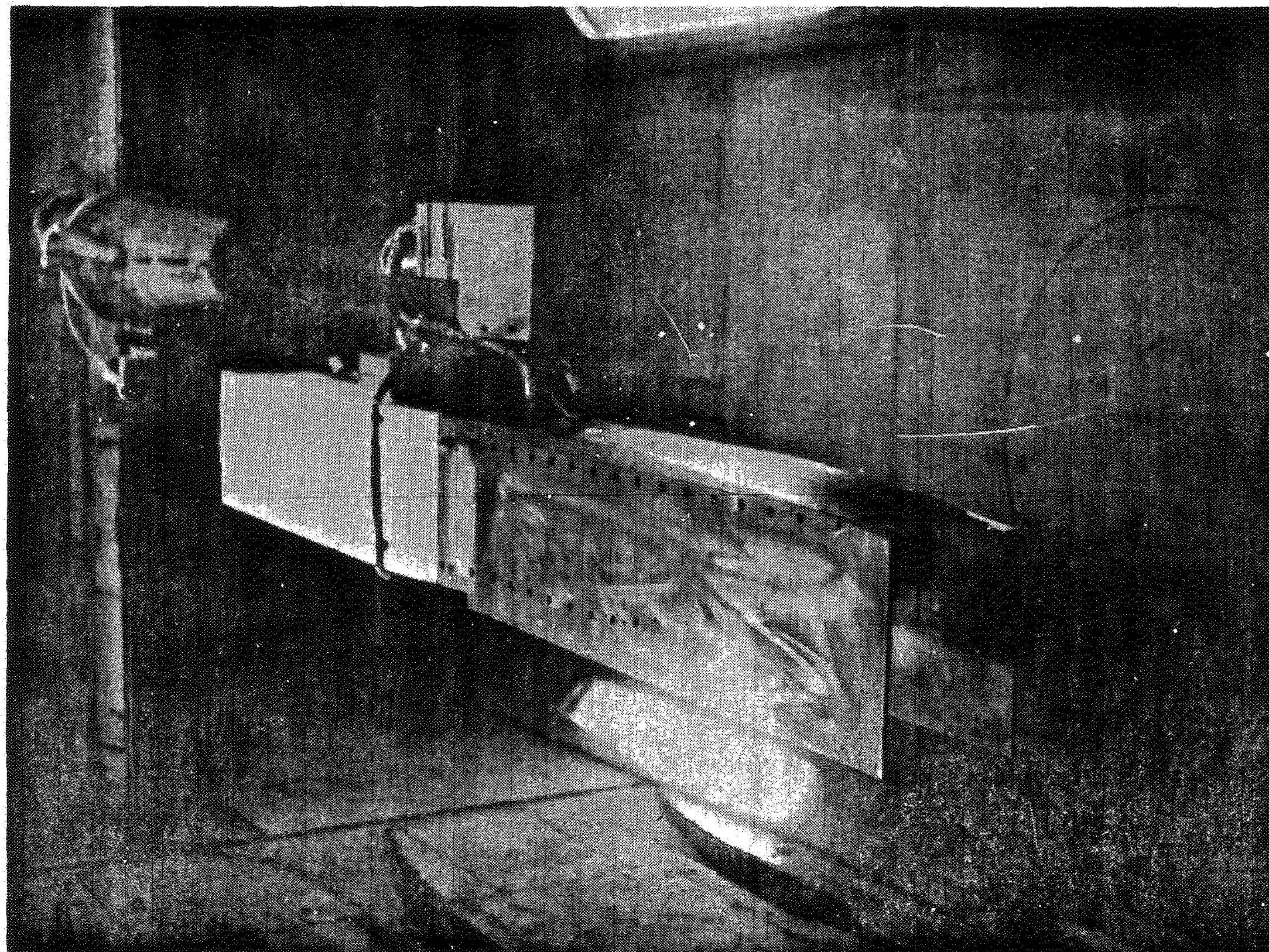

Figure 16. A pressure model on a special mount on the standard angle of attack sting.

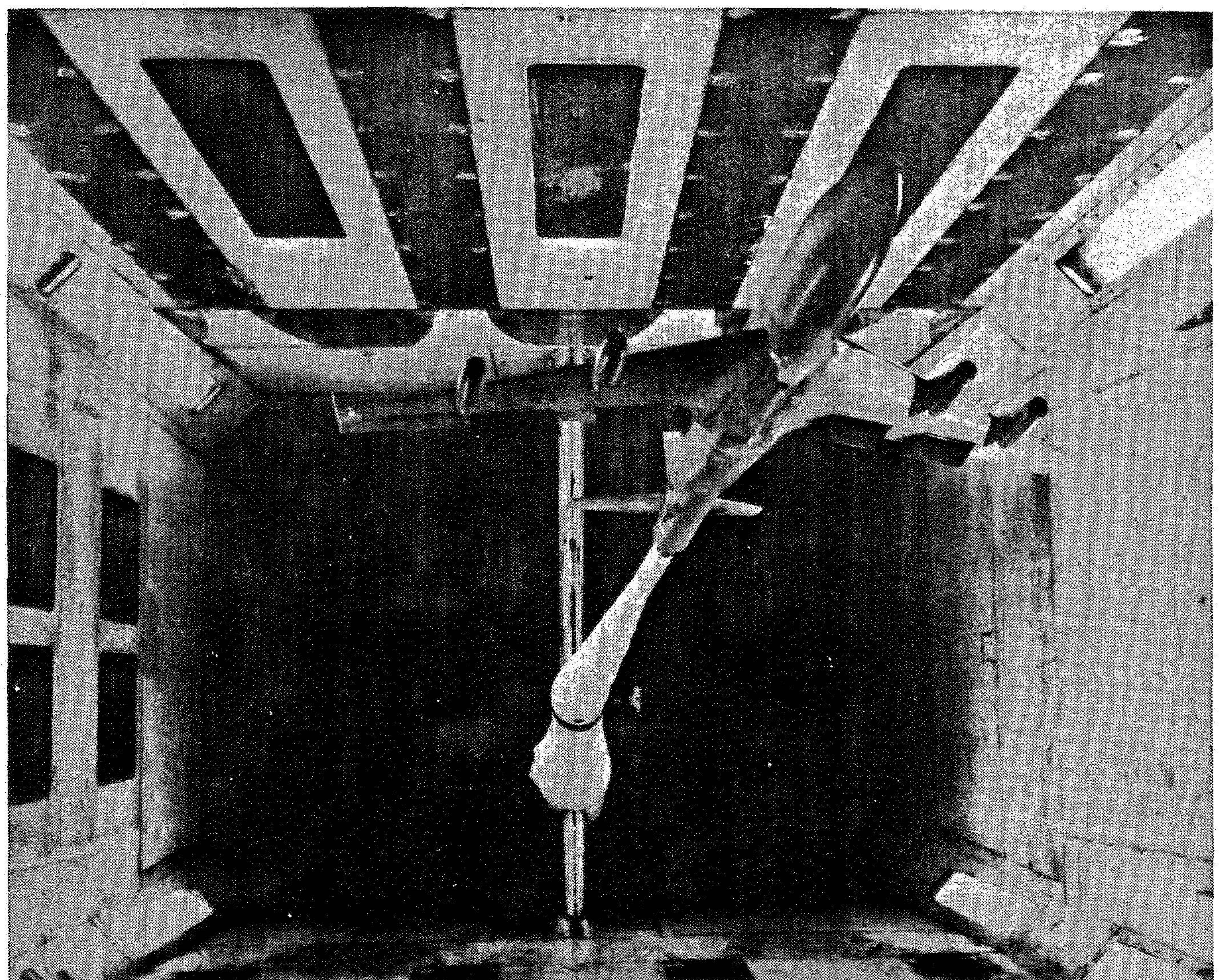

(a) Front view

Figure 17. A force and pressure model mounted on the standard angle of attack sting with a yaw coupling to obtain sideslip data.

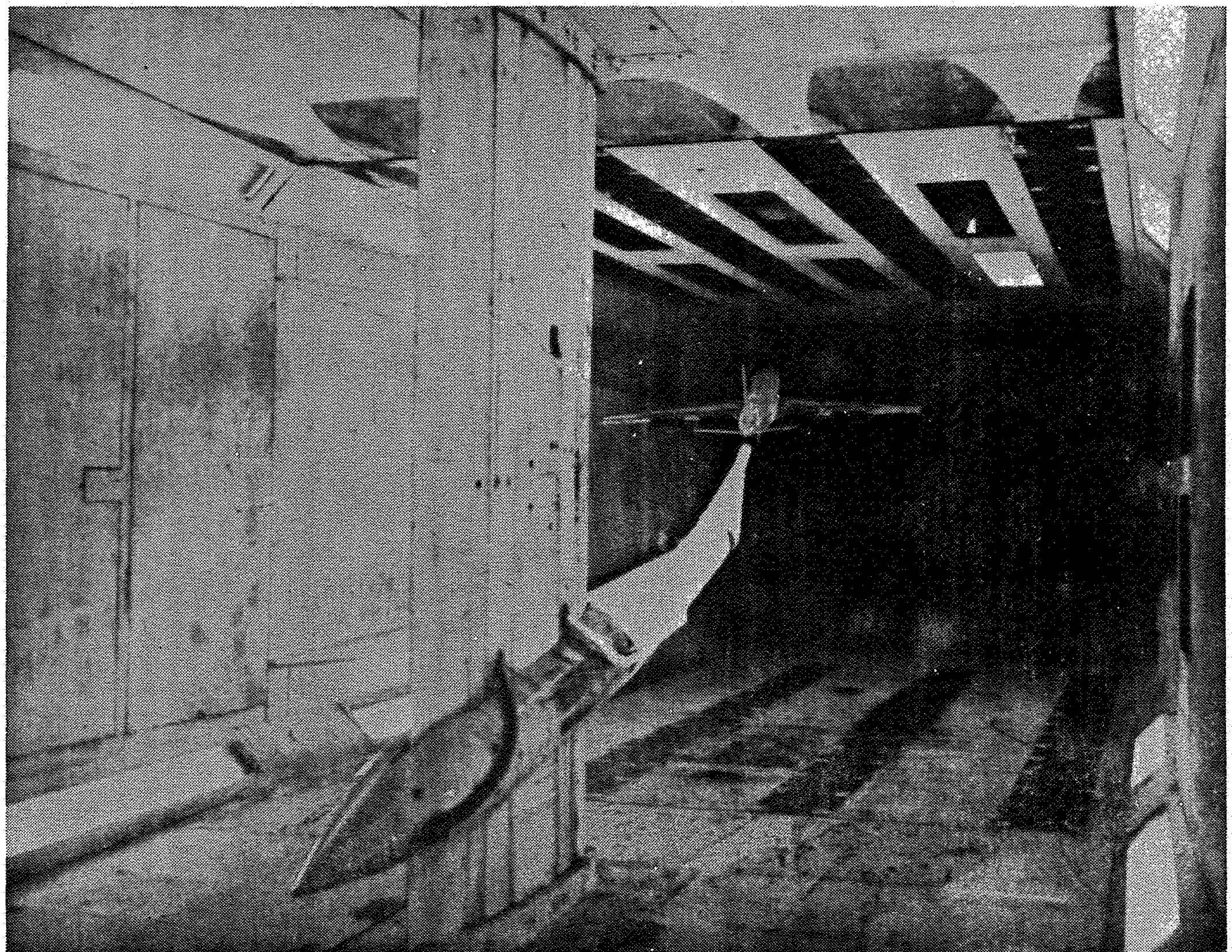

(b) Rear view

Figure 17. Concluded.

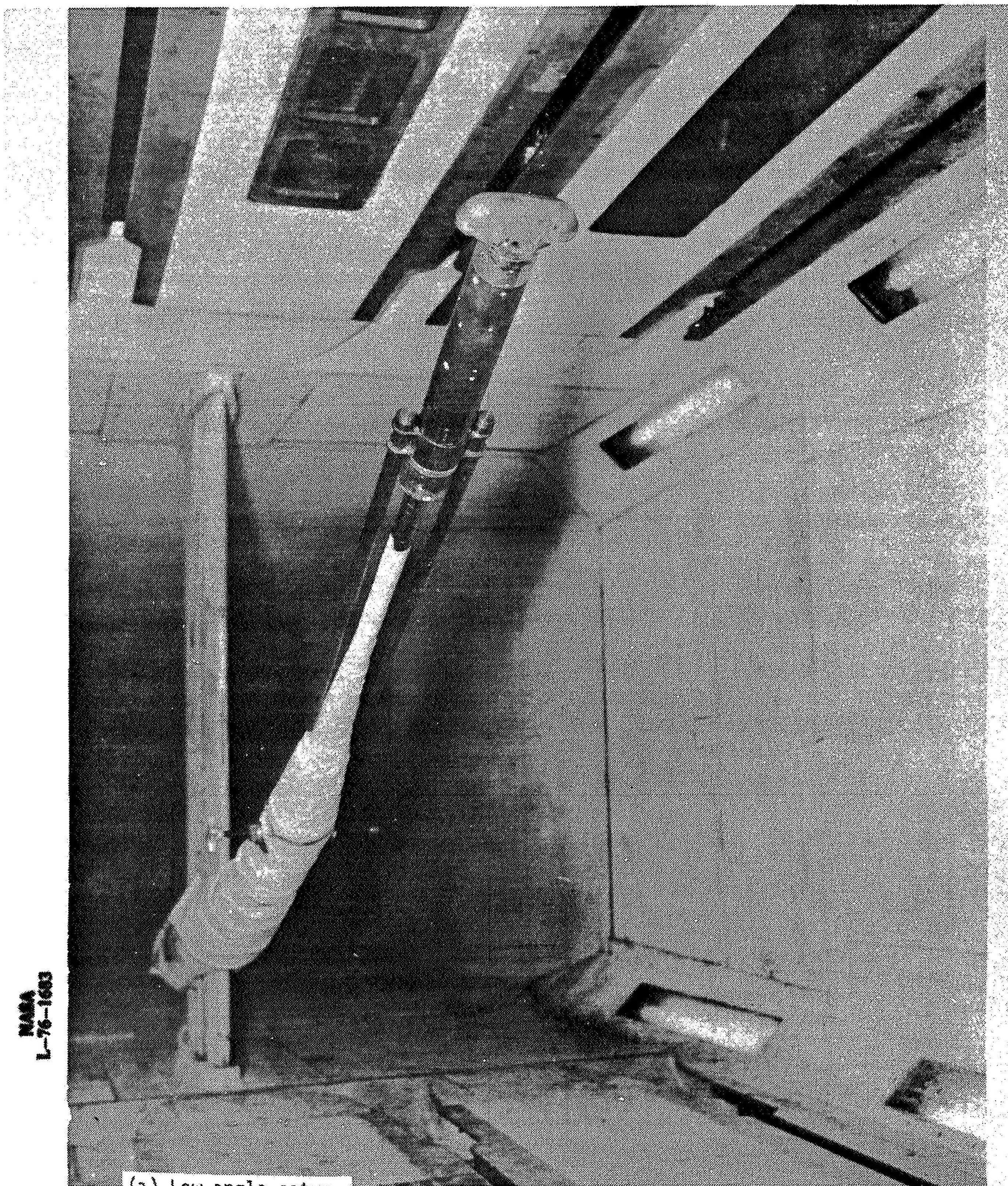

(a) Low angle setup.

Figure 18. A force model on standard and special mounts on the standard angle of attack sting.

ORIGINAL PAGE IS
OF POOR QUALITY

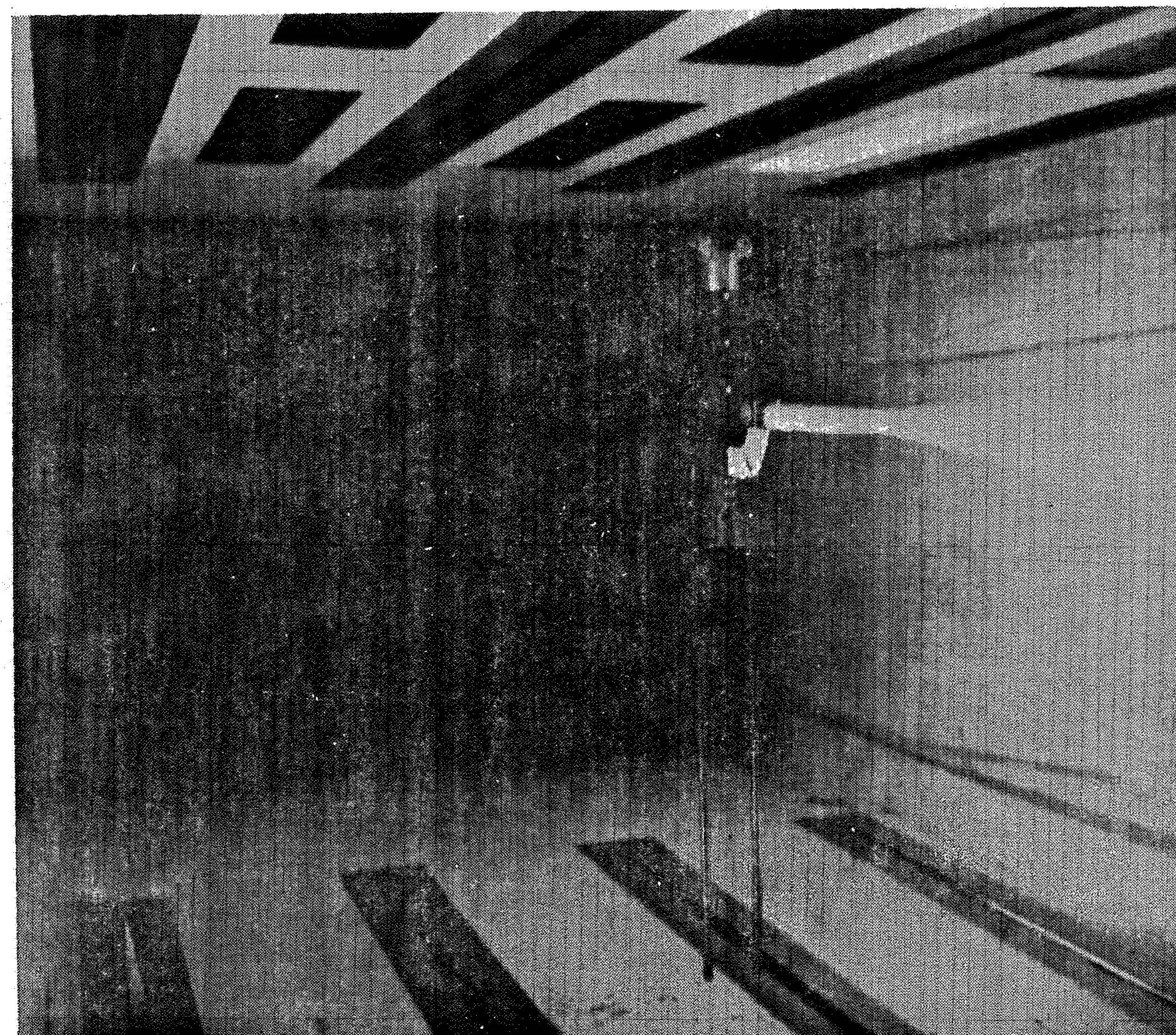

(b) High angle setup.

Figure 18. Concluded.

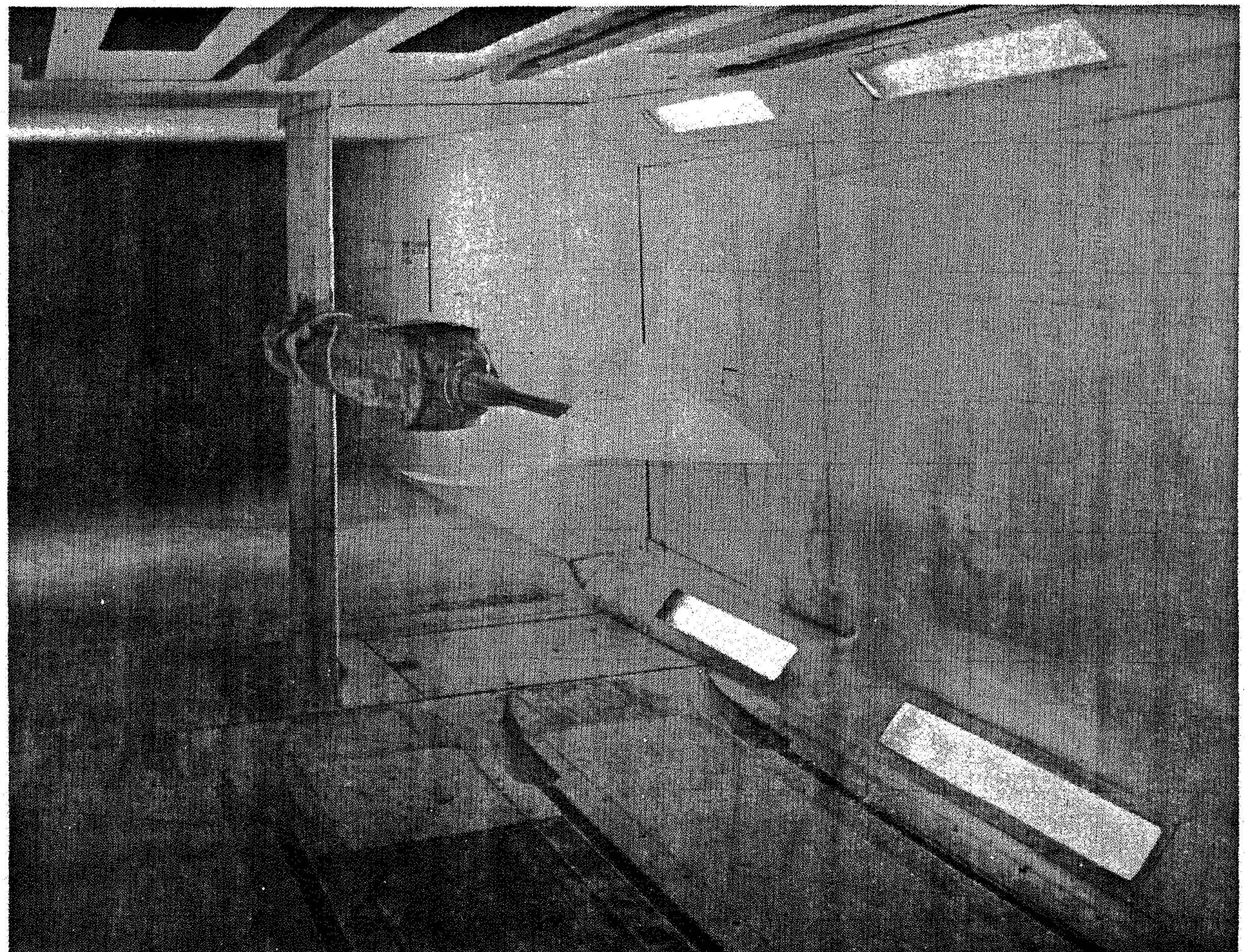

Figure 19. A force model mounted on the high angle stability sting.

ORIGINAL PAGE IS
OF POOR QUALITY

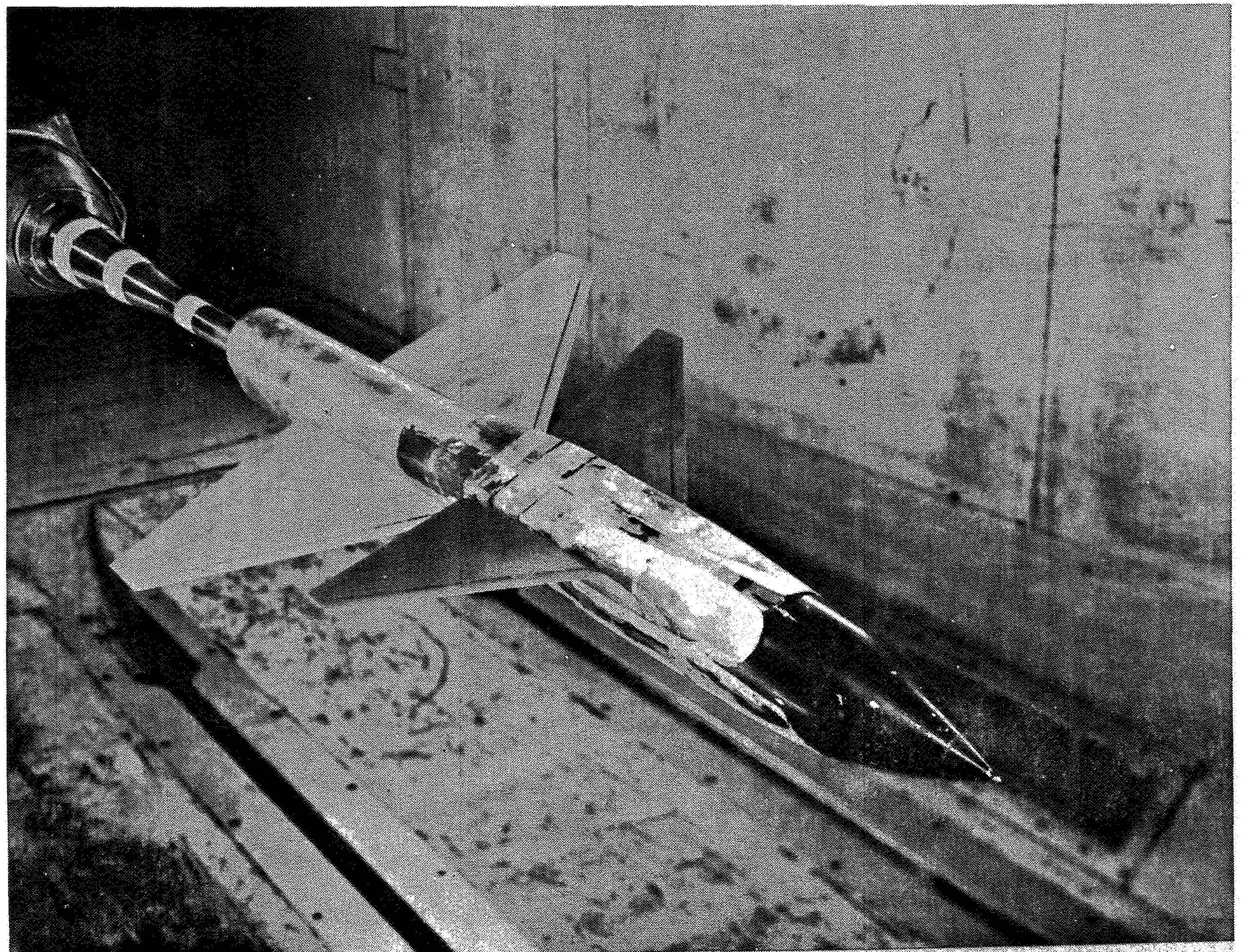

Figure 20. Force models mounted on the high angle stability sting.

Figure 20. Concluded.

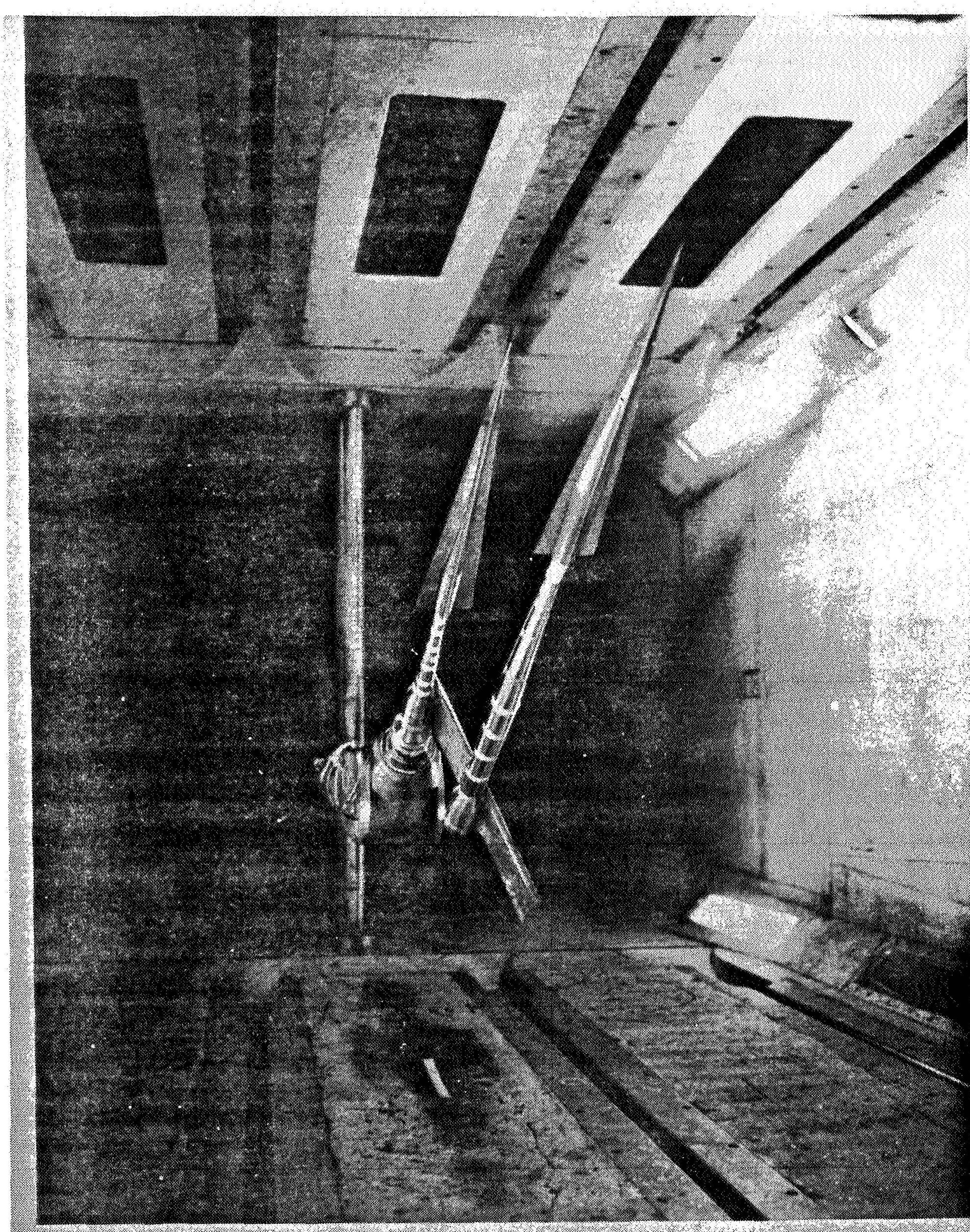

Figure 21. A pair of force models on a special mount on the high angle stability sting

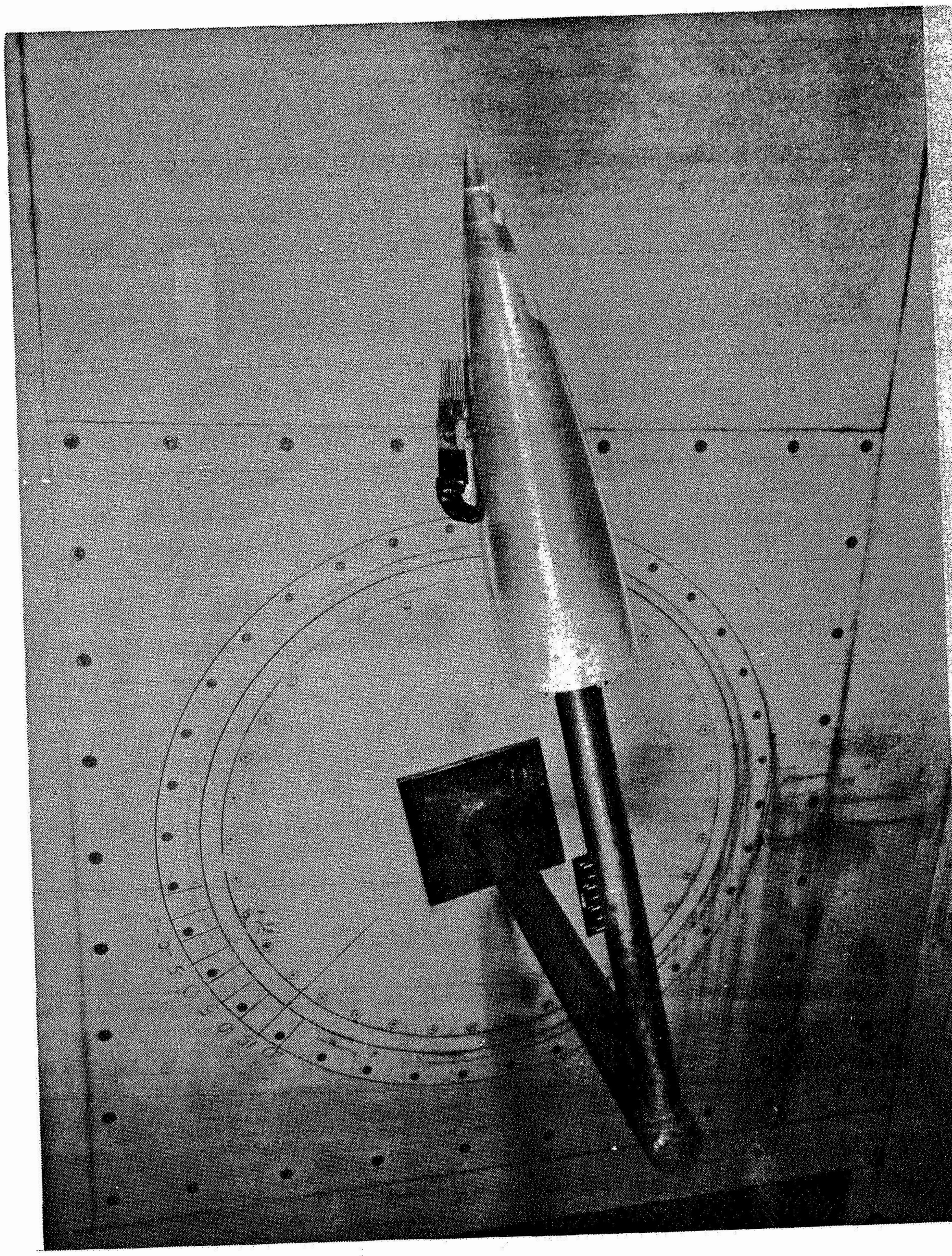

Figure 22. A model mounted on the side wall turntable.

ORIGINAL PAGE IS
OF POOR QUALITY

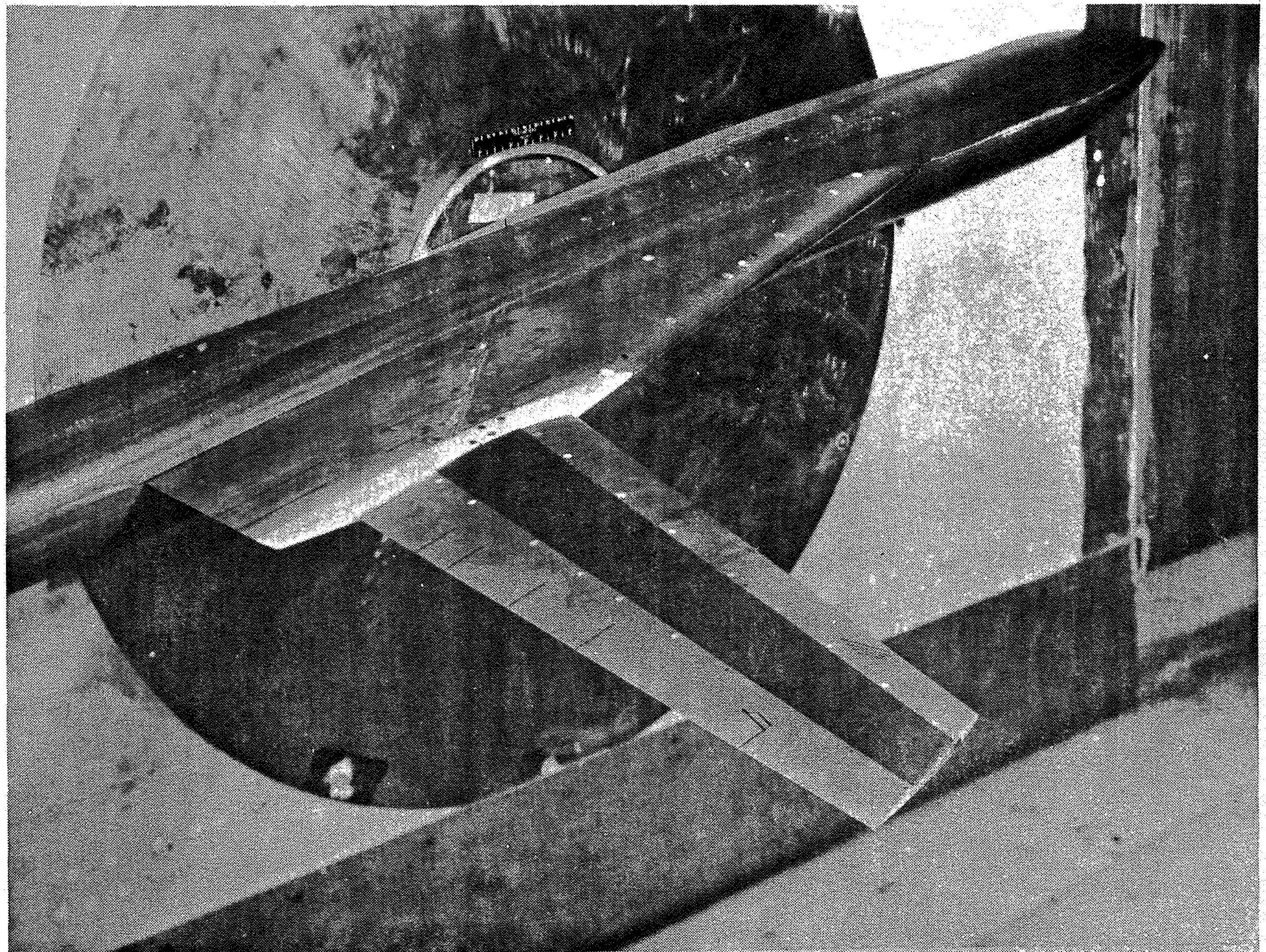

Figure 23. A semispan pressure model mounted on the side wall turntable boundary layer splitter plate.

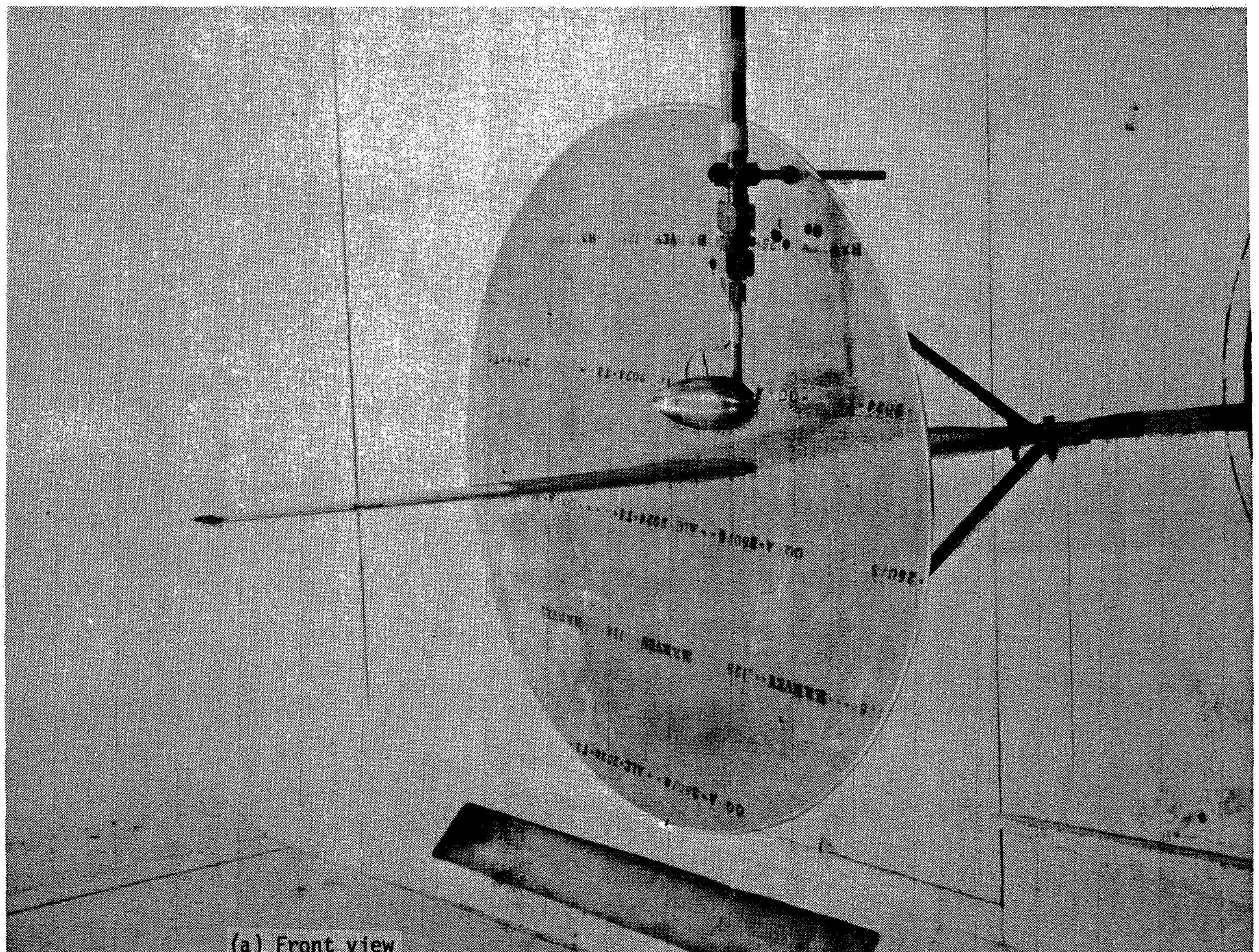

(a) Front view

Figure 24. A semispan pressure model with a high pressure air engine simulator mounted on the side wall turntable with a reflection plane.

ORIGINAL PAGE IS
OF POOR QUALITY

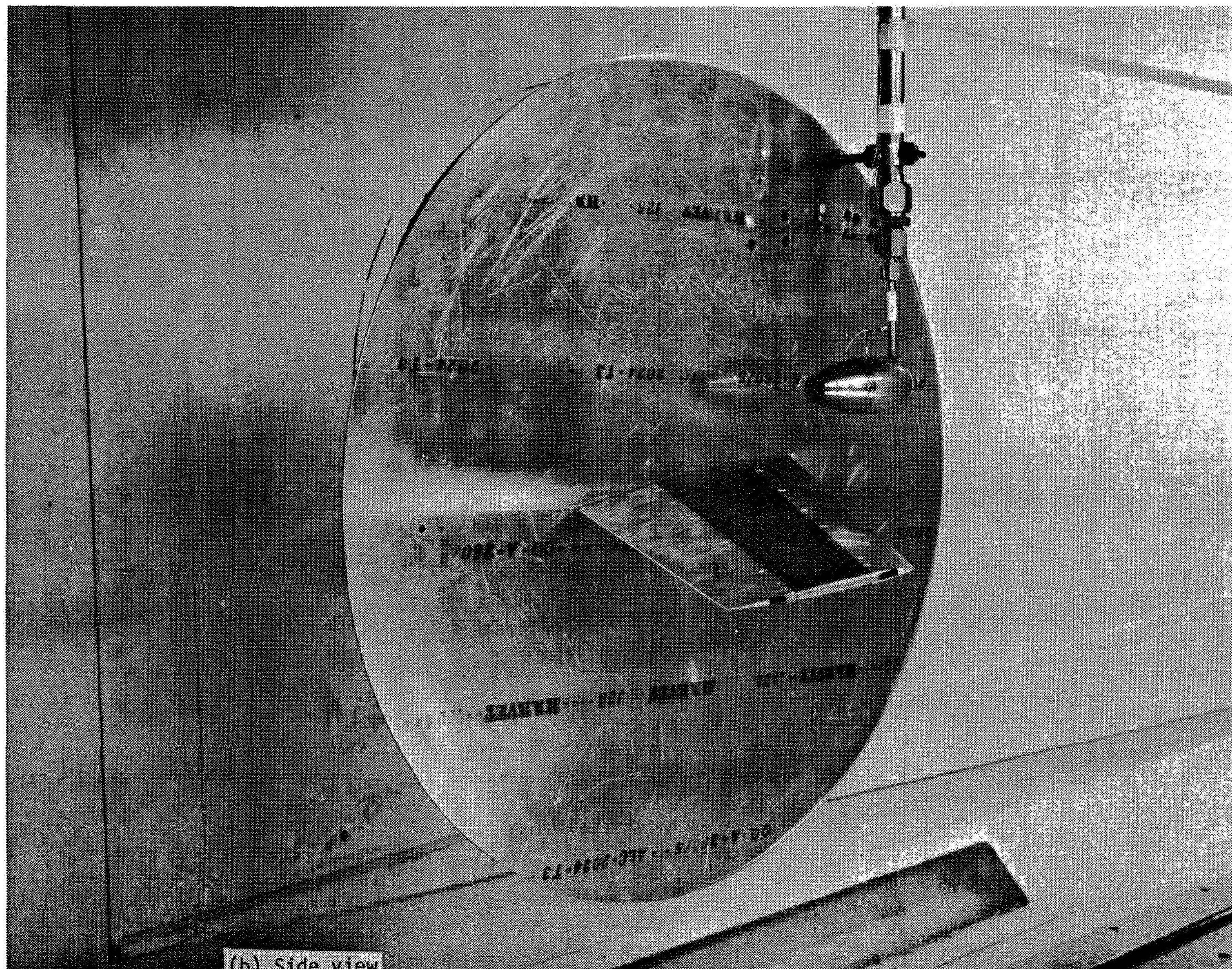

(b) Side view

Figure 24. Concluded.

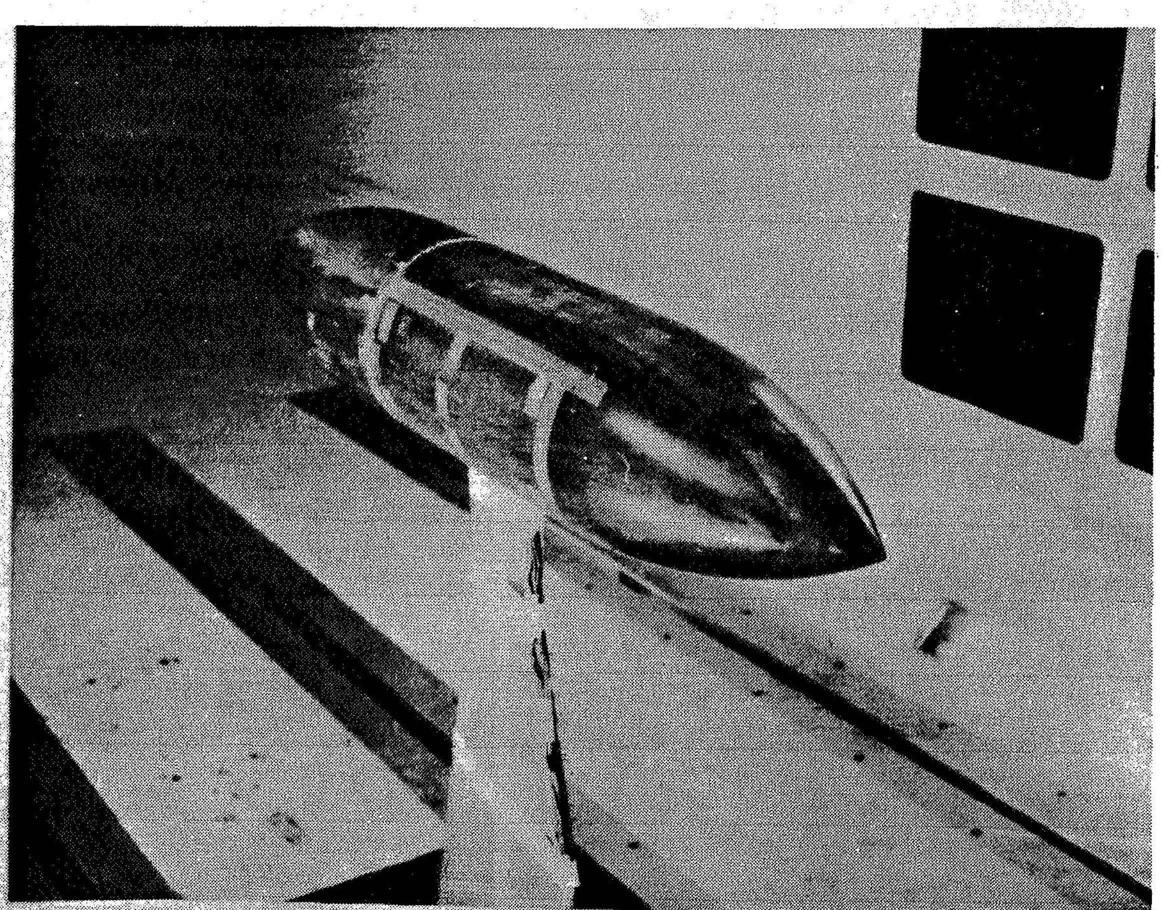

Figure 25. A force and pressure model mounted on a fixed strut.

ORIGINAL PAGE IS
OF POOR QUALITY

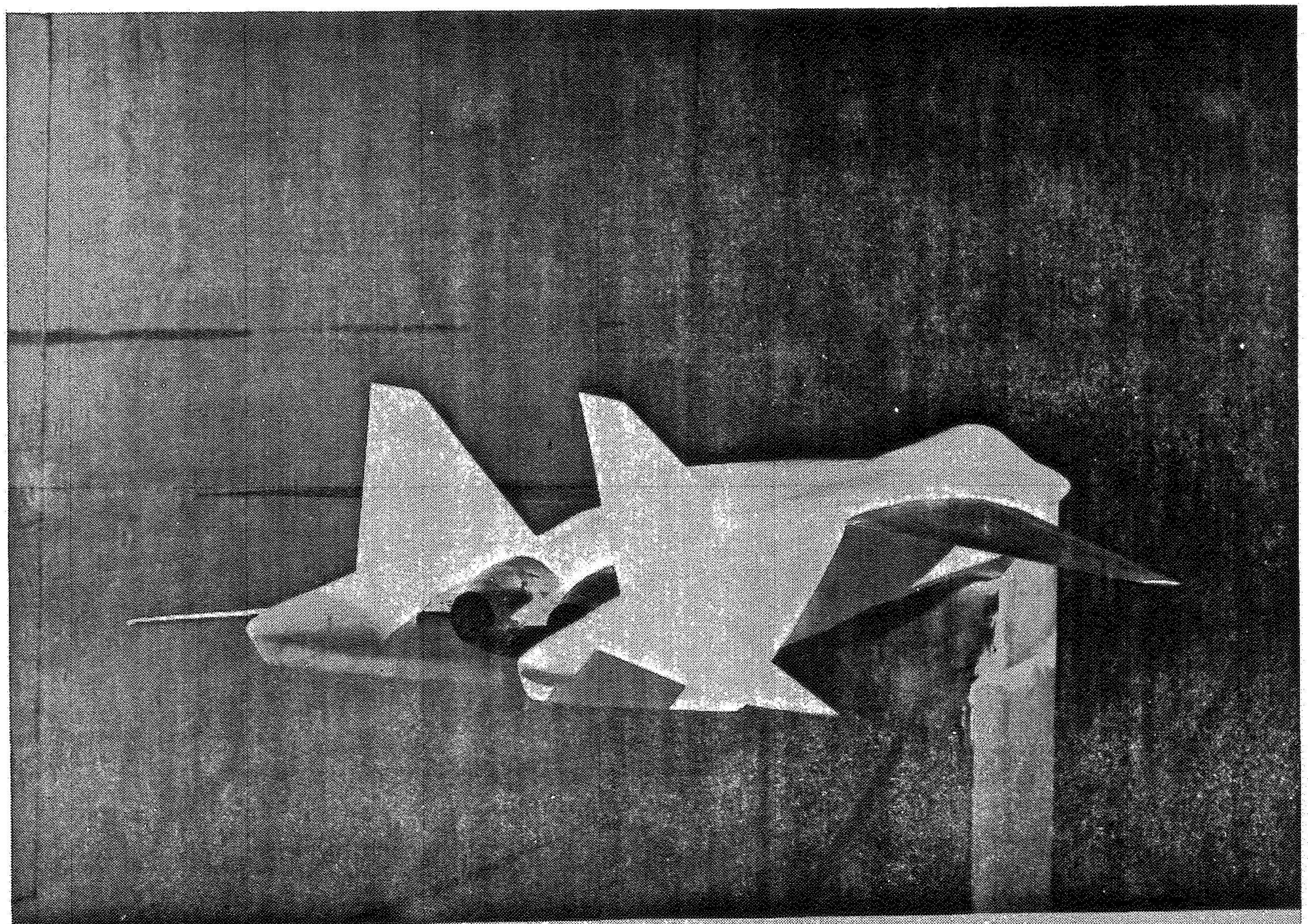

Figure 26. A pressure model with high pressure air engine simulators mounted on a fixed strut.

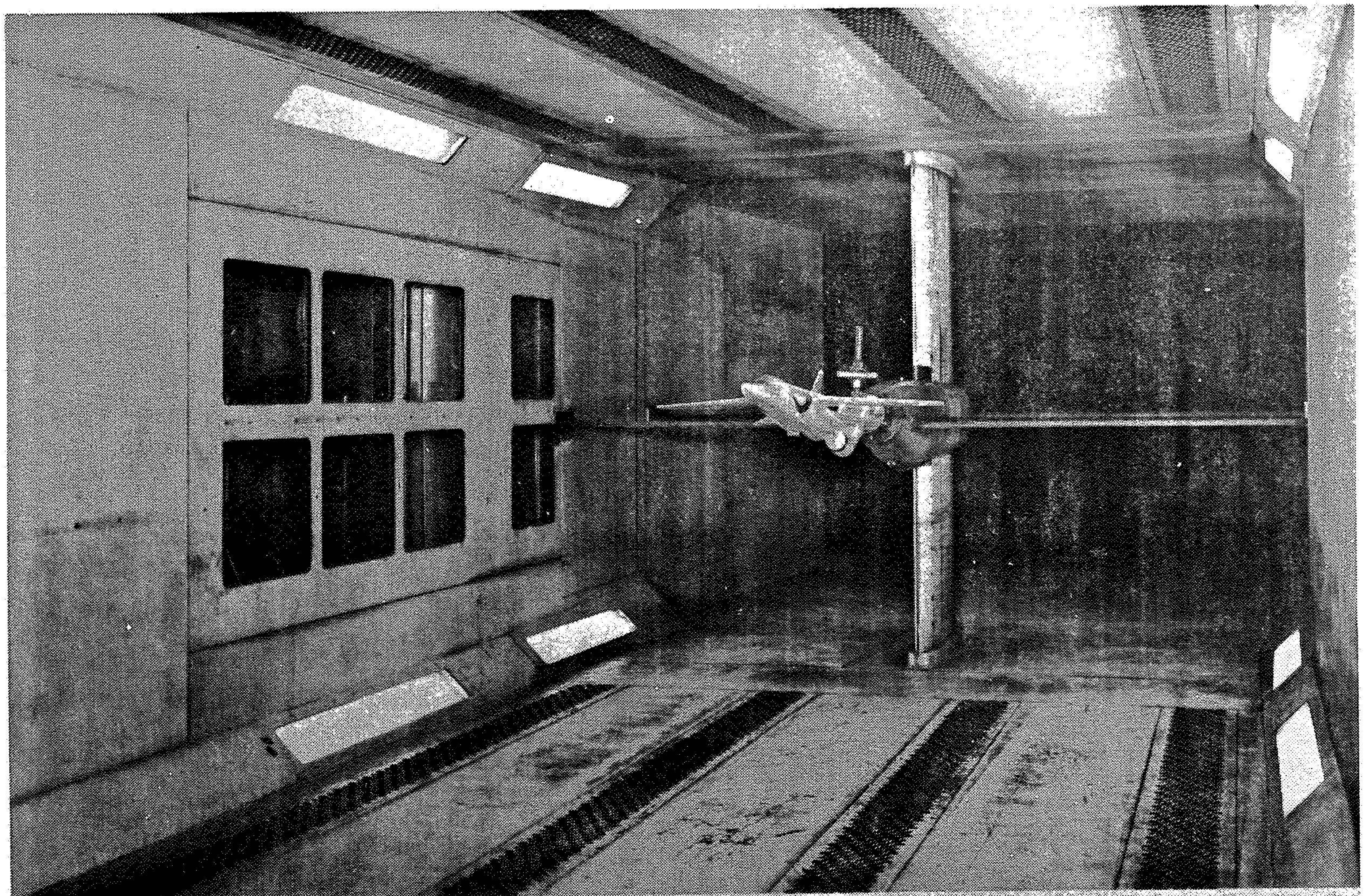

Figure 27. Dynamic stability models mounted on the steady state roll rig at an angle of attack.

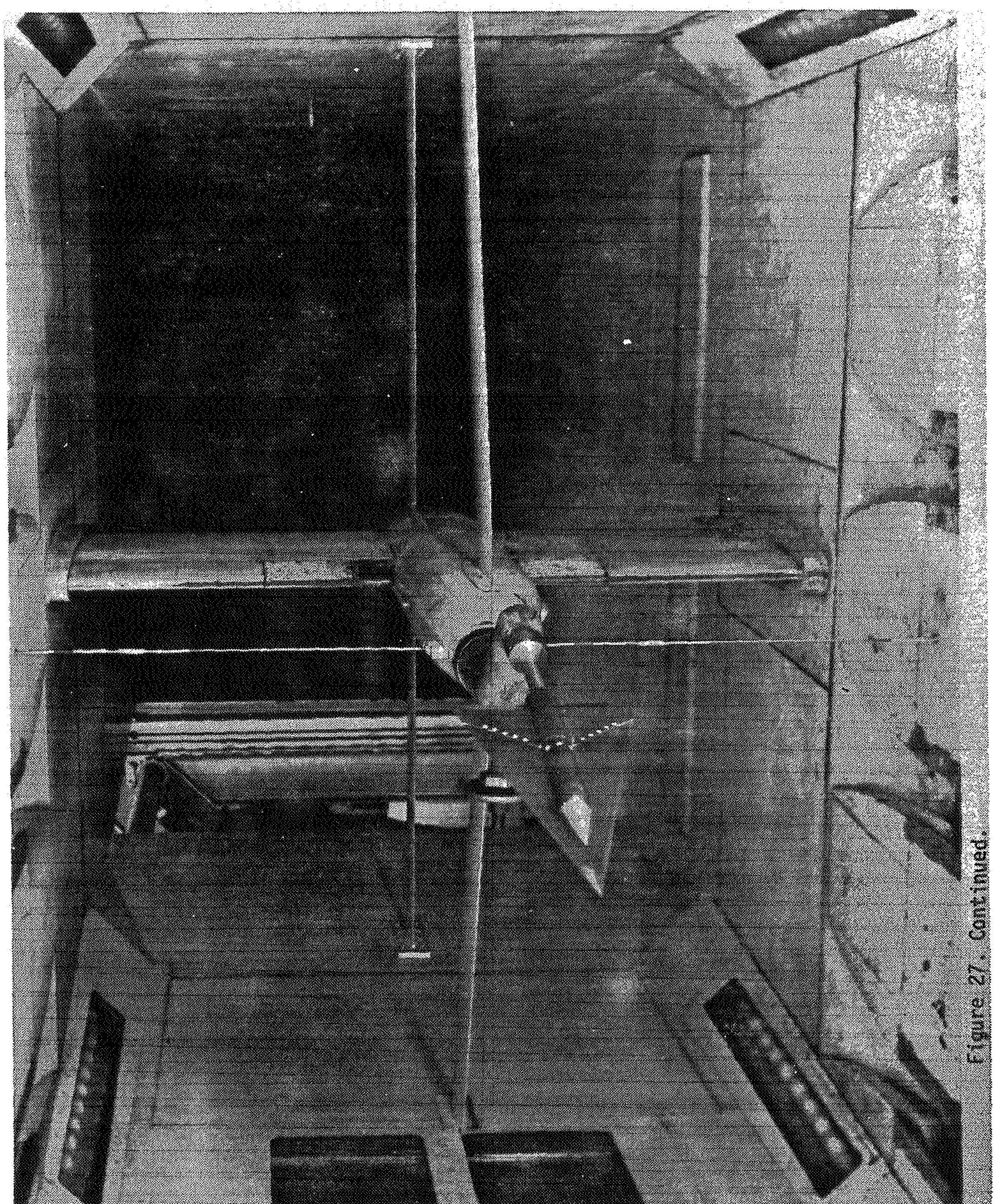

Figure 27. Continued.

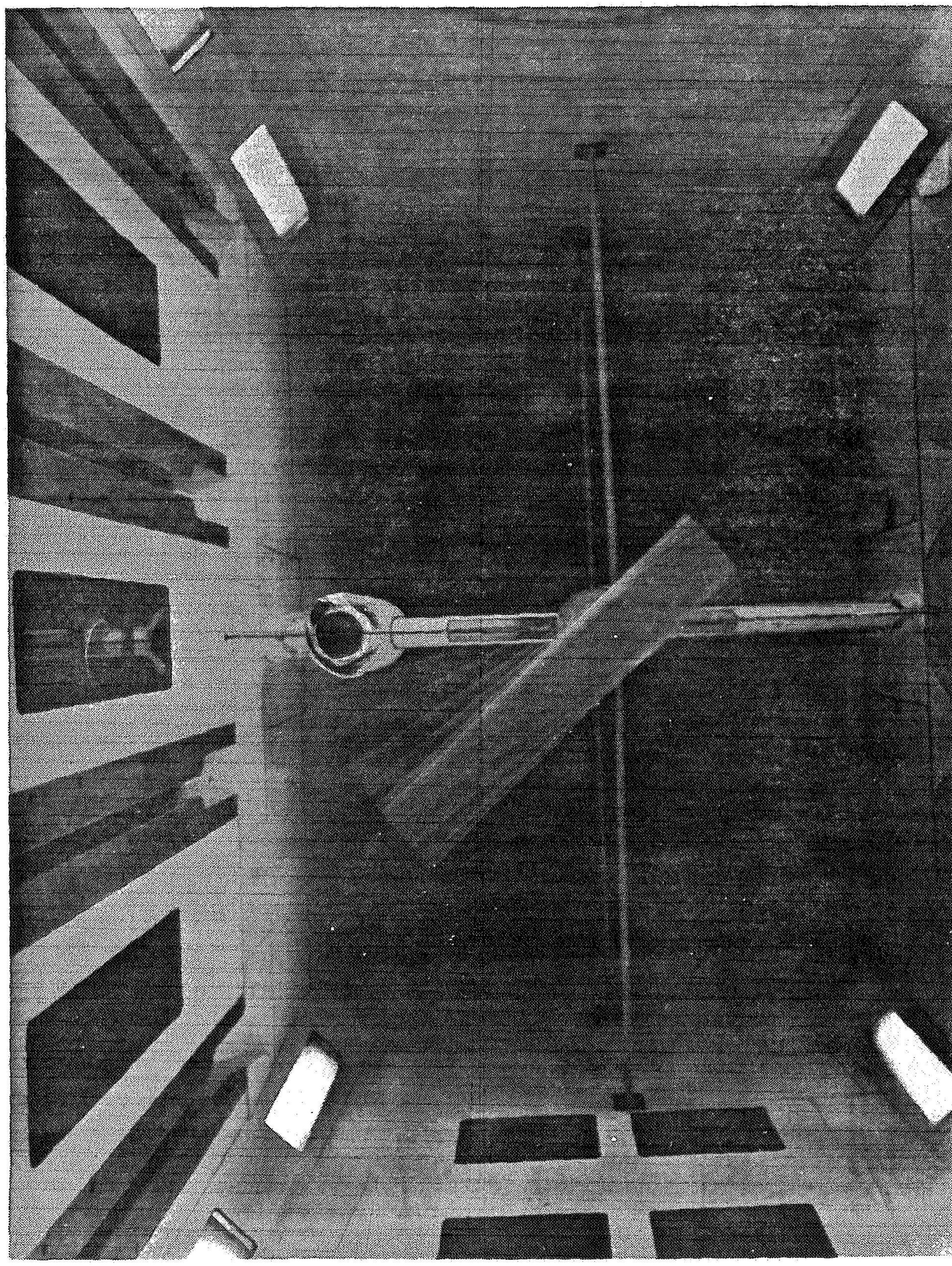

Figure 27. Concluded.

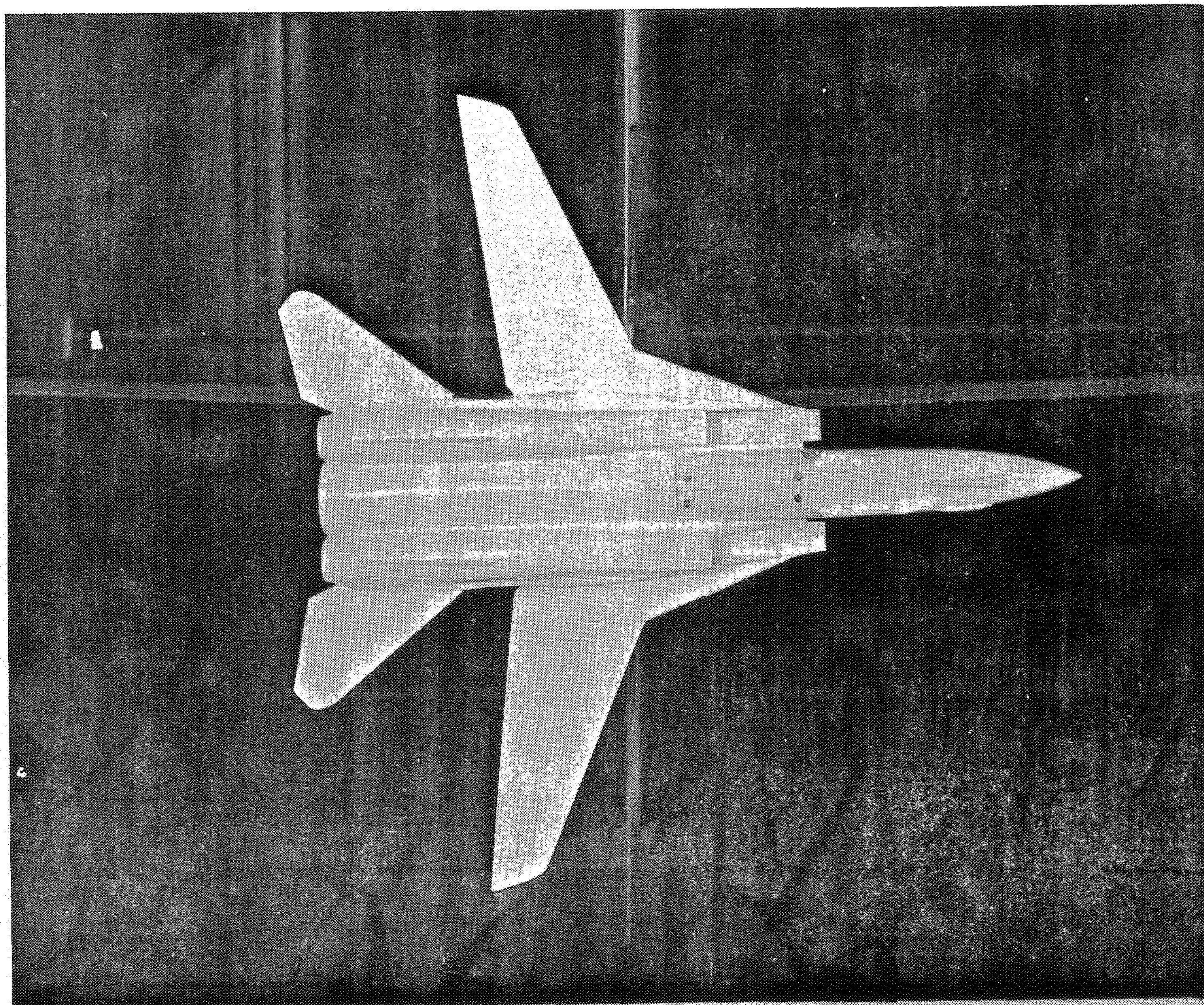

(a) Front view.
Figure 28. A dynamic stability model mounted on the steady state roll rig at 90° angle of attack.

L-71-9841
NASA

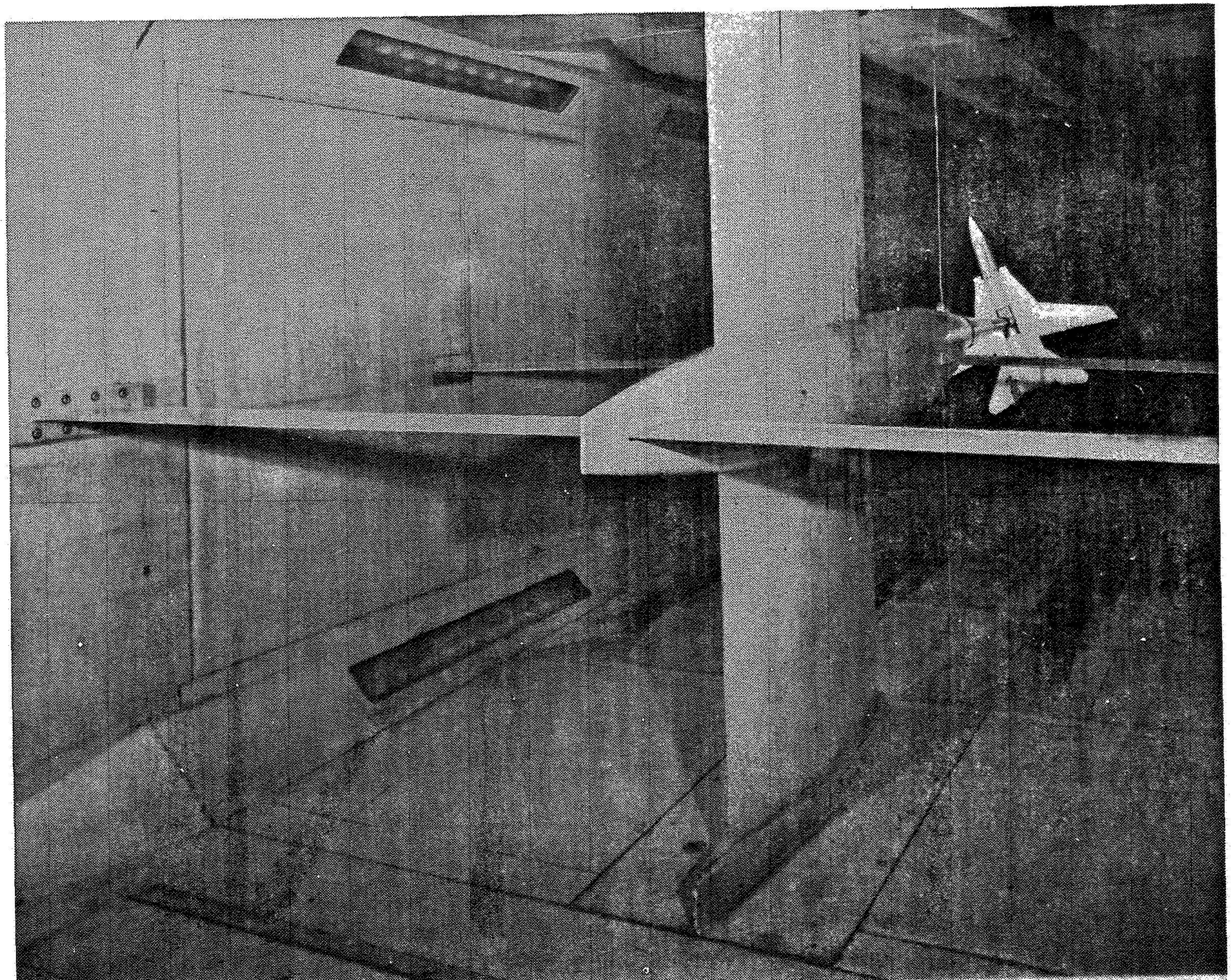

(b) Rear view.

Figure 28. Concluded.

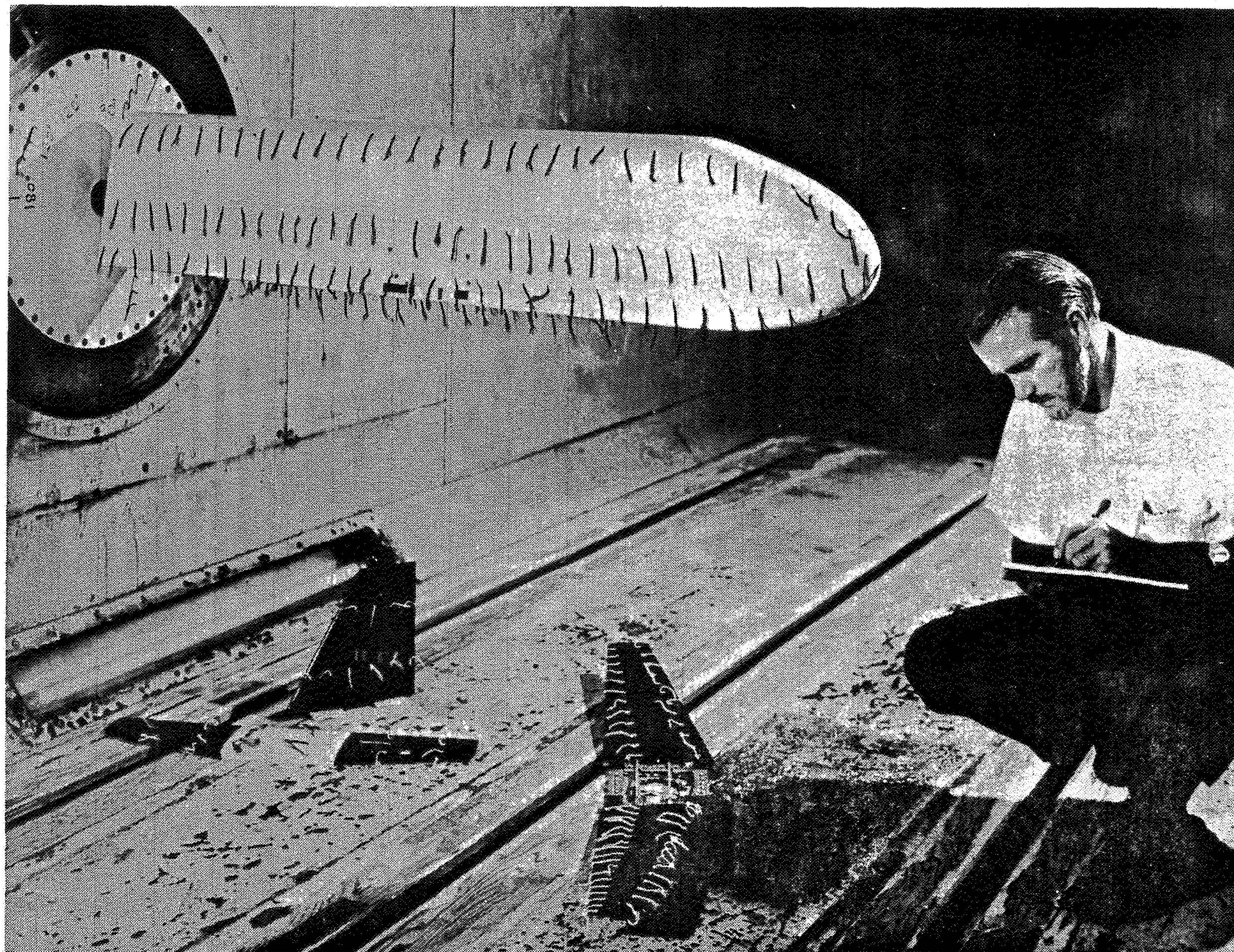

Figure 29. A dynamic stability model mounted on the roll oscillation rig on the side wall turntable.

Figure 30. A dynamic stability model mounted on the roll oscillation rig.

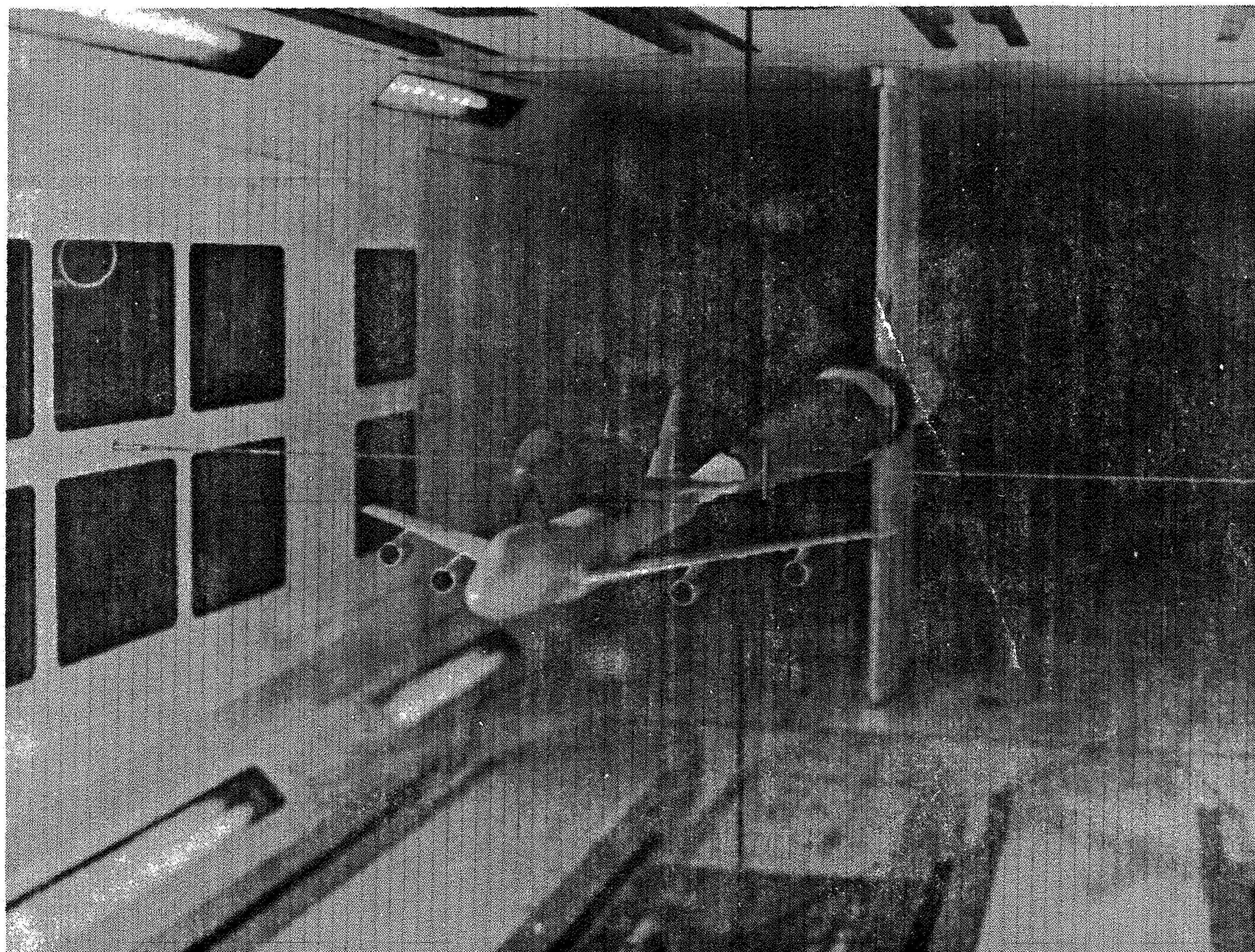

Figure 31. A dynamic stability model mounted on the pitch oscillation rig. This rig can also be setup for yaw oscillations.

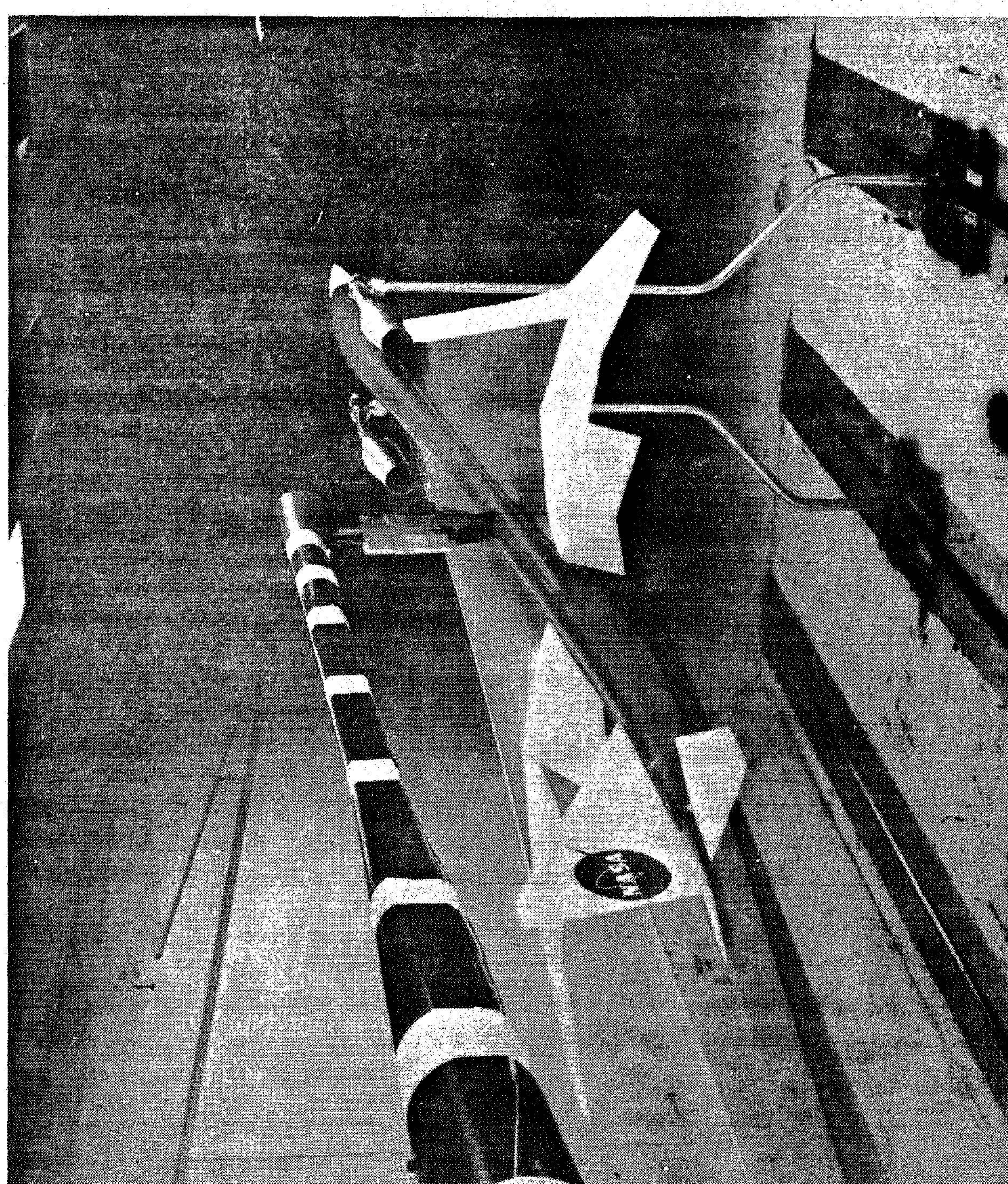

Figure 32. A force model with non-metric high pressure air engine simulators mounted on a special mount on the standard angle of attack sting.

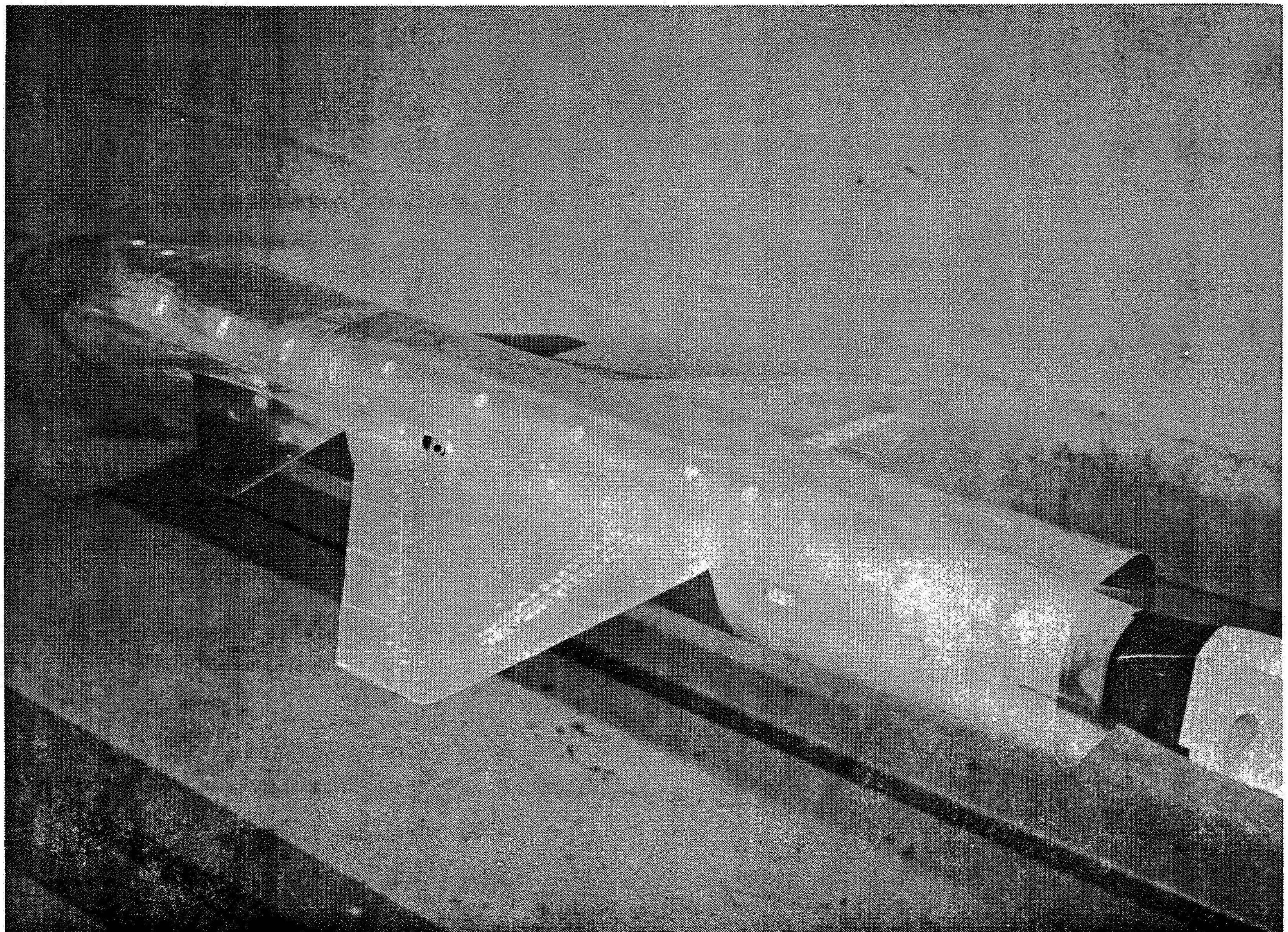

Figure 33. A force model with high pressure air simulation of spanwise blowing mounted on the standard angle of attack sting.

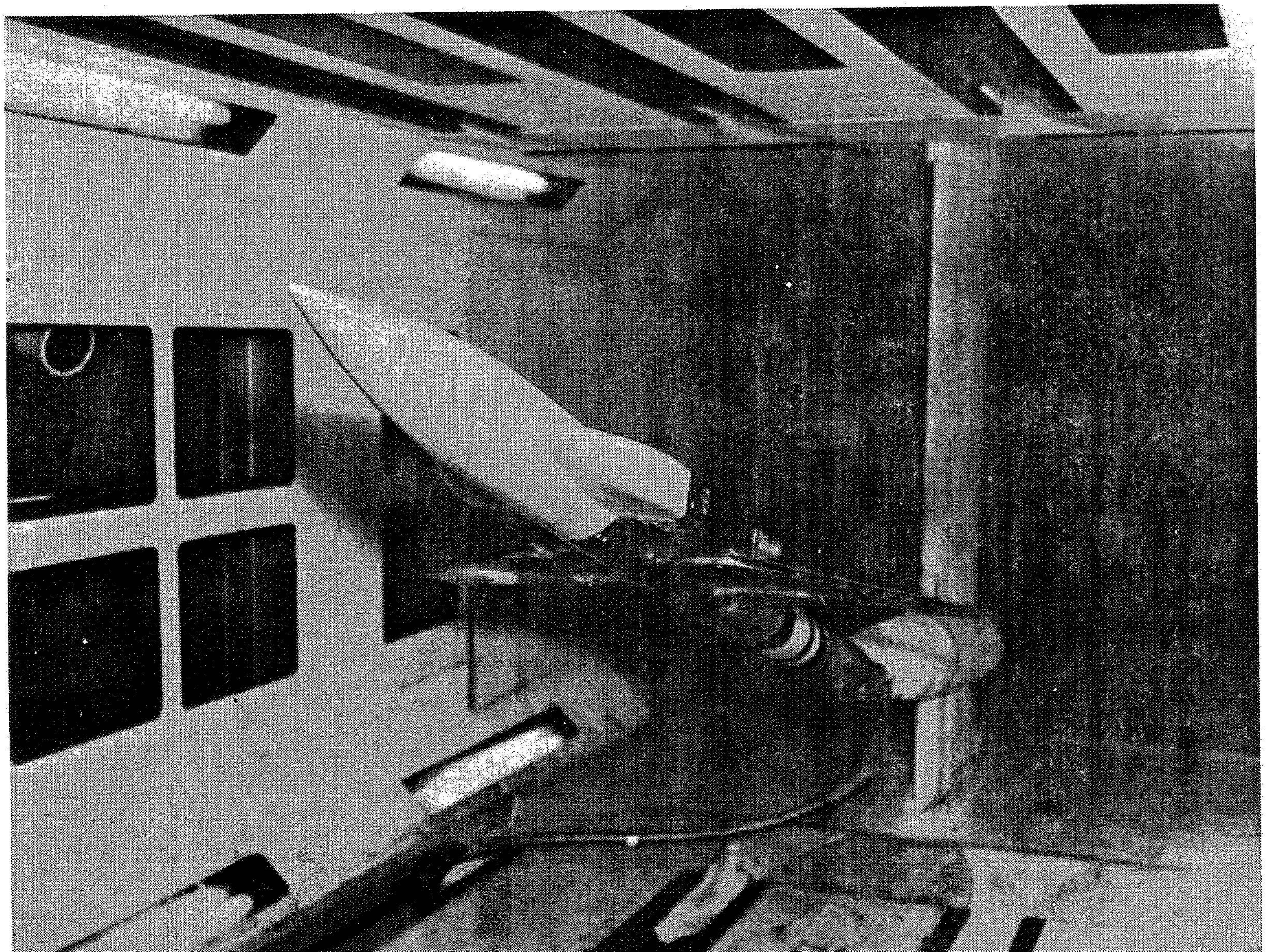

(a) Front view

Figure 34. A force model with high pressure air simulation of spanwise blowing and high pressure air engine simulators mounted on the standard angle of attack sting.

ORIGINAL PAGE IS
OF POOR QUALITY

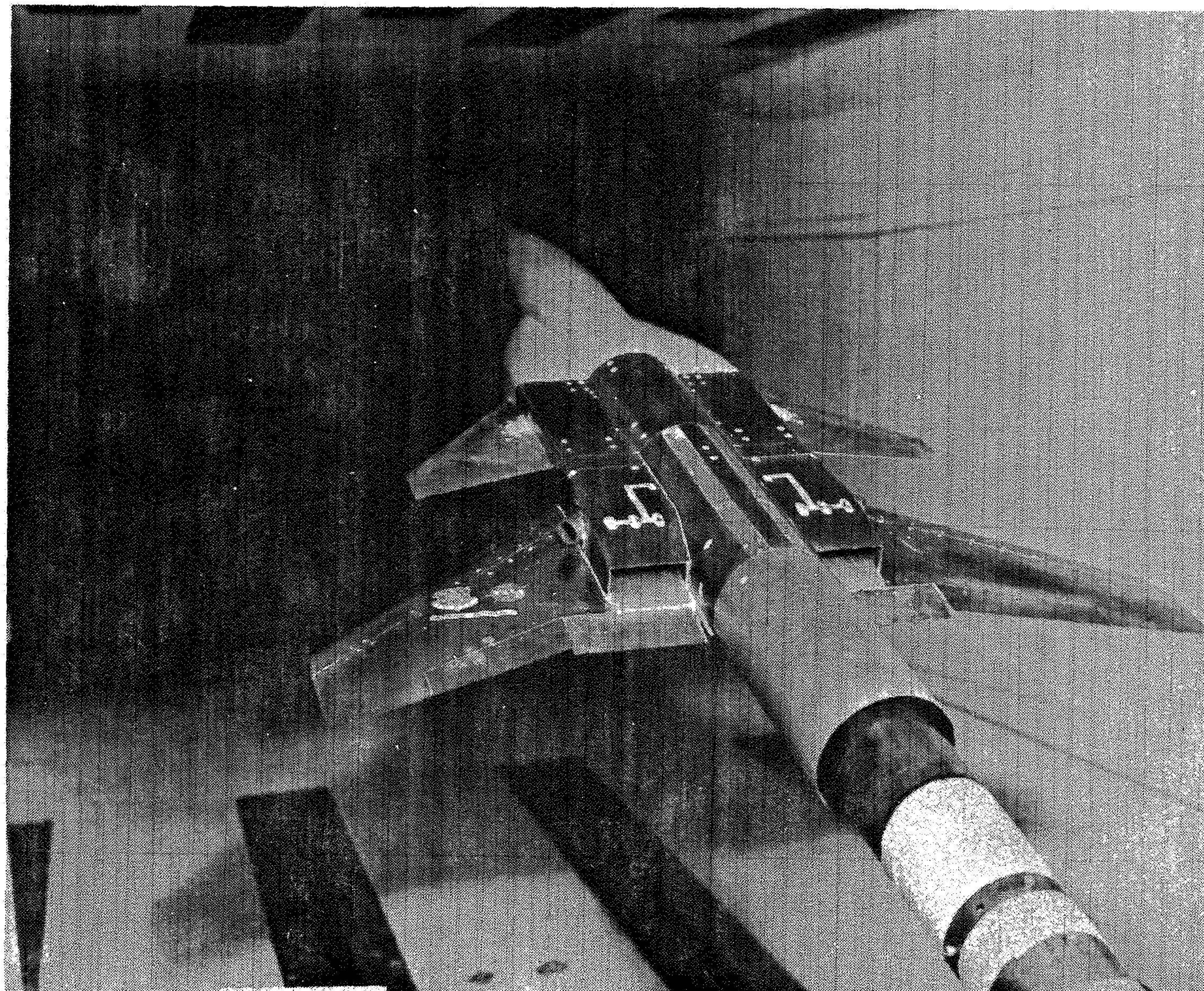

(b) Rear view
Figure 34. Concluded.

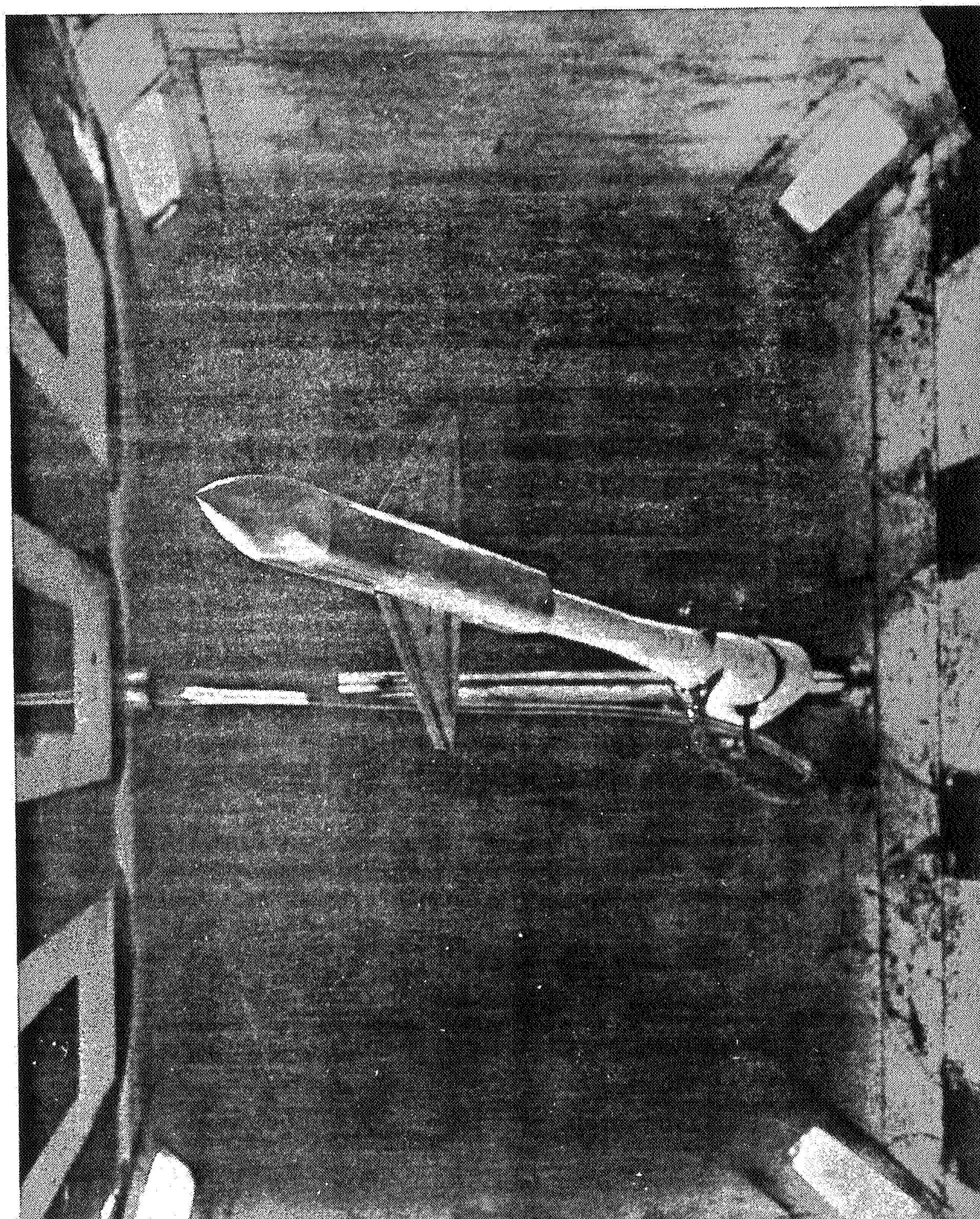

Figure 35. A force model with high pressure air simulation of a strake mounted at a sideslip angle on the standard angle of attack sting set up for the pitch range of 10° to 30°.

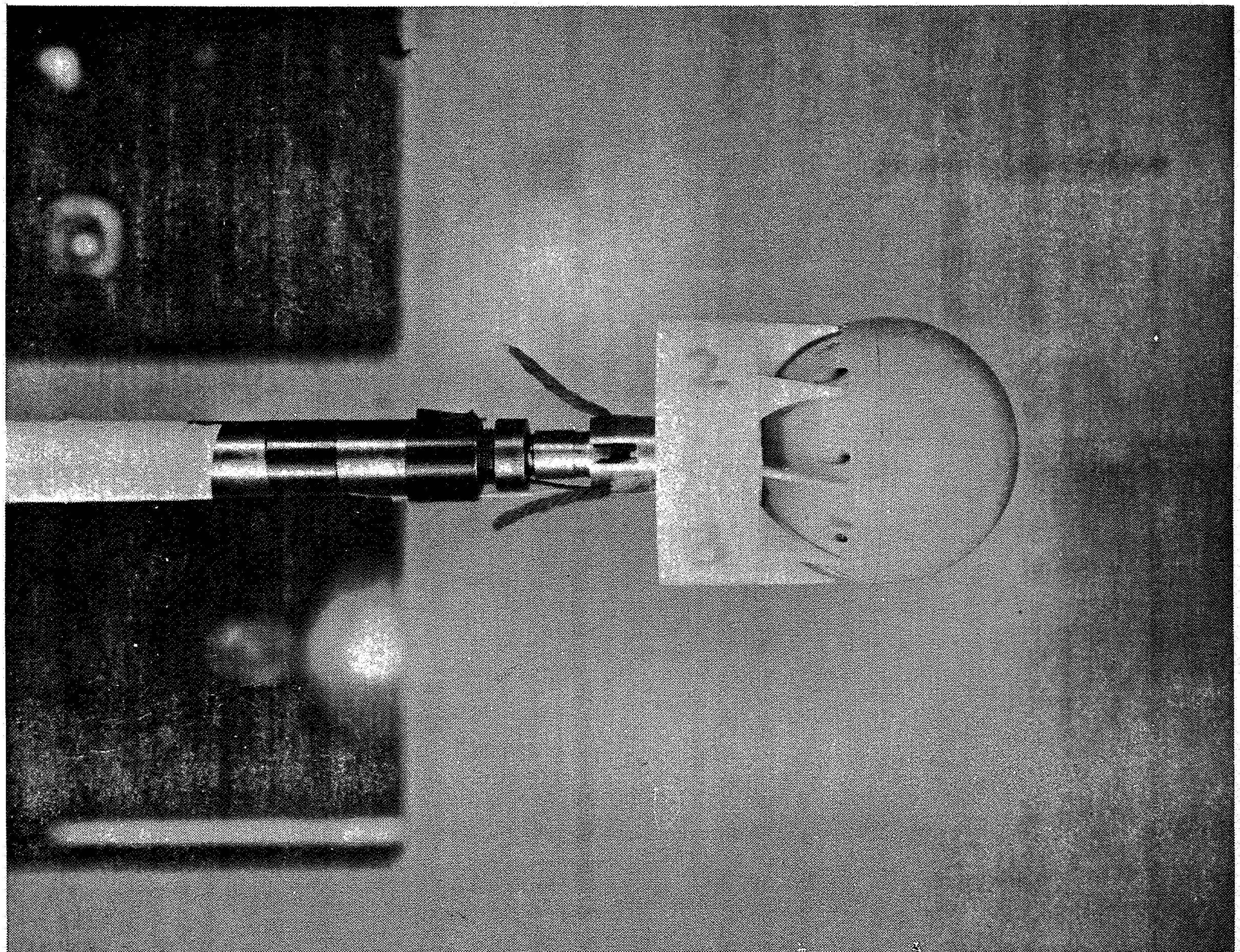

Figure 36. Free spinning force model mounted on the standard angle of attack sting.

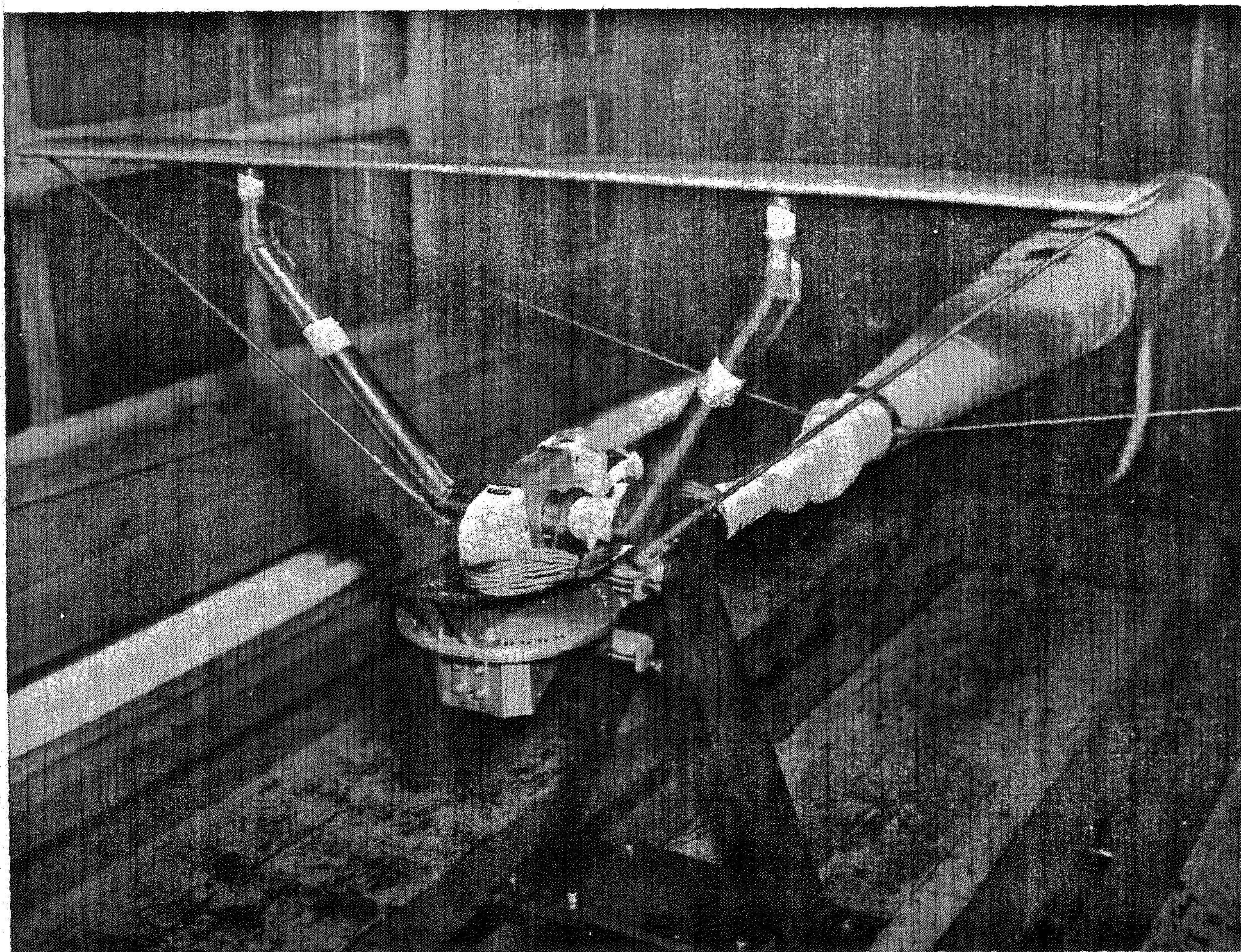

Figure 37. A pressure model mounted on a special rigid support for precision flow field velocity measurements.

ORIGINAL PAGE IS
OF POOR QUALITY

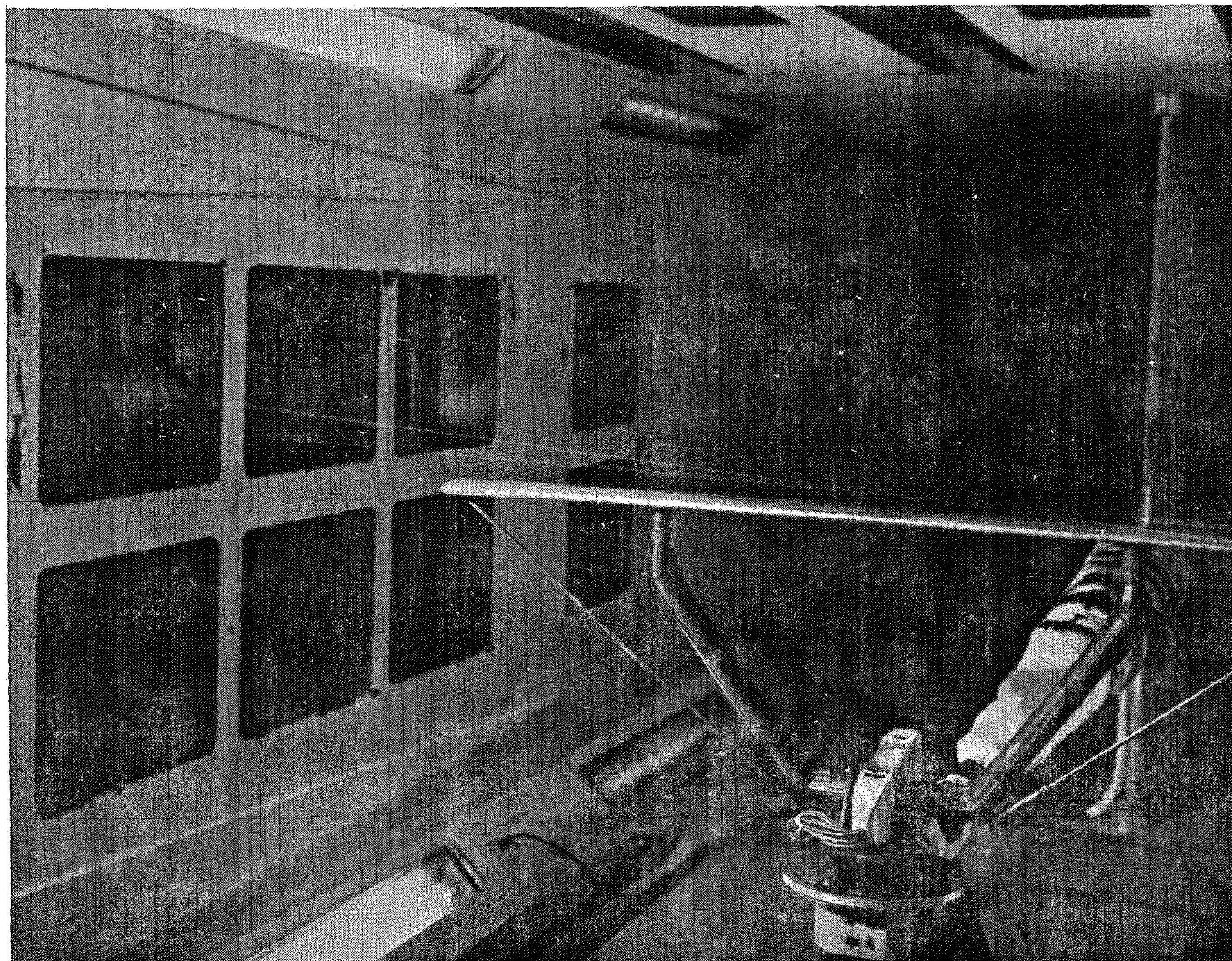

Figure 37. Concluded. The light beams of the laser velocimeter are shown.

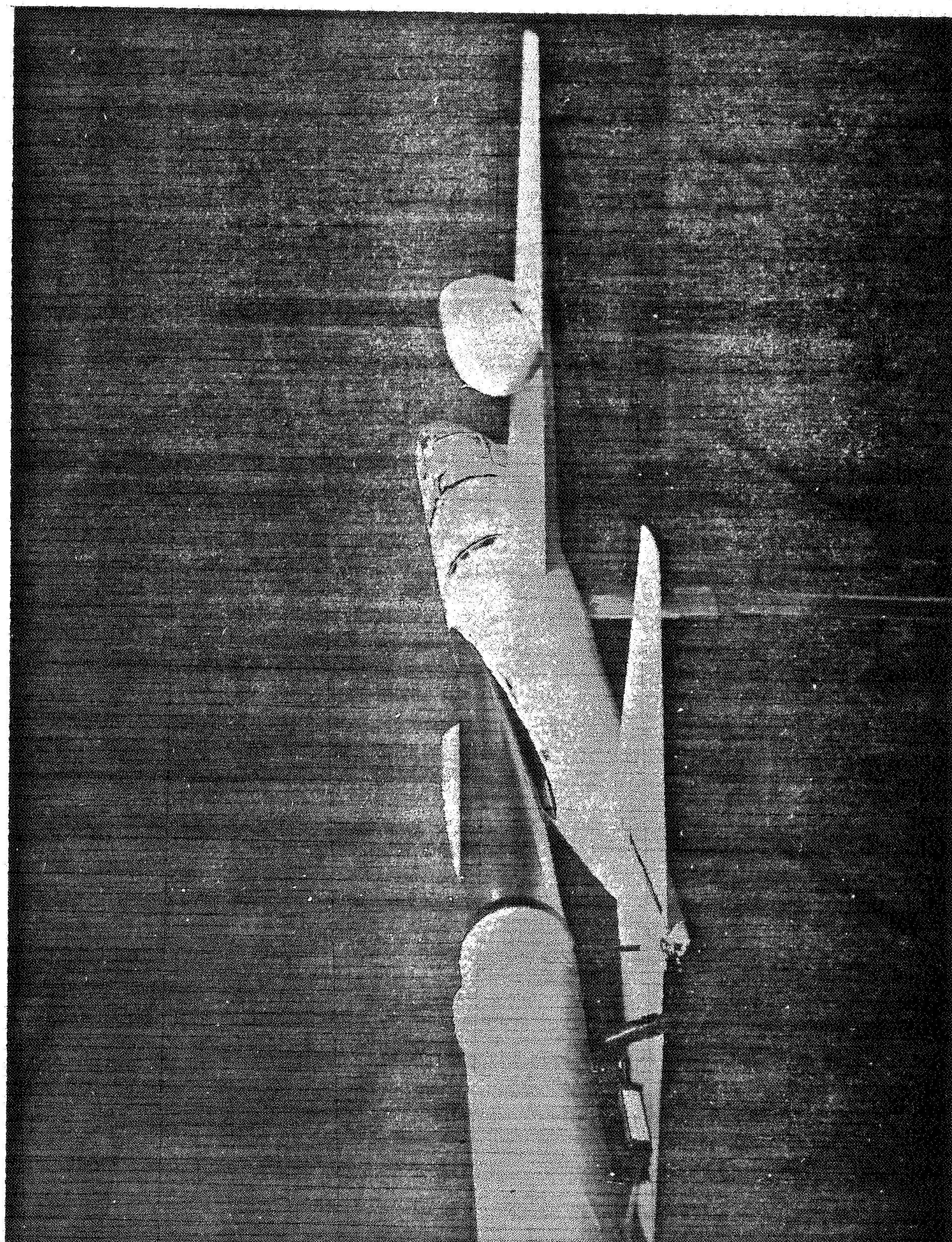

Figure 38. A force model mounted on a fixed strut with a dummy sting to determine sting tare effects.

ORIGINAL PAGE IS
OF POOR QUALITY

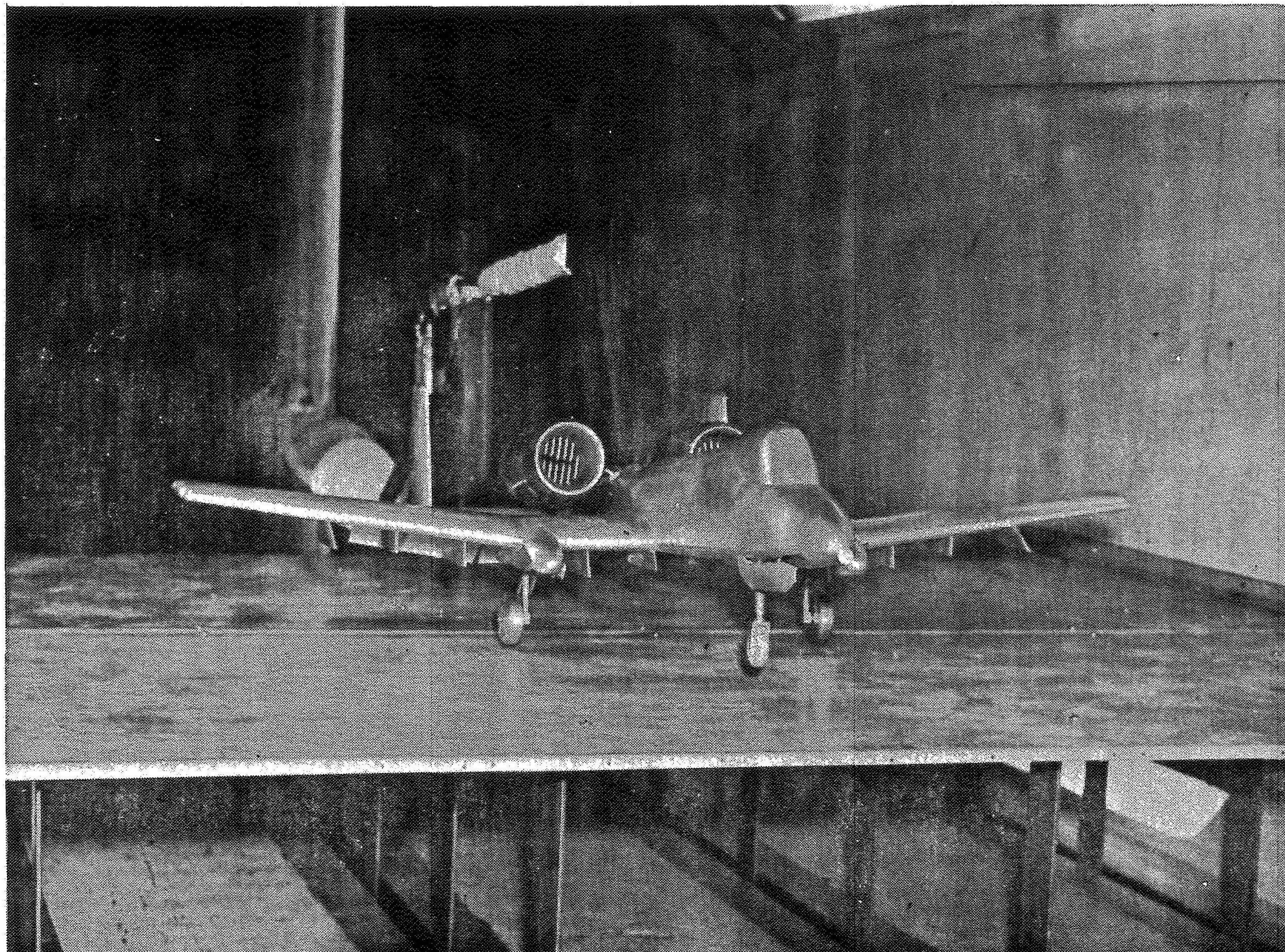

Figure 39. A force model with high pressure air engine simulation mounted on the standard angle of attack sting for testing in the presence of a fixed ground plane.

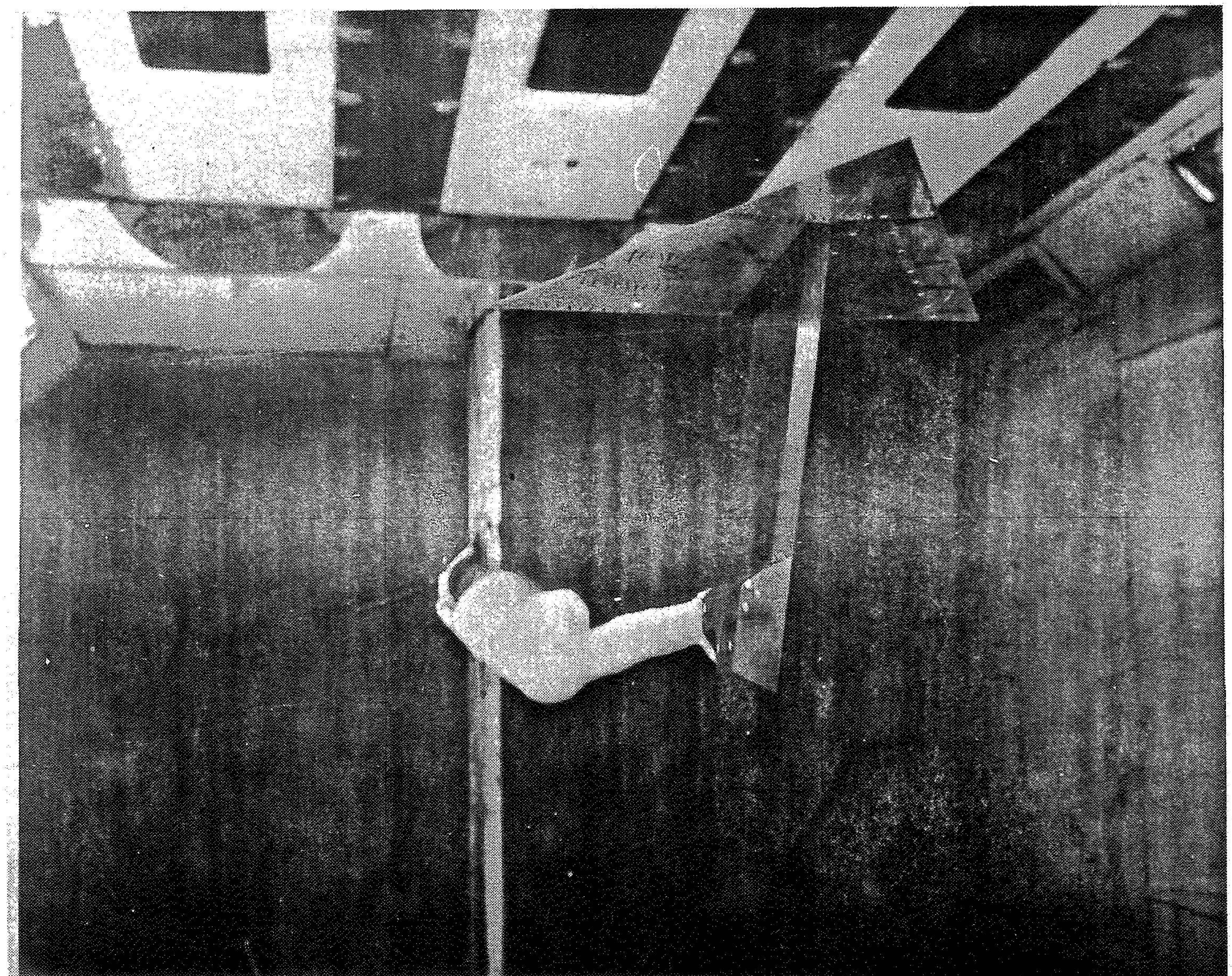

Figure 40. A pressure wing mounted on a special mount on the standard angle of attack sting.

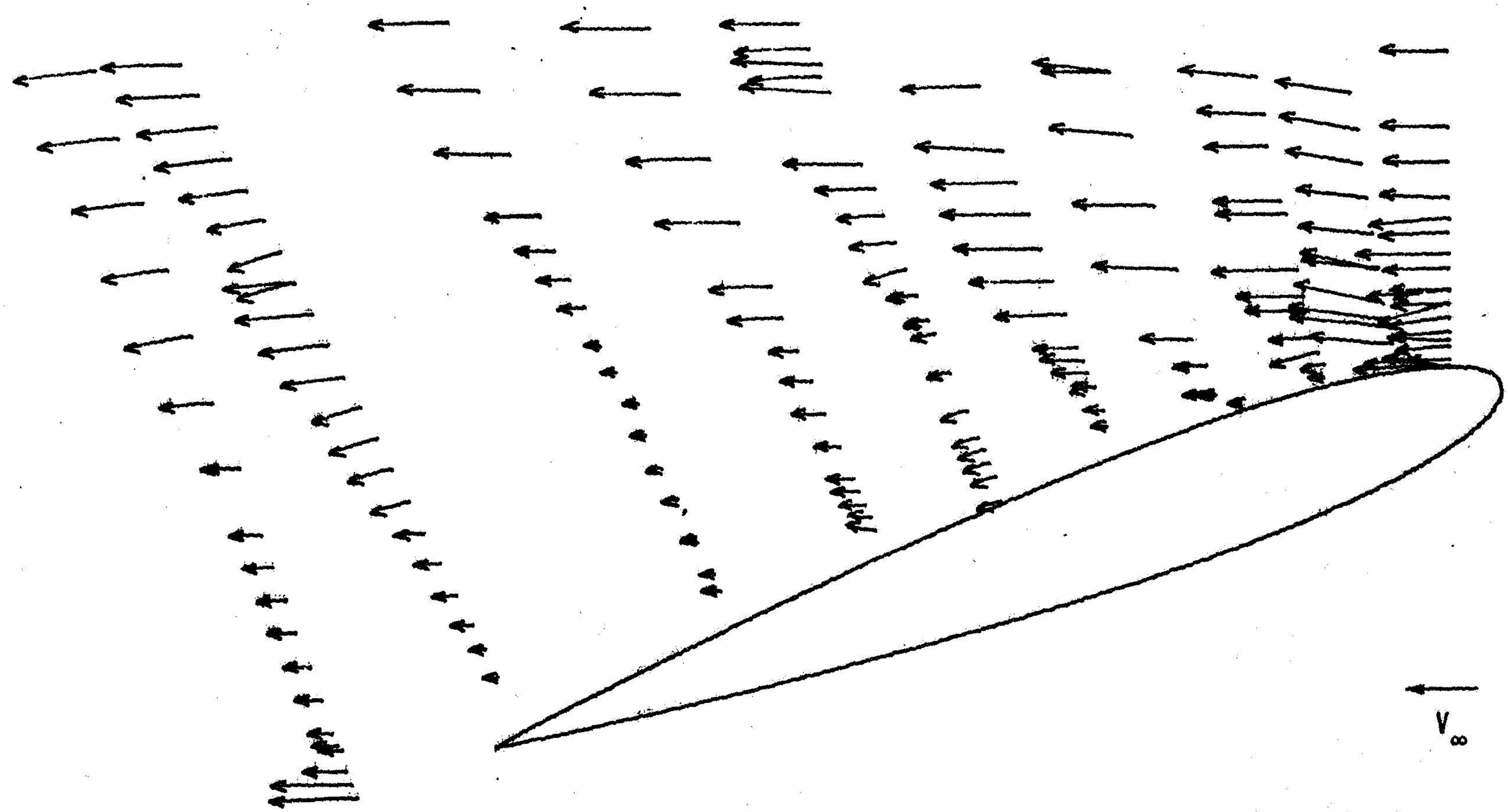

(a) Mean velocities with all velocities shown in the prime direction.

Figure 41. Laser velocimeter data for the NACA 0012 airfoil of figure 39 at a Mach number of .49 and an angle of attack of 19.5°.

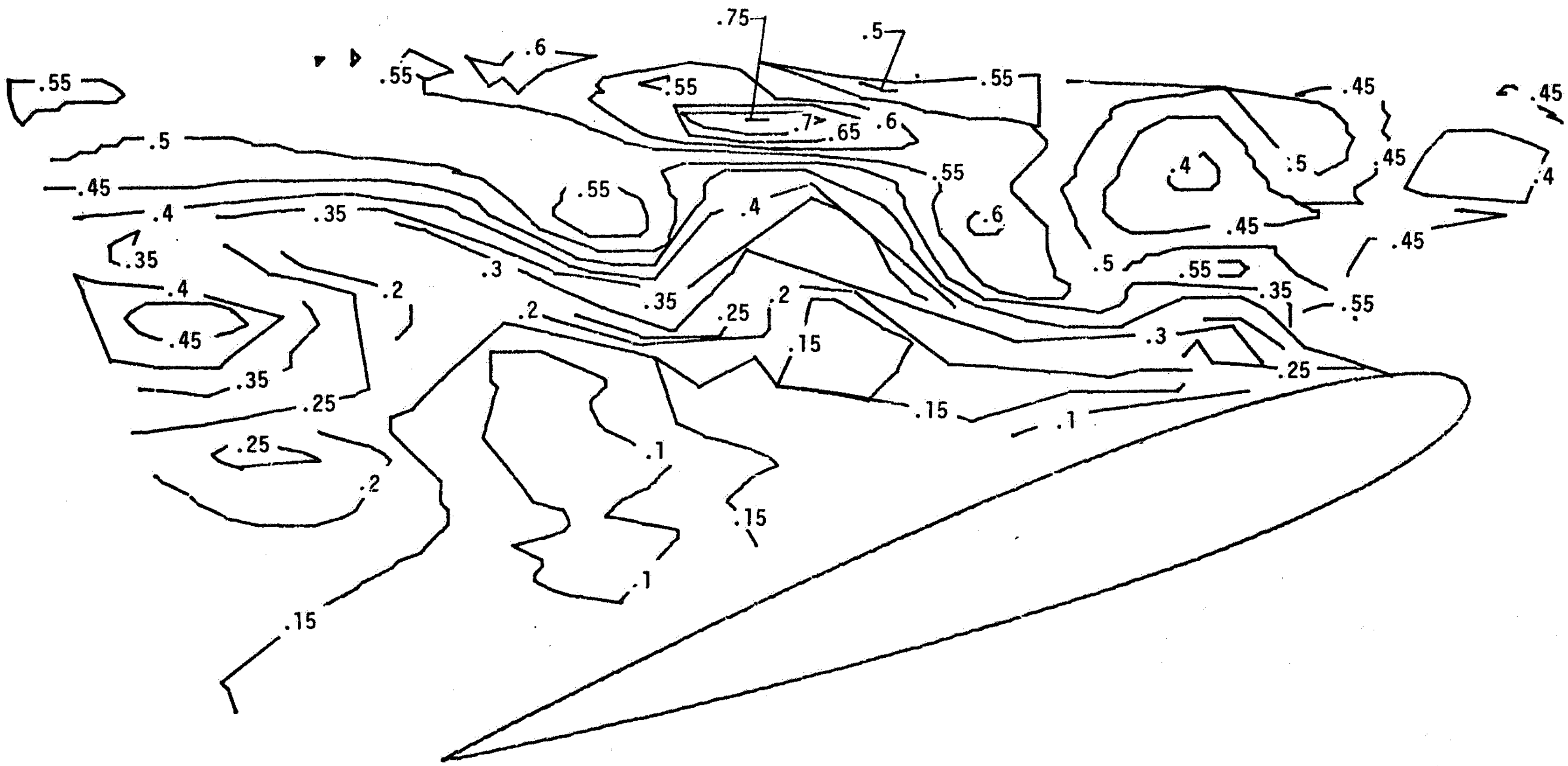

(b) Contours of constant Mach number based on the average resultant velocity corrected for velocity bias.

Figure 41. Continued.

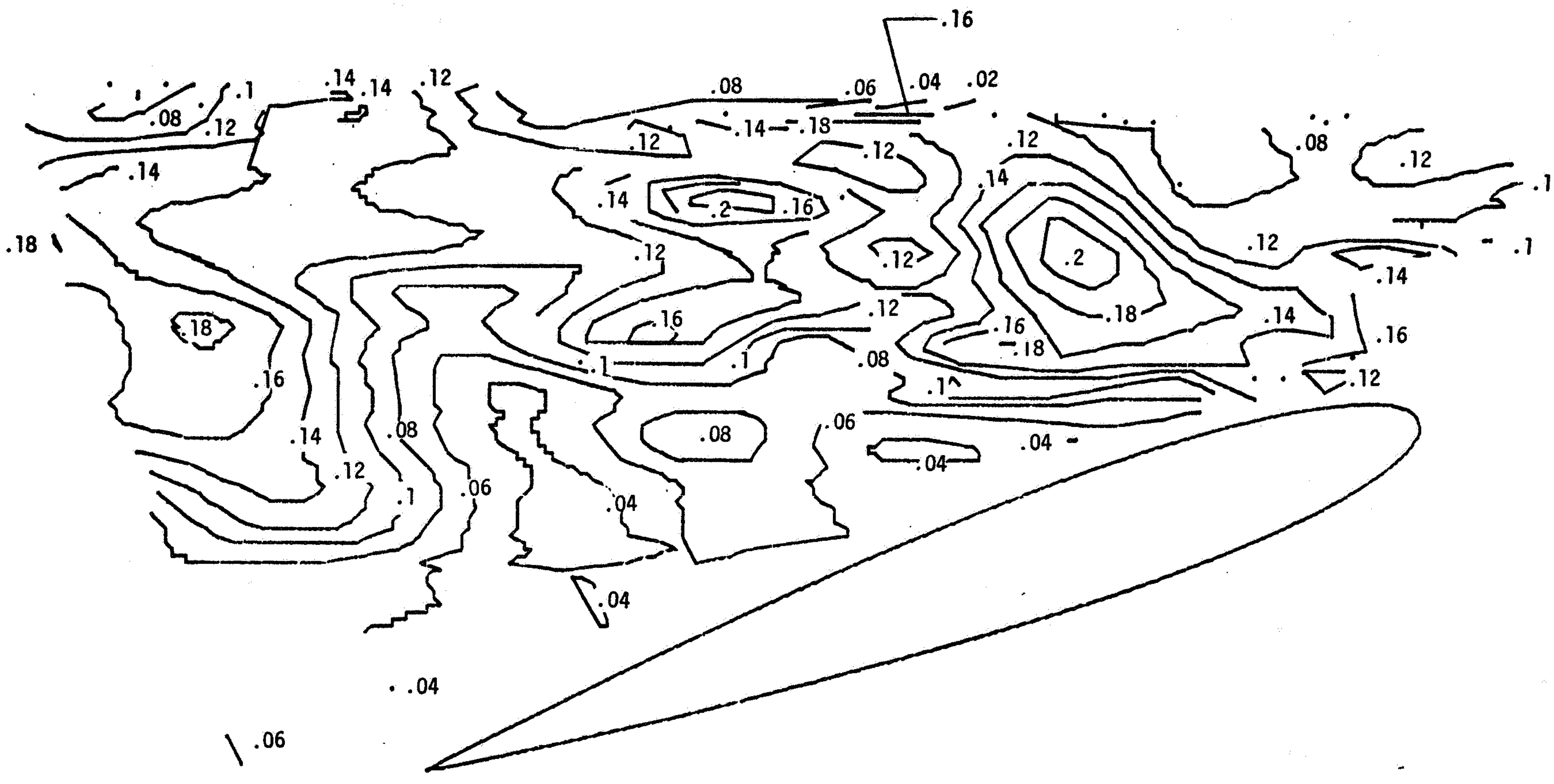

(c) Contours of constant deviation from the mean velocity corrected for velocity bias and converted to Mach number.
Figure 41. Concluded.

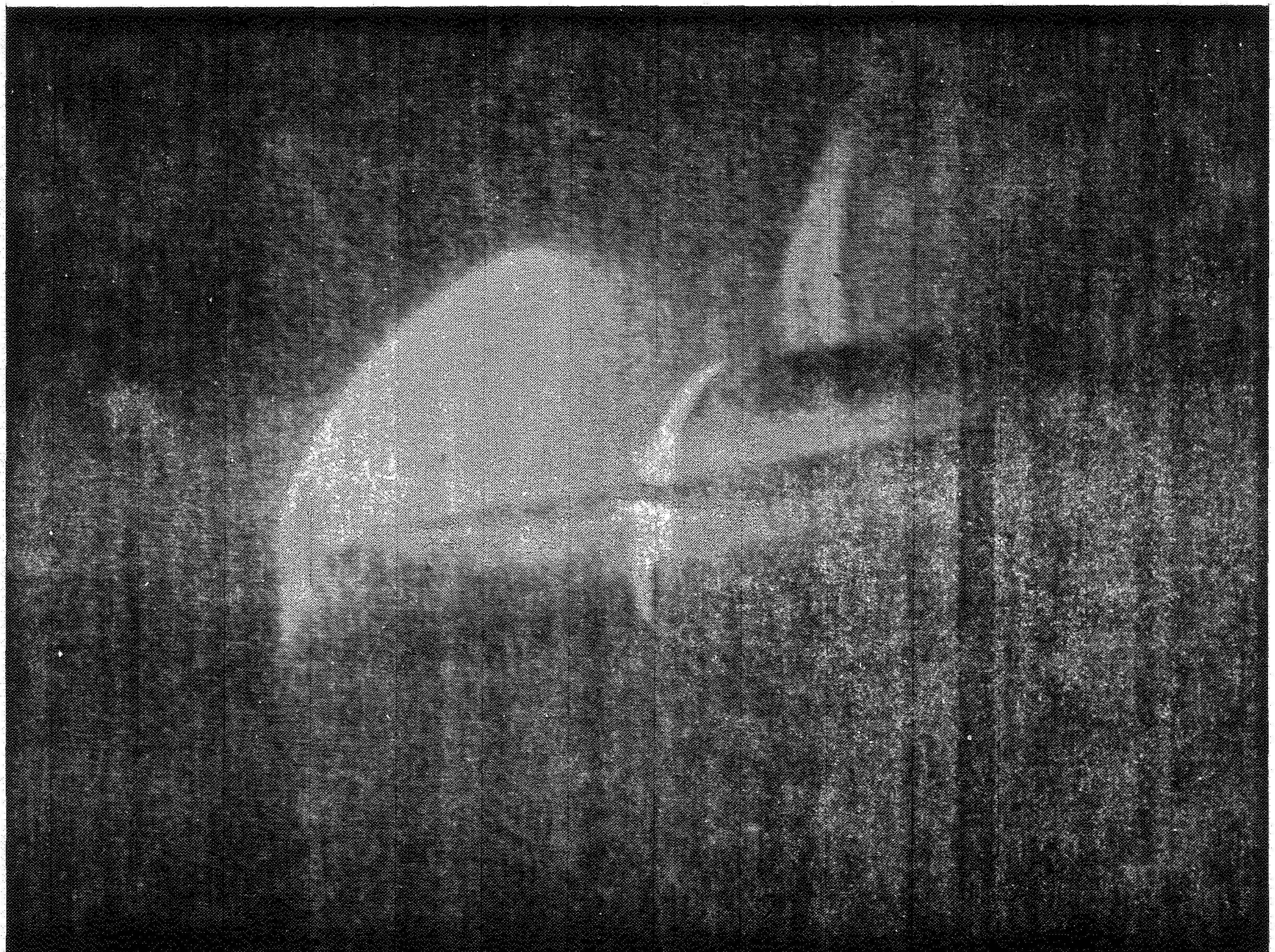

(a) Three-quarter front view showing wing vortex.

Figure 42. Flow visualization using kerosene smoke and a laser light sheet for the model of figure 30 without canard at a Mach number of .1, an angle of attack of 14°, and a roll oscillation of 1 Hz. The illumination is incident on the right half of the model.

ORIGINAL PAGE IS
OF POOR QUALITY

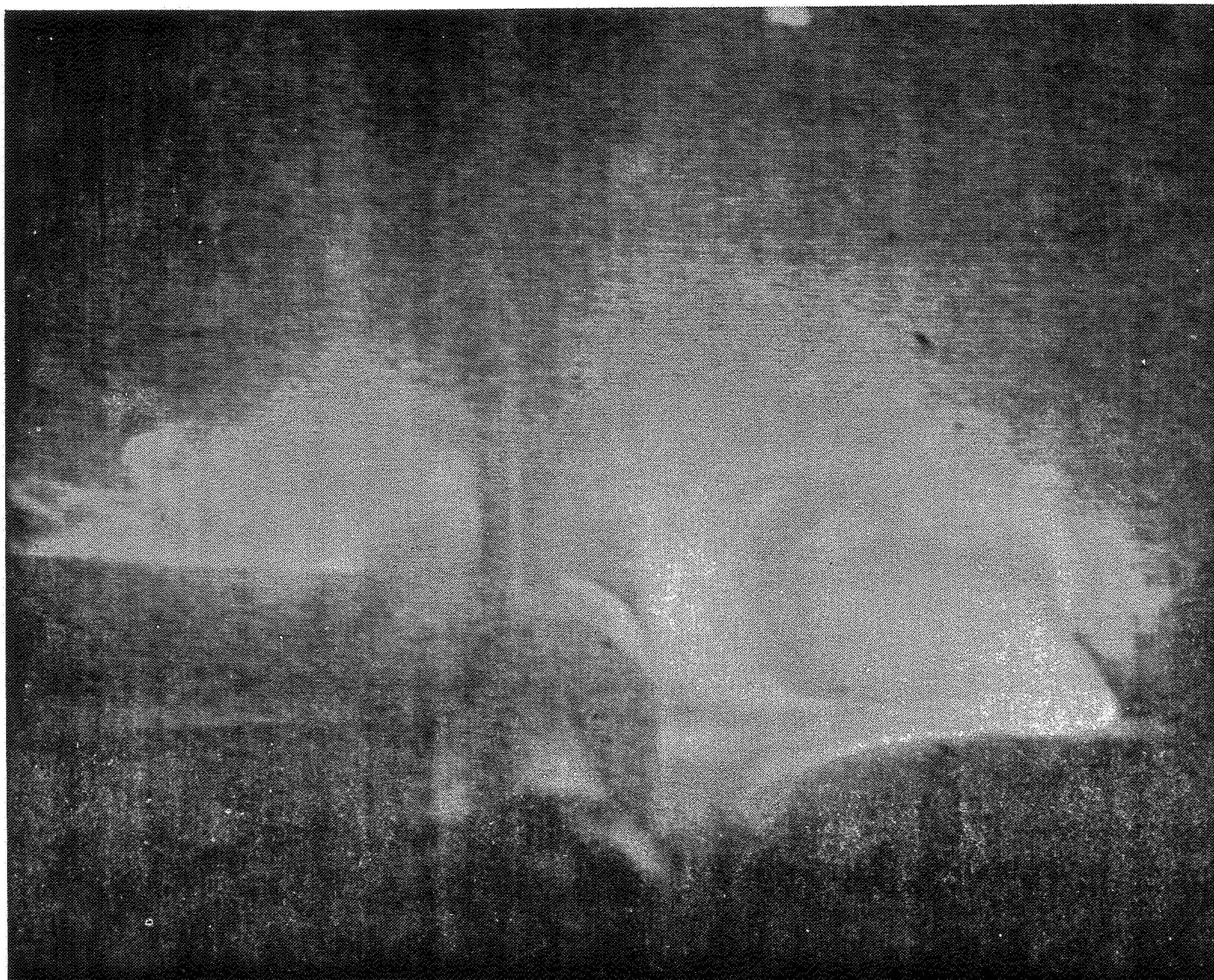

(b) Rear view showing wing vortex.

Figure 42. Continued.

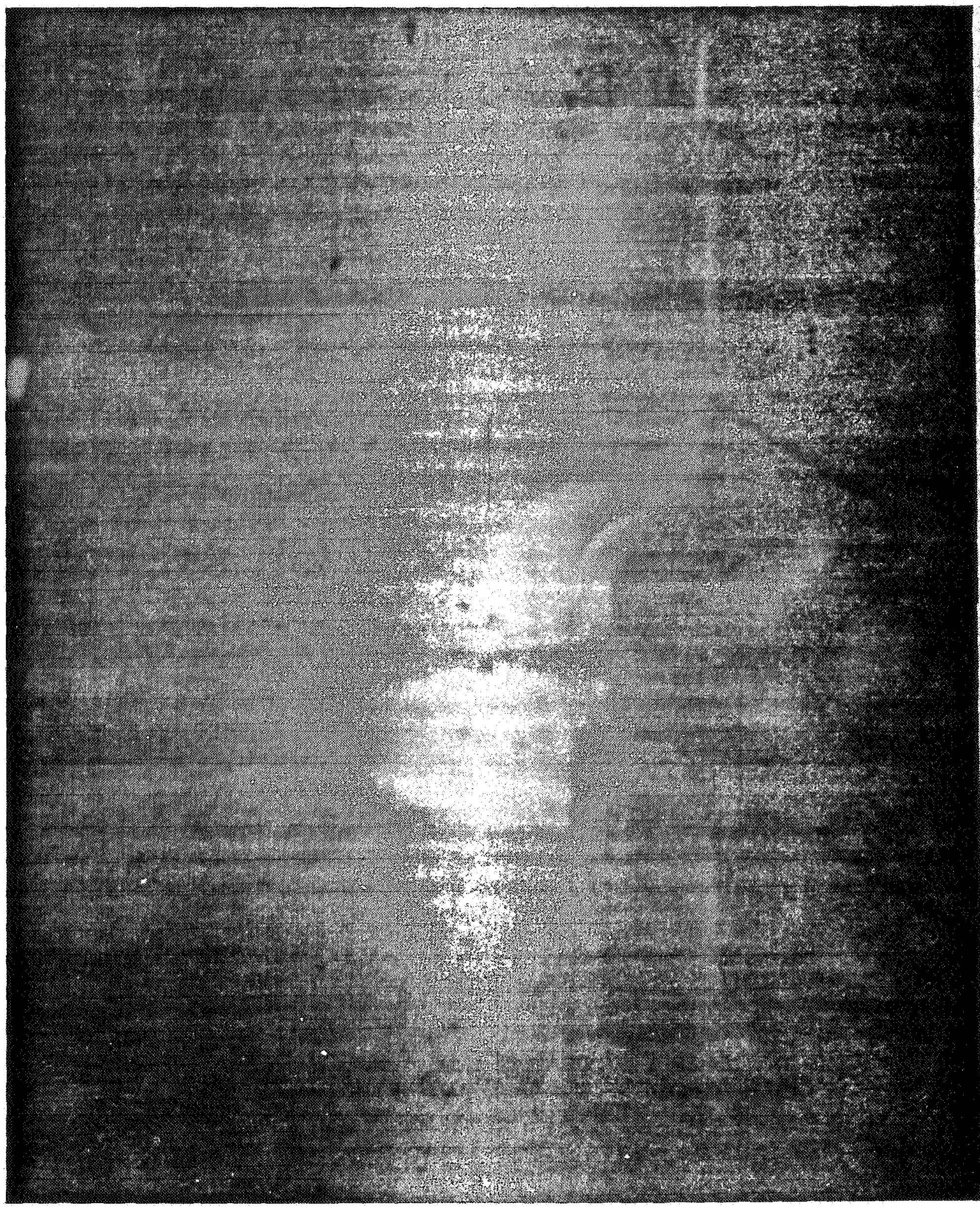

(c) Rear view showing body vortex.

Figure 42. Concluded.

ORIGINAL PAGE IS
OF POOR QUALITY